Heat Transfer Characteristics of FC-72 Flowing Upward in Vertical Small Diameter Tubes

Li, Yantao

(Degree)
博士（工学）

(Date of Degree)
2017-03-25

(Date of Publication)
2018-03-01

(Resource Type)
doctoral thesis

(Report Number)
甲第6953号

(URL)
https://hdl.handle.net/20.500.14094/D1006953

Doctoral Dissertation

Heat Transfer Characteristics of FC-72 Flowing Upward in Vertical Small Diameter Tubes

(垂直細管内を上向流動する FC-72 の熱伝達特性)

January 2017

Graduate School of Maritime Sciences

Kobe University

Yantao LI

(李延涛)

Contents

ABSTRACT

Small channel heat exchanger has the capabilities to transfer high heat flux in relatively small surface and volume. And it has been used in a wide variety of applications including electronics devices, compact heat exchangers, refrigeration evaporators and condensers and so on. However, several fundamental issues for small channel heat transfer still exist and further study is necessary.

The aim of this thesis is to contribute to a better understanding of the underlying physical phenomena in single-phase and two-phase flow boiling heat transfer in small channels. For this purpose, a set of experimental apparatus cable of testing a wide range of parameters such as tube inner diameter, heated length, flow rate, inlet liquid temperature as well as exponential period of exponentially increasing heat input was designed. It is mainly composed of a flow loop section, a heat input control system, a data acquisition system and a test section assembly. The test section assembly was designed and machined to ensure a fully developed turbulent flow in the test tube without leakage, provide a mean of heating the test tube uniformly, and facilitate the installation of measurement instruments. The measuring instruments were carefully calibrated and associated experimental uncertainties were thoroughly analyzed. Hence, the present experimental facility can be utilized to provide important data necessary to

understand heat transfer characteristics in small diameter tubes. FC-72 was selected as the test liquid as its low viscosity and surface tension are critically required for the single-phase and two-phase flow boiling heat transfer in small flow channels.

Prior to experiments on heat transfer in small channels, pool boiling experiments were conducted since the essential characteristics of the pool boiling CHF are retained in flow boiling CHF. The study of pool boiling is necessary for better understanding of flow boiling and its CHF. Chapter 3 presents and discusses the boiling heat transfer experiments results. The steady state and transient CHF data for a wide range of exponential period, system pressure and liquid subcooling were measured and studied. It was found that the steady state CHF increase with the increase of subcoolings. And although the steady CHF data for one atmosphere are in agreement with conventional correlations, the CHF data for sub-atmospheric pressures show higher values. The transient CHF values under sub-atmospheric pressures could be divided into two groups based on exponential periods, corresponding to short period region and long period region. The data in long period could be explained with conventional hydrodynamic instability (HI) mechanism. The data in short period could be described with explosive-like heterogeneous spontaneous nucleation (HSN) mechanism.

The steady state heat transfer process of turbulent forced convection of FC-72

through small diameter tubes was experimentally investigated. The effects of Reynolds number, Prandtl number, ratio of the viscosity in the bulk to that at the wall (μ/μ_w) and ratio of heated length to inner diameter (L/d) on turbulent heat transfer were studied in detail. It was found that the heat transfer coefficient increases with the increase of flow velocity, μ/μ_w and Prandtl number, and decrease of L/d .The experimental data were also compared with the values calculated by classical correlations for conventional sized channels. The results indicated that the classical heat transfer correlations are not adequate for calculation of the heat transfer coefficient in small diameter tubes. It is assumed that the roughness effect enhances the heat transfer rate in small sized channels. The Nusselt numbers for inner diameter of 1 and 1.8 mm depend on Reynold number in a different manner compared to that for inner diameter of 2.8 mm, which agrees with conventional correlations. The deviation from conventional heat transfer correlations increased as the Reynold numbers increase. The turbulent heat transfer correlations for FC-72 flow in tubes with diameters of 1, 1.8 and 2.8 mm have been developed respectively based on the experiment data. The differences between experimental and predicted Nusselt numbers are within ±15%.

The transient heat transfer process due to exponentially increasing heat inputs for turbulent flow of FC-72 was schematically investigated for different combinations of

parameters such as flow velocity, inlet liquid temperature, period of exponentially increasing heat inputs and test tube geometry. The effects of flow velocity, exponential period and tube inner diameter on transient turbulent heat transfer process were explored. It was found that the relation between transient Nusselt number and Fourier number, *Fo*, with flow velocity as a parameter shows the same trend as heat tranfer coefficient versus exponential period for each velocity. It was clarified that the transient turbulent heat transfer due to exponentially increasing heat inputs could be analyzed by introducing a dimensionless time, *Fo*. It was also found that the increment of transient state data relative to the steady state is higher for smaller diameter. It might be assumed that the effect of heat conduction contribution increases with a decrease of tube inner diameter. The empirical correlations for transient turbulent heat transfer caused by exponentially increasing heat inputs on small diameter tubes were developed based on the effects of Fourier number and tube inner diameter. The empirical correlations present the experimental data within ±25%.

Finally the subcooled flow boiling heat transfer experiments were conducted with FC-72 in vertical tube with inner diameter of 1 mm and effective length of 26.2 mm for exponentially increasing heat input with periods of 81.31 ms to 16.04 s. The flow velocity varied from 3 to 5 m/s and the inlet liquid temperature changed from 293 K to

333 K at a fixed outlet pressure of 300 kPa. The steady state flow boiling CHF values increase with increase of flow velocity, inlet subcooling and outlet subcooling because in such a situation a higher heat flux is required to initiate and sustain bubble activity. Empirical correlations combing velocity and subcooling have been proposed. The transition to film boiling process can be categorized into two types, representing two different CHF mechanisms. The transition from non-boiling to film boiling through FDNB and the transition from non-boiling region to film boiling through a short nucleate boiling are named as type 1 and type 2 process. Type 1 occurs at steadily increasing heat inputs and could be explained by conventional HI mechanism. Type 2 appears for rapid increasing heat inputs and it is induced by the explosive-like HSN from originally flooded cavities. The transient flow boiling CHF values first increase with a decrease in exponential periods up to a maximum CHF, then those decrease down to a minimum one and again increase with a decrease in exponential period. The transient CHFs due to exponentially increasing heat input could be divided into first and second group for long and short periods. The first group data correspond to type 1 process. The second group data correspond to type 2 process.

ACKNOWLEDGEMENTS

I would like to express my gratitude to my supervisor, Professor Fukuda Katsuya, for his support, guidance and encouragement during my PhD study. His guidance improved my research ability; his financial support enabled me to focus on study in the last year; his hardworking sprit encouraged me to follow him. He availed himself for discussion at any time although he has many other important responsibilities. Without his profound comments and advises, this work would not have been possible.

I also wish to thank Professor Liu Qiusheng for his constructive advises throughout the years. His humble and cautious attitude toward research is and will always be valuable assets to me.

Much appreciation is also expressed to Professor Dan Tomohisa and Professor Mimura Haruo for the thorough review of this thesis.

I am deeply thankful to the Japan Ministry of Education, Science and Culture for granting me a fully funded scholarship and an opportunity to pursuit my PhD study.

I would also like to thank my seniors and my friends, Mr. Yamane and Mr. Sutopo, for passing me the knowledge about the experimental facility and giving their kind and useful advices. I acknowledge Dr. Zhao Zhou for his help and cooperation in the design and manufacture of the test section. I am also grateful to the technician Mr. Ogawa and

Assistant Professor Shibahara Makoto for their support and help in the daily work.

Special thanks to Dr. Wang Jingzhu for her constant encouragement. My gratitude also goes to the doctoral students in my laboratory, Dr. Min and Dr. Wang Li, thank you for making the lab such a pleasant and stimulating place to study.

Kind and warm care from my Japanese host family, the Inoues, is also acknowledged.

Last but not least, I would like to express thanks to my parents and my brother for their love, encouragement and support all the time.

NOMENCLATURE

a, b	constant in Eq. (2.10)
Br	Brinkman number
C	constant in Eq. (4.15)
c_p	specific heat at constant pressure, J/kg K
d	inner diameter of the test tube, m
d_{re}	reference diameter in Eq.(4.7), 0.001 m
d_o	outer diameter of the test tube, m
D_h	hydraulic diameter, m
f	friction factor
Fo	$=\alpha\tau/r_i^2$, Non-dimensional time, Fourier number
Gr_H	Grashot number
h	heat transfer coefficient, W/m^2 K
I	current flowing through standard resistance, A
K_1	constant in Eq. (3.5)
K_2	constant in Eq. (3.6)
L	heated length, m
L_e	entrance length, m
m	mass of test tube, kg/m^3
Nu, Nu_d	$= hd/\lambda,$ Nusselt number, transient Nusselt number
$Nu_{d,st}$	steady state Nusselt number
$Nu_{d,tr}$	transient Nusselt number
$(Nu_{d,tr})_{\text{cal}}$	calculated transient Nusselt number
P	pressure, Pa
P_{in}	pressure at inlet of heated section, Pa
P_{ipt}	pressure measured by inlet pressure transducer, Pa
P_l	pressure in liquid, Pa
P_{out}	pressure at outlet of heated section, Pa
P_{opt}	pressure measured by outlet pressure transducer, Pa
Pr	$=c_p\mu/\lambda$, Prandtl number
P_v	pressure in vapor, Pa
Q	heat input per unit volume, W/m^3
Q'	volumetric flow rate, m^3/s
Q_0	initial exponential heat input, W/ m^3
q	heat flux, W/m^2

q_{cr}	critical heat flux, W/m^2
$q_{cr,sub}$	subcooled critical heat flux, W/m^2
q_i	incipient boiling heat flux, W/m^2
r	test tube radius, m
r_i	test tube inner radius, m
r_o	test tube outer radius, m
r*	critical radius of spherical bubble, m
R_1 *to* R_3	resistance in a double bridge circuit, Ω
Re Re_d	$=ud/v$, Reynolds number
R_s	resistance of standard resistance, Ω
R_T	resistance of test tube, Ω
S	surface area, m^2
T	temperature, K
T_{sat}	saturation temperature, K
T_{in}	Incipience surface temperature, K
T_{in}	inlet liquid temperature, K
T_L	average bulk liquid temperature, K
T_{out}	outlet liquid temperature, K
$(T_{out})_{cal}$	calculated outlet liquid temperature, K
T_s	heater inner surface temperature, K
t	time, s
ΔT_c	superheat corresponding to CHF, K
ΔT_i	superheat corresponding to boiling incipience, K
ΔT_L	$=(T_s-T_L)$, surface temperature difference between heater inner surface temperature and average bulk liquid temperature, K
ΔT_{sat}	surface superheat, K
ΔT_{sub}	liquid subcooling, K
$\Delta T_{sub,in}$	inlet liquid subcooling, K
$\Delta T_{sub,out}$	outlet liquid subcooling, K
u	flow velocity, m/s
V	volume, m^3
V'	voltage signal, V
V_{FM}	voltage signal of flow velocity, V
V_1	voltage drop across standard resistance, V
V_R	voltage drop across the test heater, V
V_1	unbalance voltage of a double bridge circuit, V

V_{TLi}	voltage signal of inlet temperature, V
V_{TLo}	voltage signal of outlet temperature, V
α	thermal diffusivity, m^2/s
β	coefficient of volume expansion, 1/K
γ	aspect ratio
δ	wall thickness, m
σ	surface tension, N/m
λ	thermal conductivity, W/(m·K)
μ	viscosity, $N \cdot s/m^2$
μ_w	viscosity at tube wall temperature, $N \cdot s/m^2$
ρ	density, kg/m^3
ρ_l	liquid density, kg/m^3
ρ_v	vapor density, kg/m^3
τ	exponential period, s
υ	kinematics viscosity of the fluid, m^2/s

Subscripts

a	average
c	conduction
cal	calculated
h	hydraulic
in	inlet
out	outlet
L	liquid
s	surface

FIGURE LIST

TABLE LIST

CHAPTER 1

Introduction

1.1 Research Background

1.1.1 Basic concept of heat transfer in small channels

1.1.1.1 Flow channel classification

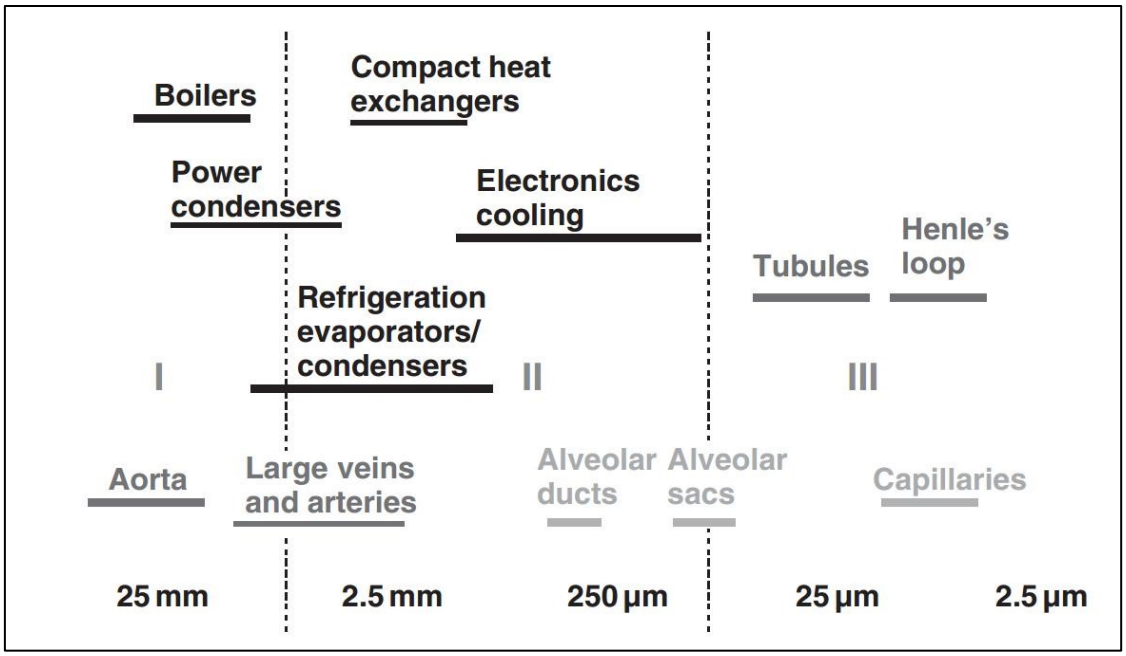

Fig. 1.1 Range of channel diameters employed in various applications [1]

A flow channel serves for liquid flowing so that the heat transport process from the wall surface to liquid is accomplished. Fig. 1.1 shows the ranges of channel dimensions employed in various systems. A shift from larger diameters, on the order of 10–20 mm, to smaller diameter channels occurs with the development of mini and micro technology.

Since the dimensions of interest are in the range of a few tens or hundreds of micrometers to several millimeters, they are assumed to be small channels for science and engineering associated with processes at this scale.

A flow channel classification proposed by Mehendale et al. [2] classifies the dimension from 1 to 100 μm as microchannels, 100 μm to 1 mm as meso-channels, 1 to 6 mm as compact passages, and greater than 6 mm as conventional passages.

Table 1.1 Flow channel classification scheme

Conventional channels	$d > 3$ mm
Minichannels	3 mm $\geq d >$ 200 μm
Microchannels	200 μm $\geq d >$10 μm
Transitional Microchannels	10 μm $\geq d >$1 μm
Transitional Nanochannels	1 μm $\geq d >$0.1 μm
Nanochannels	0.1 μm $\geq d$

Kandlikar and Grande [1] slightly modified the above classification method, and proposed a more general scheme as shown in Table 1.1. This classification scheme is generally adopted in literature.

1.1.1.2 Small flow channel applications

Small flow channel cooling method has been widely used due to the capabilities to transfer high heat flux in relatively small surface and volume. The heat removal enhancement is achieved through increase of heat transfer coefficient and heat exchange surface (for a certain volume) with the decrease of channel size accompanying with a higher pressure drop. A balance between heat transfer enhancement and pressure drop for different applications leads to different channel dimensions. Fig. 1.1 shows the main applications with corresponding channel dimensions range, including electronics cooling, compact heat exchangers, refrigeration evaporators and condensers and so on. The details are described as follows.

a) Electronics cooling

The thermal load for electronic devices has risen significantly in the rescent years. Dr.Moore predicted that the number of transistors on an intergrated circuit would double every 18 months. The truth is that an exponential growth of number of transistors in circuits has been developed following the Moore Law in the past decades. This results in rapid increase of the internal resistance of the component as well as the internal heat generation. The new challenge for the coming decade is on the order of 600-1000W/cm^2 [3]. So high heat flux dissapation in compact structures requires

efficient cooling system. Single-phase and two-phase flow boiling heat tranfer inside small channels is one of the efficient canditates of maintaining desired temperature difference for these electronic devices. Fig 1.2 shows the schematic of cooling of electronic components with small channel cooling method. The basic concept of miniturization was first devolved by Tuckerman and Pease [4]. They demonstrated cooling of 7.9 W/cm^2 with a maxium temperature increase of 71℃ by reducing the channel size into micro scale. The pressure drop was also as high as 200 kPa. This is the main disadvantage of miniaturization.

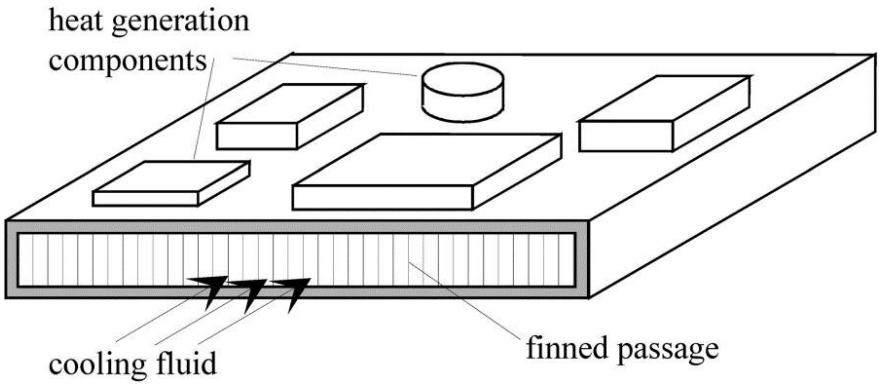

Fig. 1.2 Schematic of cooling of electronic components with small channel cooling method [5]

Colgan et al. [6] at IBM published a practical implementation of a silicon microchannel cooler as shown in Fig. 1.3 for high-power chips. They argued that it is not practical to form the microchannels directly on the chip given the high cost of

high-performance processor chips. Power densities in excess of 400 W/cm^2 are reported for a flow of 1.2 l/min at pressure drop of 30 kPa. High pressure drop with decrease of flow channel still limit the ongoing miniaturization in practice.

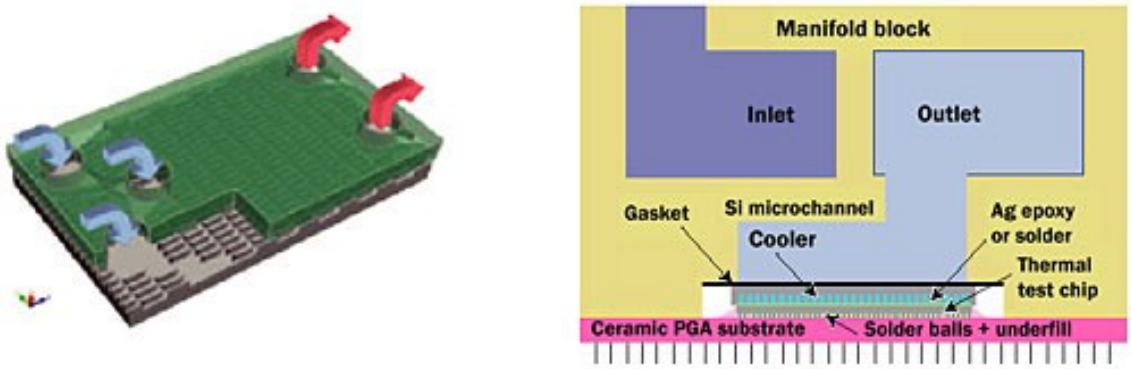

Fig. 1.3 High-performance liquid cooling technology using microchannels

As compactness increases, the heat tranfer increases and the pressure drop also increases. Higher heat tranfer coefficient comes at a cost of higher requirement of pump power. Increasing the hydraulic diameter from micro to mini scale configuration, sufficient heat tranfer coefficient can be achieved with a lower pressure drop.

b) Compact heat exchanger

Figure 1.4 shows a typical structure of compact heat exchanger. It has numerious benefits such as greater heat transfer, smaller volume and weight, higher efficiency and lower cost. Traditional compact heat exchangers have surface area densities greater than 700 m^2/m^3[7]. However, with the development of nanotechnology and fuel-cell technology, more compact and enhanced heat exchangers are being designed.

Ultra-compact heat exchangers typically have surface area densities high up to 10,000 m^2/m^3 [7]. The high heat transfer areas per unit volume of these heat exchangers could be achieved by construction techniques that result in large numbers of small channels in the range of 0.1-1 mm [1]. The compact and ultra-compact heat exchangers have also been widely used in aerospace, cryogenic, refrigeration and even nuclear industries.

For better design of those small channel applications, it is necessary to know the heat transfer characteristics of the fluid flow in small channels as precisely as possible.

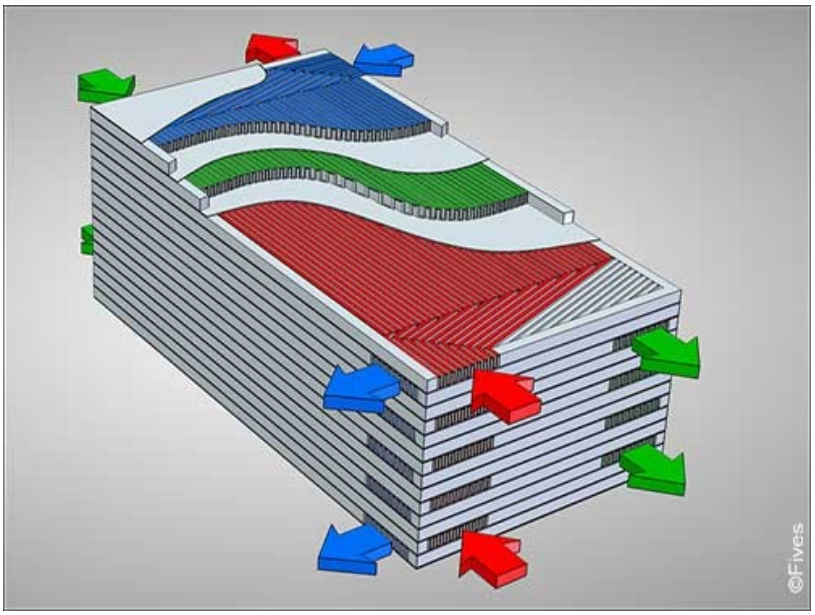

Fig. 1.4 Schematic of compact heat exchanger

1.1.1.3 Coolant used in the single-phase cooling in small flow channel

Small channel cooling is possible by various medium like liquid and gas. Water and air are the most popular coolants used in the past years. Air has a limit about 100 W/cm^2

because air has less heat capacity and lower density. Water is used for high heat flux removal due to its high thermal conductivity, high convective heat transfer coefficient and high heat capacity. However, it may damage the electronic devices when it leaks out because of its electrical conductivity. In practice, dielectric coolant is preferred for electronic devices. Flurinert liquid like FC-72 is selected as a coolant over other dielectric fluids because of relatively high thermal conductivity, high latent heat of vaporization and low viscosity.

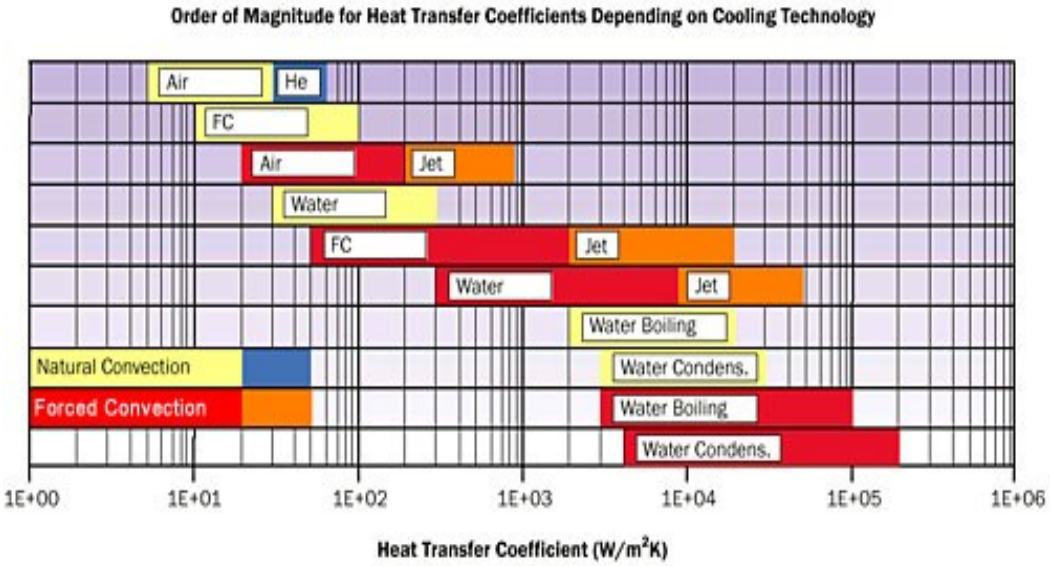

Fig. 1.5 Range of overall heat transfer coefficients for different fluids and cooling modes

1.1.2 Fundamentals of boiling heat transfer

Boiling is the process of evaporation associated with vapor bubbles in liquid. The two basic boiling types are pool boiling and flow boiling. The former is boiling on the

heated surface submerged in a pool of liquid, while the latter occurs in a flowing stream of liquid. Both of them are effective heat transfer methods to increasingly stringent thermal management requirements in various areas because of the high performance due to latent heat of vaporization. Flow boiling is considerably more complicated than pool boiling, owing to the coupling between hydrodynamic and boiling heat transfer process. Pool boiling is simpler experimentally than flow boiling but the results can be incorporated in the descriptions of the more complicated regimes of flow boiling.

1.1.2.1 Nucleation and bubble formation

Nucleation that occurs at nucleation sites at a solid-liquid interface is called heterogeneous nucleation. Nucleation without preferential nucleation sites is homogeneous nucleation, which occurs spontaneously and randomly within the liquid.

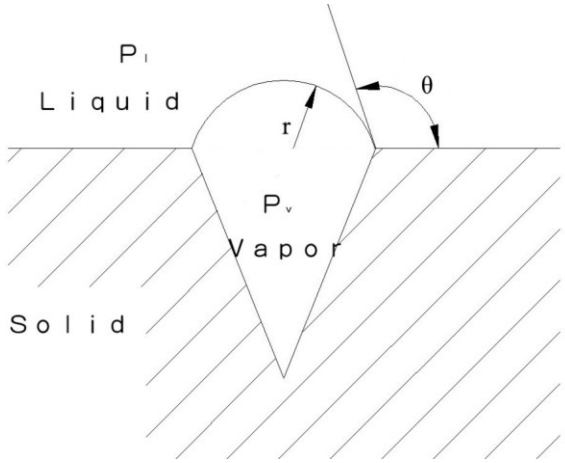

Fig. 1.6 Nucleation from a cavity

For the case of heterogeneous nucleation, most of the proposed theories assume that nucleation is initiated in cavities in which a gas or vapor preexists. A simple model, which is represented by a cavity in the surface with a spherically shaped bubble emerging from it, is shown in Fig.1.6. The bubble will be in mechanical equilibrium when the pressure difference between the inside and the outside of the bubble is balanced by the forces of surface tension.

$$(P_v - P_l)\pi r^{*2} = 2\pi r^* \sigma \tag{1.1}$$

From Equation (1.2), the following Young-Laplace equation can be obtained,

$$P_v - P_l = 2\sigma / r^* \tag{1.2}$$

Where

P_v＝pressure in vapor

P_l＝pressure in liquid

σ＝surface tension of liquid

r*＝critical radius of spherical bubble

The vapor superheat $\Delta T(=T_v-T_{sat})$ corresponding to $\Delta P(=P_v-P_l)$ is required to maintain a bubble of radius, r^*, at equilibrium. The superheat for homogenous nucleation is very large and is difficult to obtain in the presence of surfaces. The

heterogeneous nucleation requires less superheat and is in addition a function of the angle of contact between the vapor and solid. The contact angle is related to the surface tension of the liquid. This contact angle is affected by wettability of the surface, shape of the surfaces, local temperature gradients, etc. The extent of how a surface can catalyze or facilitate the nucleation depends on the contact angle. The smaller the angle (or the stronger the wetting of the surface), the lower the free energy change, and the lower the nucleation barrier will be.

With sufficient high superheat, the bubble emerges from the cavity and starts to grow on the flat surface outside the cavity, the bubble will grow and detach from the surface as the buoyant force exceeds the surface tension force if the liquid is at or above the saturation temperature. There the bubbles collapse because the temperature of bulk fluid is not as high as at the heat transfer surface, where the bubbles were created. In the condition of high subcooling, the bubble will collapse without leaving the heated surface, or it will detach and immediately collapse into the subcooled liquid.

1.1.2.2 Typical pool boiling curve

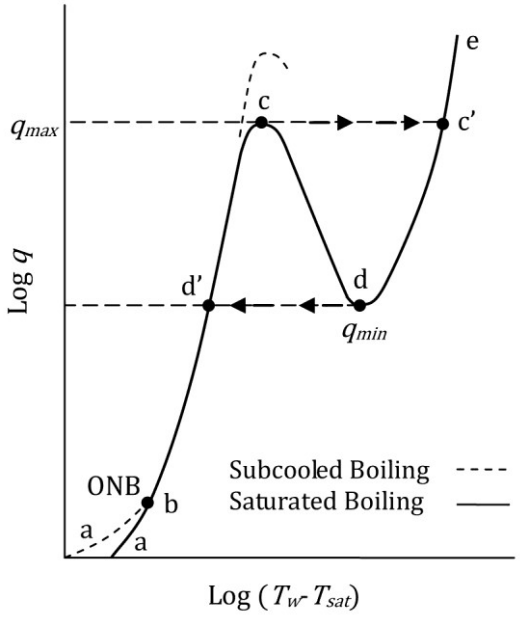

Fig. 1.7 Pool boiling heat transfer curve

The typical boiling curve for heat flux against surface superheat is plotted in Fig. 1.7. This curve can be divided into four regions based on the vapor behaviors, namely natural convection, nucleate boiling, transition boiling and film boiling.

Region I: Single-phase natural convection (a-b). ΔT is so small that the fluid motion and heat transfer is dominated by single-phase natural convection. With the increase of superheat, bubble inception or the onset of nucleate boiling at point b will occur.

Region II: Nucleate boiling (b-c). ΔT is large enough that the nucleation of vapor bubbles occurs at the heating surface. As the superheat continuously increases, the number of nucleation sites increases. As a result, vapor patches and columns are formed close to the surface. After that, the vapor generation rate is so high that the surface is

blanketed with an unstable vapor film. Meantime the maximum heat flux, $q_{max,}$ is reached at point c. The maximum heat flux is also termed as critical heat flux (CHF).

Region III: Transition boiling (c-d). In this region, a part of the heated surface undergoes film boiling while other parts are under nucleate boiling. It is characterized by the existence of an unstable vapor blanket over the heating surface that releases large patches of vapor at more or less regular intervals.

Region IV: Film boiling (d-e). Film boiling is characterized by a layer of vapor film which continuously covers the heat surface when the heat flux reaches the minimum heat flux, q_{min}, or the Leidenfrost point, at point d. The heat transfer occurs by conduction through the vapor film instead of a liquid film. The vapor film is such stable that the temperature increases, radiation becomes significant and thus increases the heat transfer rate with the increasing of superheat.

1.1.2.3 Pool boiling CHF

The pool boiling CHF can be easily described as the change of the heat transfer regime from nucleate boiling to film boiling. Two models from Zuber and Sakurai are well accepted for explanation of pool boiling CHF mechanism.

a) Hydrodynamic instability (HI)

Zuber's hydrodynamic instability model [8] has been considered as the most likely mechanism. He suggested that the number of the nucleation sites is so large and the vapor generation rate is so high that the area between the bubble columns for liquid flow to the heating surface is reduced under high heat flux. The relative velocity is then so large that the liquid-vapor interface becomes unstable, essentially starving the surface of the liquid and causing the formation of a vapor blanket.

b) Heterogeneous spontaneous nucleation (HSN)

The critical heat fluxes (CHFs) occur from the levitation of liquid on cylinder surface at transition to film boiling not only from transient heat conduction process but also from steadily natural convection. The phenomena were observed by Sakurai et al.[9] for the pool boiling heat transfer due to exponentially increasing heat inputs, $Q_0\exp(t/\tau)$, in liquid nitrogen. It was suggested that the CHFs occur due the explosive-like HSN in initially flooded cavities on cylinder surface for inducing the incipient boiling process. These CHFs become lower than those estimated from the CHF correlation based on the HI model.

1.1.2.4 Flow boiling regime

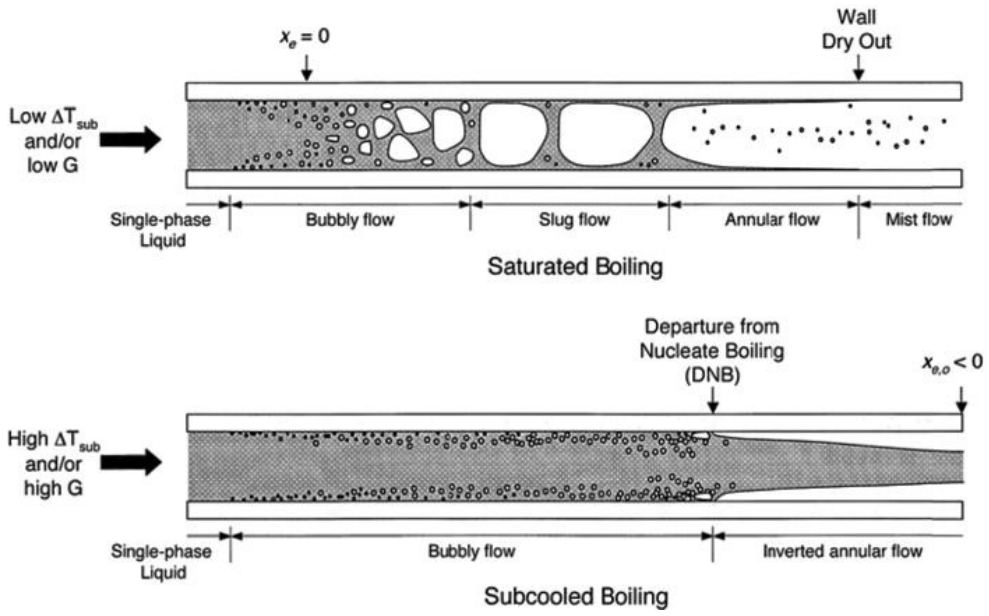

Fig. 1.8 Saturated and subcooled flow boiling regime

As shown in Fig. 1.8, the saturated flow boiling regimes include single-phase liquid, bubbly flow, slug flow, annular flow and mist flow. However, high subcooled flow boiling is usually employed for higher heat flux. The generated bubbles would condense in contact with subcooled liquid and the bubbles are usually very small.

1.2 Literature Review

A literatures review summarizes the previous analytical and experimental studies on pool boiling, single-phase heat transfer and two-phase flow boiling in small diameter. The details will be stated separately as follows.

1.2.1 Pool boiling heat transfer

Extensive studies on the pool boiling heat transfer in non-wetting and wetting liquids under wide ranges of pressures and subcoolings due to exponentially increasing heat inputs, $Q_0\exp(t/\tau)$, were reported by Sakurai and his associates [9, 10], Fukuda et al [11, 12], Park [13] and Sutopo [14]. The wide investigations on water and other wetting liquids such as ethanol, liquid nitrogen, and liquid helium have been performed for a wide range of exponential periods, pressures and liquid subcoolings, effect of surface condition on CHF, and the photographic observation on vapor and bubble behavior at transitions to film boiling. The exponential periods represent increasing rate of heat inputs and surface superheats. They observed three kinds of transition of boiling heat transfer process are the transition from the non-boiling regime to film boiling or direct transition (type 1), the transition from non-boiling to fully developed nucleate boiling (FDNB) (type 2), and the transition from non-boiling regime to film boiling with increasing heat flux or semi-direct transition (type 3). The direct transitions at incipient boiling surface superheat in the liquids were well explained by the assumption that the incipient boiling occurs due to the explosive boiling, named the explosive-like heterogeneous spontaneous nucleation (HSN) in originally flooded cavities at the HSN surface superheat. They also found that the CHF can be were classified clearly into the

first, second, and third groups for long, short, and intermediate periods, respectively.

1.2.2 Single-phase heat transfer

1.2.2.1 Steady state forced convection heat transfer

Table 1.2 summarizes the small channel heat transfer studies by different researchers with a comparison with conventional theory. The results show clear deviations of heat transfer prediction compared with conventional theory. More studies summarized in Table 1.2 indicate an under-prediction of the measured Nusselt numbers by conventional correlations. These studies are reviewed in detail as follows.

Several investigators claimed higher Nu_d values than those predicted by correlations based on conventional theory. Wu and Little [15] tested the heat transfer characteristics of N_2 flowing through microchannel heat exchangers. It was found average Nusselt numbers higher than those predicted by the conventional correlations for fully developed laminar flows and for fully developed turbulent flows. The authors reported that the very large relative roughness of the microchannels could improve heat transfer coefficients. Choi et al. [18] presented experimental data on the Nusselt numbers for Reynolds numbers ranging between 50 and 20,000. They found that the Nusselt number was larger than the prediction of the Colburn analogy. They also found that the Nusselt number in both laminar and turbulent flow depends on Reynold number in a different

Table 1.2 Summarize of studies on heat transfer in small channels

Reference	Nusselt number	D_h(μm)	Cross section	Test fluid
Wu and Little [15]	Higher	55.8-72.4	Trap.	N_2
Choi et al. [16]	Higher	3-81	Circ.	N_2
Yu et al. [17]	Higher	19-102	Circ.	Water, N_2
Peng and Wang [18]	Lower	646	Rect.	Water
Peng and Peterson [19]	Lower	311-747	Rect.	Water, methanol
Acosta et al. [20]	Agree	36-990	Rect.	He
Harms et al. [21]	Agree	404	Rect.	Water
Adams et al. [22]	Higher	102-1090	Circ.	Water
Adams et al. [23]	Agree	>1200	Circ.	Water
Tso and Mahulikar [24]	Lower	717-741	Circ.	Water
Debray et al. [25]	Lower	590-2218	Rect.	Water
Kandlikar et al. [26]	Higher	620-1067	Circ.	Water
Qu and Mudawar [27]	Agree	349	Rect.	water

manner compared with conventional theory. Yu et al. [17] investigated particularly the heat transfer of nitrogen gas and water in micro tubes in the turbulent regime. The Nusselt number values in turbulent regime were considerably larger than those predicted by means of the conventional theory. Adams et al. [22] studied single-phase heat transfer in circular tubes with diameters of 0.76 and 1.09 mm with water. They reported that Nusselt numbers were usually higher than those predicted by conventional heat transfer correlations. They observed that the deviation increased as the channel diameter decreased and Reynolds numbers increased. Kandlikar et al. [26] and Lee [28] also have found the Nusselt number higher than predicted by correlations based on conventional theory.

On the other hand, some researchers have found the Nusselt number smaller than that measured for convectional sized channels. Peng and Wang [16] investigated single-phase convective heat transfer of water and methanol for fully developed turbulent flow in rectangular channels with hydraulic diameter of 646 μm. It was found that the measured Nusselt number was lower than the predicted value. Debray et al. [25] experimentally studied the convective heat transfer coefficient in a rectangular channel with hydraulic diameter of 590-2218 μm for water. They found the Nusselt numbers are lower than those predicted by the conventional Colburn correlation for turbulent flow.

The authors attributed the observed deviations to the lack of the wall heat flux uniformity at the walls of microchannel.

There have also been many other reports in which conventional correlations are able to predict single-phase heat transfer coefficients in small sized channels. Adams et al. [23] conducted experimental tests on turbulent convective heat transfer through non-circular microchannels with a hydraulic diameter of 1.13 mm. The results show that their experimental Nusselt numbers were well predicted by Gnielinski's correlation; They concluded that the hydraulic diameter of 1.2 mm can be assumed as reasonable lower limit for conventional correlations for the Nusselt number. Owahib and Palm [29] performed experiments on the single-phase forced convection through small sized channels. Their experimental results in the turbulent region were in very good agreement with the conventional correlations. Agostini et al. [30] investigated the heat transfer coefficient in circular and rectangular mini-channels with hydraulic diameters of 0.77 to 2.01 mm. They found their experimental results in the turbulent regime coincided with the Gnielinski correlation. Acosta et al. [20] and Harms et al. [21] also reported that the conventional correlations hold for small flow channels.

The possible reasons for deviations of heat transfer prediction in small channels compared with conventional theory includes experimental conditions and errors [31],

roughness effect [32], variation of physical properties [33], electrical double layer [34] and so on.

1.2.2.2 Transient forced convection heat transfer

An in-depth knowledge of transient forced convection heat transfer has become important for the precise thermal management of high-performance electrical machines, nuclear reactors and renewable energy applications like thermal solar panels [35-38]. The dynamic processes such as start-up, shut-down, power surge, and pump failure may cause thermal transients, leading to high temperature gradients and severe thermal stress. The unsteady nature of thermal load imposes a challenge in maintaining the efficiency and reliability of the applications mentioned above. Therefore, a better understanding of the transient forced convection heat transfer process for time dependent heat generation is deemed necessary for safety assessment and optimal design of the thermal components involved in the dynamic process.

A great many experimental, analytical and numerical studies have focused on the transient laminar forced convection heat transfer. Sparrow and Siegel [39] conducted an analysis of transient laminar convection in the thermal entrance region of circular tubes. They determined thermal responses to unit step changes in the wall heat flux or in the temperature. Siegel [40] analyzed transient laminar forced convection in a parallel plate

channel. The results demonstrated that the slug assumption did reveal the essential physical behavior of the systems considered, although the numerical results were somewhat in error. Fakoor-Pakdaman et al. [41, 42] analytically and experimentally studied the transient laminar forced convection heat transfer inside a circular tube under time-dependent heat flux. They expressed the transient Nusselt number as a function of dimensionless space and time. The dimensionless time was defined as $Fo=\alpha t/r_i^2$, where Fo, α, t, r_i are the Fourier number, thermal diffusivity, elapsed time and tube inner radius, respectively. Semi-analytical relationships were developed on the basis of experimental data and analytical methodology to predict the transient thermal response.

Although there are some analytical and experimental studies on transient turbulent heat transfer, only a few are focused on the transient process caused by an exponentially increasing heat generation rate, Q ($=Q_0 exp(t/\tau)$, where, Q_0 is initial heat generation rate, t is time, and τ is the exponential period of heat generation rate). Kakaç [43] numerically analyzed transient heat transfer for turbulent flow between two parallel plates for dynamic wall flux or wall temperature. The variation of the Nusselt number was presented in terms of non-dimensional space and time. The dimensionless time was defined as $Fo=\alpha t/(D_h/2)^2$, where D_h was the hydraulic diameter of the parallel-plate channel. Kawamura [44] examined the variation of heat transfer coefficient in a steady

turbulent flow through a circular tube heated stepwise with time. A numerical analysis was also conducted for the same size channel and the results of which agreed with experimental data well. Soliman and Johnson [45] analytically and experimentally studied the transient mean wall temperature change of a flat plate heated by an exponential heat source. Their solutions were 50% higher than the experimental data. Kataoka et al. [46] investigated the transient phenomenon due to exponentially increasing heat inputs with water flowing over a platinum wire inserted in a round tube. They derived the transient Nusselt number correlation by introducing one non-dimensional parameter, $\tau u/L$ (where τ, u and L represent period, velocity and heater length, respectively). Liu et al. [47-48] conducted transient experiments for parallel flow of helium gas over horizontal cylinders, flat plates and twisted plates at various exponential periods of heat generation rates. Transient heat transfer correlations were obtained for various heater configurations. Hata et al. [49] experimentally studied the transient turbulent heat transfer coefficients for water flow in tubes with relatively large inner diameters. An empirical correlation for describing the transient turbulent heat transfer was developed in terms of a non-dimensional exponential period. Although the correlation could represent the experimental data well, the non-dimensional exponential parameter seems to be meaningless for single-phase heat transfer.

1.2.3 Two-phase flow boiling heat transfer

Two-phase boiling heat transfer process and its CHF are complex phenomena because they involve wide variables such as: mass flow rate, mass dryness fraction, liquid density, gas density, liquid viscosity, gas viscosity, surface tension, surface roughness, and pipe inclination. Many experimental studies have been conducted on this topic and several correlations and physical models have been developed to explain the phenomena. High CHF could be obtained by using small diameter tube with short heated length. Extensively studied have been conducted for flow boiling in conventional large geometries. There is limited data available for flow boiling CHF in small channels [50-51].

The earlier study on subcooled flow boiling in small sized channels was performed by Peng et al. [52]. They reported that nucleation in small channels requires larger superheats. Bubble generation and growth was said to require a minimum amount of space, the evaporating space. Hapke et al. [53] studied the onset of nucleate boiling in a vertical pipe with an inner diameter of 1.5 mm. They figured out that the superheat necessary to initiate boiling to be essentially higher than that of larger tubes for the same values of heat and mass flux. Larger heat fluxes lead to an increase in the wall superheat at the onset of nucleate boiling (ONB).

There are still inconsistencies in the experimental CHF results in small sized channels. The discrepancy is large on the influence on CHF of inlet subcooling, pressure, and inner diameter [50-51].

1.3 Research Motivations

Detailed literature review on pool boiling and single-phase and two-phase flow boiling heat transfer is presented in section 1.2. It indicates that several fundamental issues for pool boiling and heat transfer in small channels still exist.

1.3.1 Pool boiling heat transfer issue

The pool boiling phenomena have been extensively studied for atmospheric pressure and higher ones. Nevertheless, there are only a few experimental works which are focused on the transient pool boiling under sub-atmospheric pressures. The generalized mechanism for the pool boiling phenomenon under sub-atmospheric pressures still needs to be clarified.

1.3.2 Single-phase heat transfer issue

1.3.2.1 Steady state turbulent heat transfer issue

1) There is still disagreement among the researchers about if the conventional

empirical constants and correlations are available for small diameter channels.

2) The channel diameter at which departure from single phase conventional theory occurs is still not clear.

3) Some publications reported different dependence of Nusselt number on Reynold number in the fully developed turbulent regime.

4) Important parameters that might result in a deviation from the conventional theory should be confirmed.

Carefully designed and systematic experimental investigation is still necessary before final conclusions can be drawn.

1.3.2.2 Transient turbulent heat transfer issue

1) Many experimental studies of transient forced convection heat transfer were conducted with water or gas. There has been a lack of systematic experimental data on FC-72 flowing in tubes. FC-72 is ideal coolant for small channel cooling due to its low viscosity and low surface tension.

2) The transient phenomenon caused by exponentially increasing heat generation was investigated by few researchers and it is still not clarified. The effect of the period of heat generation rate on the transient heat transfer still need to be clarified.

3) For small channel heat transfer, the channel dimensions may play a role in

transient heat transfer process.

1.3.3 Flow boiling heat transfer issue

The most important issue in flow boiling is the flow boiling CHF mechanism. Although many CHF models have been proposed, they are valid under certain conditions. The HSN model proposed by Sakurai [10] for pool boiling is expected to explain the flow boiling CHF caused by exponentially increasing heat inputs.

1.4 Research Objectives

As discussed above, some of the heat transfer process is still unclear and need more research. Although the ultimate research objective is to study the flow boiling heat transfer and CHF in small diameter tubes, the study on pool boiling and single-phase heat transfer is also necessary. The knowledge of pool boiling and single-phase heat transfer could contribute to the understanding the flow boiling heat transfer process. As a result, the objectives of the current study include:

1) To design an experimental system elaborately to ensure the uncertainties in measurements at small channel dimension including geometrical dimensions and operating parameters to be minimized.

2) To obtain experimental data at various experimental conditions (velocities, inlet liquid temperatures, test tube geometries .etc).

3) To study the effect of flow parameters and tube geometries on the heat transfer process.

4) To evaluate and correlate the experimental data. Then discuss the physical mechanism for single-phase and flow boiling heat transfer in vertical small diameter tubes.

1.5 Outline of Current Thesis

The current thesis is organized as follows.

In Chapter 1, section 1.1 introduces the research background including the basic knowledge on boiling heat transfer. Section 1.2 presents a literature review on pool boiling and single-phase and flow boiling heat transfer. Section 1.3 and section 1.4 propose the research motivations and objectives based on the literature review in section 1.2. Finally the outline of the thesis is presented in section 1.5.

Chapter 2 presents a detailed description for the experimental apparatus, the test section, the test fluid, the data measurement, data reduction as well as uncertainty analysis. The apparatus for pool boiling tests and single-phase and two-phase flow

boiling experiments are introduced separately.

Chapter 3 presents and discusses the pool boiling heat transfer results. Section 3.1 introduces the experimental conditions. Section 3.2 describes the time dependence of pool boiling characteristics. The heat transfer coefficients in non-boiling region are discussed in section 3.3. Section 3.4 and 3.5 describe the steady state and transient pool boiling curve and the vapor behaviors. Finally the experimental results on steady state and transient pool boiling CHF are presented in section 3.6 and 3.7.

In chapter 4, the steady state and transient turbulent heat transfer results are presented in section 4.1 and section 4.2 separately. Firstly introduce the experimental conditions. Then describe the characteristics of heat input. The effects of flow parameters and tube geometries are discussed. Finally the steady state and transient turbulent heat transfer correlations are presented.

Chapter 5 presents the subcooled flow boiling heat transfer results. This chapter is organized as follows. Section 5.1 introduces the experimental conditions. Section 5.2 presents the heat transfer coefficient in non-boiling region. The time-dependency of boiling characteristics are described in section 5.3. Two kinds of transition from non-boiling region to film boiling are described in section 5.4. Section 5.5 presents the effect of velocity and subcooling on CHF. Section 5.6 discusses the transient CHF for

various periods.

Chapter 6 gives the conclusions on pool boiling heat transfer and single-phase and subcooled flow boiling heat transfer in vertical small diameter tubes.

References

[1] S. G. Kandlikar, and W. J. Grande, Evolution of microchannel flow passages – thermohydraulic performance and fabrication technology, Heat Transfer Eng., 24(1), (2003) 3–17.

[2] S. S. Mehendale, , A. M. Jacobi, , and R. K. Shah, , Fluid flow and heat transfer at micro- and meso-scales with applications to heat exchanger design, Appl. Mech. Rev., 53,(2000) 175–193.

[3] S. G. Kandlikar, heat tranfer and fluid flow in minichannels and microchannels, Elsevier Ltd, (2006).

[4] D. B. Tuckerman and R. F. W. Pease, "High performance heat sink for VLSI," IEEE Electron Dev. Lett., vol. EDL-2, no. 5, May (1981) 126–129.

[5] Bengt Sundén and Gongnan Xie, Thermal Analysis of Air-Cooled Electronic Units With Integrated Offset Strip-Fin Heat Sink, Journal of Electronic Packaging, Vol. 136-2 (2014).

[6] Colgan, E., et al., "A Practical Implementation of Silicon Microchannel Coolers for High Power Chips," Proceedings of 21st Semi Therm Symposium, San Jose, CA, (2005) 1-7.

[7] Kakac, S. and Liu, H., "Heat Exchangers: Selection, Rating and thermal Design,"

CRC Press, pp. 903-904, Chapter 9, 1998.

[8] Zuber N., , Hydrodynamic Aspects of Boiling Heat Transfer, AECU-4439, USAEC(1959).

[9] Sakurai, A., Shiotsu, M., Hata, K., New Transition Phenomena to Film Boiling due to Increasing Heat Inputs on a Solid Surface in Pressurized Liquids. In: Instability in Two Phase Flow Systems, vol. HTD-260:Fed-169, 1993, ASME, New York, 27–39.

[10] Sakurai, A. "Mechanism of Transitions to Film Boiling at CHFs in Subcooled and Pressurized Liquids Due To Steady and Increasing Heat Inputs", Nuclear Engineering and Design, Vol. 197, (2000) 301-356.

[11] Fukuda, K., Liu, Q., Park, J., and Kida, H. "Pool Boiling Critical Heat Flux of Highly Wetting Liquid", Journal of the JIME, Vol. 39 No. 10, (2004) 25-32

[12]Fukuda, K., Shiotsu, M., and Sakurai, A. "Effect of Surface Conditions on Critical Heat Fluxes for a Horizontal Cylinder in a Pool of Water at Pressures due to Exponentially Increasing Heat Inputs", Nuclear Engineering and Design, Vol. 200, (2000) 55-68.

[13] Park, J. "Subcooled Pool Boiling CHFs for Various Liquids due to Steady and Transient Heat Input", Ph.D Thesis, Graduate School of Science and Technology, Kobe University. (2006)

[14] P.F. SUTOPO, K. FUKUDA, Q. LIU, Direct Transition Phenomena in Pool Boiling of FC-72, J. Therm. Sci. Technol. 5 (2010) 206–221.

[15] P. Wu, W.A. Little, Measurement of friction factors for the flow of gases in very fine channels used for microminiature refrigerators, Cryogenics 24 (1983) 273–277.

[16] S.B. Choi, R.F. Barron, R.O. Warrington, Fluid flow and heat transfer in microtubes, in: Micromechanical Sensors, Actuators and Systems, ASME DSC, vol. 32, Atlanta, GA, (1991) 123–134.

[17] D. Yu, R.O. Warrington, R. Barron, T. Ameel, An Experimental and Theoretical Investigation of Fluid Flow and Heat Transfer in Microtubes, Proceedings of ASME/JSME Thermal Engineering Joint Conf., Maui, HI, 1995, 523–530.

[18] Peng, X.F., Wang, B.X., Forced Convection and Fluid Flow Boiling Heat Transfer for Liquid Flowing Through Microchannels, International Journal of Heat and Mass Transfer, Vol. 36, No. 14, (1993) 3421-3427.

[19] X.F. Peng, G.P. Peterson, The effect of thermofluid and geometrical parameters on convection of liquids through rectangular microchannels, Internat. J. Heat Mass Transfer 38 (1995) 755–758.

[20] R.E. Acosta, R.H. Muller, W.C. Tobias, Transport processes in narrow (Capillary) channels, AIChE J. 31 (1985) 473–482.

[21] T.M. Harms, M.J. Kazmierczak, F.M. Gerner, Developing convective heat transfer in deep rectangular microchannels, Internat. J. Heat Fluid Flow 20 (1999) 149–157.

[22] Adams, T., Abdel-Khalik, S. I., Jeter, S. M., and Qureshi, Z. H., An Experimental Investigation of Single-phase Forced Convection in Microchannels, International Journal of Heat and Mass Transfer, vol. 41, no. 6–7, (1998) 851–857.

[23] T.M. Adams, M.F. Dowling, S.I. Abdel-Khalik, S.M. Jeter, Applicability of traditional turbulent single phase forced convection correlations to non-circular microchannels, Internat. J. Heat Mass Transfer 42 (1999) 4411–4415.

[24]C.P. Tso, S.P. Mahulikar, Experimental verification of the role of Brinkman number in microchannels using local parameters, Internat. J. Heat Mass Transfer 43 (2000) 1837–1849.

[25] F. Debray, J.P. Franc, T.Maitre, S. Reynaud, Mesure des coefficient de transfert thermique par convection forcée en mini-canaux, Mec. Ind. 2 (2001) 443–454.

[26] S.G. Kandlikar, , S. Joshi, S. Tian, Effect of surface roughness on heat transfer and fluid flow characteristics at low Reynolds numbers in small diameter tubes, heat transfer engineering, 24(3) (2013), 4-16.

[27] W. Qu, I. Mudawar, Experimental and numerical study of pressure drop and heat transfer in a single-phase micro-channel heat sink, Internat. J. Heat Mass Transfer

45 (2002) 2549–2565.

[28] P-S. Lee, S. V. Garimella, and D. Liu, Investigation of Heat Transfer in Rectangular Microchannels, International Journal of Heat and Mass Transfer, vol. 48, no. 9, (2005) 1688–1704.

[29] Owahib, W., Palm, B., Experimental Investigation of Single-phase Convective Heat Transfer in Circular Micro Channels, Experimental Thermal and Fluid Science 28, (2004) 105–110.

[30] B. Agostini, A. Bontemps, B. Thonon, Effects of Geometrical and Thermophysical Parameters on Heat Transfer Measurements in Small Diameter Channels, Heat Transfer Engineering, 27, (2006) 14-24.

[31] S.G. kandlikar, microchannels and minichannels- History, Terminology, claffication asmd current research needs, 1st Int. Conf. on microchannels and minichannels, Rochester, N.Y., April 24-25 (2003).

[32] G. Gamrat, m. Favre-marinet, and S. Le Person, Modelling of roughness effects on heat transfer in thermally fully developed laminar flows through microchannels, Int. j. Thermo. Sci, 48 (2009) 2203-2214.

[33] B.X. Wang., X.F. Peng, Experimental investigation on liquid forced convection heat transfer through microchannels, Int. J. Heat Mass Transfer, Vol.37, (1994)

73-82.

[34] G.M. Mala, D. Li, J.D. Dale, Heat transfer and fluid flow in microchannels, Int. J. Heat Mass Transfer 40 (1997) 3079–3088.

[35] A. Boglietti, S. Member, A. Cavagnino, D. Staton, M. Shanel, M. Mueller, and C. Mejuto, Evolution and modern approaches for thermal analysis of electrical machines, IEEE Trans. Ind. Elect., 56(3), (2009) 871–882.

[36] Xiuqing Li, Renaud Le Pierres, Stephen John Dewson , Heat exchangers for the next generation of nuclear reactors, Proceedings of ICAPP ’06 Reno, NV USA, June 4-8, (2006).

[37] J. B. Garrison, Optimization of an integrated energy storage scheme for a dispatchable solar and wind powered energy system," Proceedings of the ASME 6th International Conference on Energy Sustainability, San Diego, CA, July 23–26, (2012).

[38] K. Bennion and M. Thornton, Integrated vehicle thermal management for advanced vehicle propulsion technologies : Integrated vehicle thermal management for advanced vehicle propulsion technologies, NREL report, (2010) 1–15.

[39] E. M. Sparrow, and R. Siegel, Thermal entrance rgion of a circular tube under transient heating conditions,” Third U. S. National Congress of Applied Mechanics,

(1958) 817–826.

[40] R. Siegel, , Heat transfer for laminar flow in ducts with arbitrary time variations in wall tempearture, Trans. ASME, 27(2), (1960) 241–249.

[41] M. Fakoor-Pakdaman, M. Ahmadi, M. Bahrami, Unsteady laminar forced-convective tube flow under dynamic time-dependent heat flux, J. Heat Transfer, 136, (2014) 041706-1-9.

[42] M. Fakoor-Pakdaman, M. Ahmadi, M. Bahrami, Temperature-aware time-varying convection over a duty cycle for a given system thermal-topology, Int. J. Heat Mass Transf. 87, (2015) 418–428.

[43] S. Kakaç, Transient forced convection heat transfer in a chnannel, Wärme- und Stoffübertragung, Vol. 1, (1968) 169-176.

[44] H. kawamura, Experimental and analytical study of transient heat tranfer for turbulent flow in a circular tube, int. J. heat Mass Tranfer, 20 (1977) 443-450.

[45] M. Soliman, H.A. Johnson, Transient heat transfer for forced convection flow over a flat plate of appreciable thermal capacity and containing an exponential timedependent heat source. Int. J. Heat Mass Transf 11(1), (1968) 27–38.

[46] I. Kataoka, A. Serizawa, A. Sakurai, Transient boiling heat transfer under forced convection. Int. J. Heat Mass Transfer 26(4), (1983) 583–595.

[47] Q. Liu, K. Fukuda, Transient heat transfer for forced convection flow of helium gas. JSME Int. J. Ser B 45(3), (2002) 559–564.

[48] Q. Liu, K. Fukuda,Z. Zheng, Theoretical and experimental studies on transient heat transfer for forced convection flow of helium gas over a horizontal cylinder. JSME Int. J. Ser B, (2006)。

[49] K. Hata, N. Kai, Y. Shirai, S. Masuzaki, Transient turbulent heat transfer for heating of water in a short vertical tube, J. Power Energy Syst. 5, (2011) 414–428.

[50] D.D. Hall, I. Mudawar, Critical heat flux (CHF) for water flow in tubes—I., Int. J. Heat Mass Transf. 43 (2000) 2573–2604.

[51] D.D. Hall, I. Mudawar, Critical heat flux (CHF) for water flow in tubes—II., Int. J. Heat Mass Transf. 43 (2000) 2605–2640.

[52] Peng X.F., Hu H.Y., Wang B.X., Boiling nucleation during liquid flow in microchannels, Int. J. Heat Mass Transfer 41 (1998) 101-106.

[53] Hapke I., Boye H., Schmidt J., Onset of nucleate boiling in minichannels, Int. J. Thermal Sciences 39 (2000) 505-513.

CHAPTER 2

Experimental Apparatus and Methods

A set of experimental apparatus was developed by Sakurai and Shiotsu [1] to investigate the steady and transient pool boiling phenomena under one atmosphere and sub-atmospheric pressures. It consists of test section assembly, measurement instruments, data acquisition and heat input control system and so on. To investigate single-phase and two-phase flow boiling heat transfer characteristics in small diameter tubes, this experimental apparatus was modified to be capable of testing a wide range of parameters such as tube inner diameter, heated length, flow rate, inlet liquid temperature as well as exponential period of exponentially increasing heat input. The measuring instruments were carefully calibrated and associated experimental uncertainties were thoroughly analyzed. Hence, the present facility can be utilized to provide important data necessary to understand single-phase and two-phase flow boiling heat transfer characteristics in small diameter tubes.

This chapter describes the experimental apparatus and method for pool boiling tests and single-phase and two-phase flow boiling experiments respectively.

2.1 Pool Boiling Experiments

The experimental apparatus for pool boiling at one atmosphere and sub-atmospheric pressures is presented in this section. Meanwhile, the methods for control of experimental conditions and data reduction are also described.

2.1.1 Pool boiling apparatus

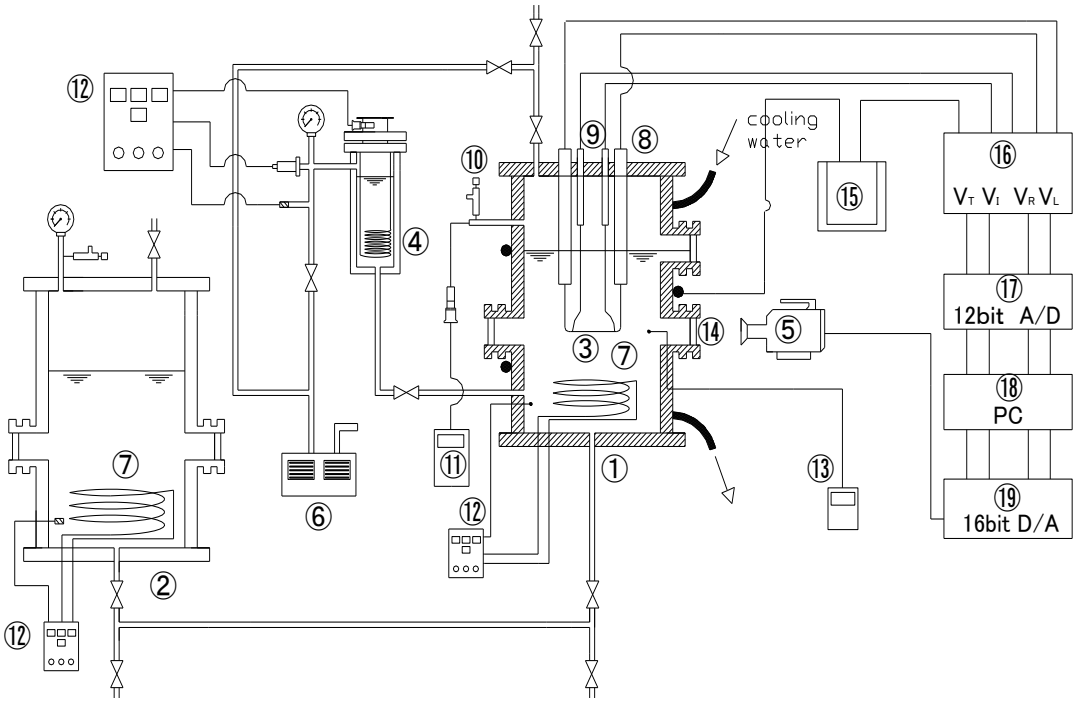

① Boiling vessel
② Auxiliary vessel
③ Test Heater
④ Pressurizer
⑤ High speed video camera
⑥ Vacuum pump
⑦ Sheathed Heater
⑧ Current conductor
⑨ Potential conductor
⑩ Pressure relief valve
⑪ Pressure gauge
⑫ Temperature controller
⑬ Digital voltmeter
⑭ Sight port
⑮ Heating system
⑯ Amplifier
⑰ A/D converter
⑱ Personal computer
⑲ D/A converter

Fig. 2.1 Schematic diagram of pool boiling apparatus

The experimental apparatus used to measure the steady and transient pool boiling phenomena is shown schematically in Fig. 2.1. Its details are also presented in the previous works [2, 3]. It mainly consists of a boiling vessel, a pressurizer, a feed water system, a heat input control and data reduction system. The boiling vessel with two sight ports is a cylindrical stainless steel pressure vessel of 20-cm inner diameter and 60-cm in height capable of withstanding pressure up to 5 MPa. The boiling vessel is connected with a liquid feed tank through pipe and valves. Two current conductors and two potential conductors are mounted at the upper side of the vessel and pass through the cylinder cover to support the test heater horizontally in the center of boiling vessel. The current conductors also pass direct current to heat the test heater. The vessel is equipped with a pressure transducer for measuring the system pressure. And a sheathed 1-mm diameter K-type thermocouple is placed near the test heater to measure the bulk liquid temperature. The liquid temperature in the boiling vessel is adjusted by a sheathed heater installed at downside of the vessel and the cooling water running through cylinder wall. The vessel is kept warm by micro heaters and thermal isolation with lagging materials. To achieve subcooling conditions, the pressurizer is used to keep a proper pressure corresponding to desired saturation temperature. A high speed video camera (1000FPS) is used to observe and record the bubble behaviors.

2.1.2 Test section

A platinum horizontal cylinder of 1.0 mm in diameter and 90 mm in length was used as the test heater to measure steady state and transient pool boiling phenomena as shown in Fig. 2.2. Two 50-μm diameter platinum wires were spot-welded as potential taps at around 20 mm from each end of the cylinder heater. The effective length of the heater between the two potential taps was 49.8 mm. The test heater was annealed to maintain the material at even properties. Its electrical resistance-temperature relation was measured in water baths with a precision double bridge circuit. The result is expressed by Eq. (2.1). The measuring accuracy was estimated to be within ±0.5 K. The test section is a Commercial Surface (CS) without any treatment or finish on the surface. However, to minimize possible dirt or solid carbons, they were cleaned with ethanol before mounted into the cylinder vessel.

$$R = R_0(1 + \alpha T + \beta T^2) \tag{2.1}$$

Where α and β are the resistance temperature coefficients. For the cylinder used in this study, α and β are determined as $\alpha=3.974603\times10^{-3}$ and $\beta=-0.5880\times10^{-6}$.

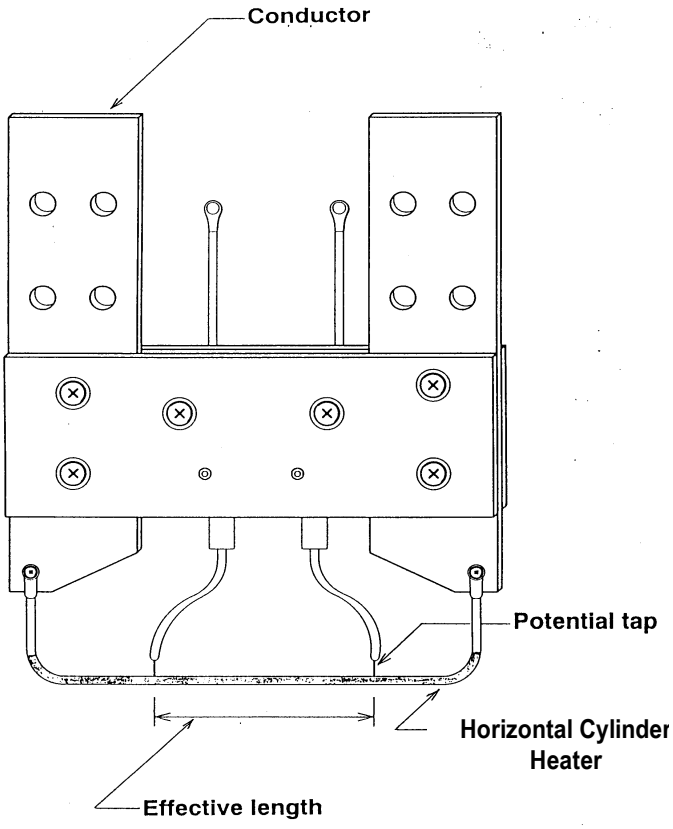

Fig. 2.2 Test Heater

2.1.3 Test fluid- water

Water has been used as one of the most popular coolants due to its advantages of high thermal conductivity, high heat capacity, low cost and so on. Water cooling has also several disadvantages like causing scale, corrosion and contamination. The properties of water are listed in Table 2.1 in comparison with FC-72. Pure water is adopted as the test fluid in the pool boiling experiments for comparison with previous research work with water, thus verifying the validation of experimental apparatus and methods.

Table 2.1 Properties of water and FC-72

Properties	FC-72	Water
Boiling point (1atm) [°C]	56	100
Liquid specific heat [kJ/(kg·K)]	1.1	4.19
Liquid density [kg/m^3]	1680	997
Latent heat of vaporization [J/g]	88	2257
Liquid thermal conductivity [W/(m·K)]	0.057	0.61
Surface tension [10^{-3}N/m]	10	72
Kinematic viscosity [$10^{-6}m^2/s$]	0.38	0.8926
Dynamic viscosity [centipoise]	0.64	0.89
Critical temperature [K]	176	374
Critical pressure [MPa]	1.83	22
Ozone depletion potential	0	0
Electrical resistivity [ohm·cm]	1.0×10^{15}	1.82×10^{7}

Note: All values determined at 25°C unless otherwise specified.

2.1.4 Experimental methods

2.1.4.1 Heat input and data acquisition system

The heat input control system is designed to supply exponentially increasing heat input, $Q_0 exp(t/\tau)$, to test section. Meanwhile, it also prevents real burnout of test section by means of interlock. The data acquisition system could take the voltage signals and send them to digital computer for further process.

The heat input and data acquisition system for pool boiling tests is essentially the same with that for single-phase and two-phase flow boiling experiments. Details are described in section 2.2.4.1.

2.1.4.2 Data reduction

The instantaneous average temperature of the test heater, T_a, was obtained by using double bridge circuit with aid of calibrated temperature resistance relation. The heat generation rate, Q, was calculated with the current measured with standard resistance and the voltage difference between two potential taps on the test heater.

The heat flux, q, is then obtained from the following heat balance equation for a given heat generation rate, Q:

$$q = \frac{1}{4} Q\, d - \frac{1}{4} c_h \rho_h d \frac{dT_a}{dt} \tag{2.2}$$

where, ρ_h, c_h, d, T_a, and t are density (kg/m^3), specific heat (kJ/(kg·K)), diameter

of cylinder (m), the average temperature of the test heater (K) and time (s), respectively.

The instantaneous surface temperature, $T_{s,}$ was obtained by solving the conduction equation Eq. (2.3) using a digital computer for a given heat generation rate with given surface heat flux as boundary conditions:

$$\frac{\partial T}{\partial t} = \alpha\left(\frac{\partial^2 T}{\partial^2 r} + \frac{1}{r}\frac{\partial T}{\partial r}\right) + \frac{Q}{\rho c} \tag{2.3}$$

where, α is thermal conductivity, W/(m·K). The boundary conditions are expressed as follows :

$$\frac{\partial T}{\partial r}\Big|_{r=0} = 0 \qquad -\lambda\frac{\partial T}{\partial r}\Big|_{r=R} = q \tag{2.4}$$

where, λ is thermal diffusivity, m^2/s.

The experimental error was estimated to be about ± 1 K in the heater surface temperature and $\pm 2\%$ in the heat flux.

2.1.4.3 Experimental procedure

Firstly, a boiling process for degassing of the liquid used in the experiment was performed at least for 30 minutes. Then, the liquid was fully filled in the boiling vessel with the free surface only in the pressurizer and liquid feed tank. Liquid temperatures and pressures in the boiling vessel and in the pressurizer were separately controlled to realize the desired saturated and subcooled conditions. The pressurizer is vacuumed to

achieve desired sub-atmospheric pressures. With the heat input exponentially increasing, the average heater surface temperature and heat flux were measured. A high-speed video camera system was used to observe the pool boiling phenomena and to confirm the start of boiling on the test heater surface. A video timer started simultaneously with the starting of measurement, and then the pool boiling phenomenon was recorded with the passage of time.

2.2 Single-phase and Two-phase Flow Boiling Experiments

This section begins with a description of the experimental apparatus, with special attention given to the measurement equipment and test sections. Then the working principle of the heat input and data acquisition system is explained. The calculation of the heat flux, the average temperature of test tube and the tube inner surface temperature are discussed next. A description of the experimental errors and uncertainties is also addressed. Finally the details of the experimental procedures are described.

2.2.1 Single-phase and two-phase flow boiling apparatus

The important components of the experimental apparatus used in the study of single-phase and two-phase flow boiling heat transfer are described. The measurement

of flow velocity, pressure and liquid temperature is also discussed.

2.2.1.1 Schematic diagram of experimental apparatus

The experimental apparatus used in study of single-phase and two phase flow boiling is schematically illustrated in Fig. 2.3. It is mainly composed of three primary subsystems: a flow loop section, a heat input control system and a data acquisition system. The flow loop was connected with 6.35-mm-diameter stainless steel tubes and Swagelok fittings, which could withstand system pressure up to 1 MPa. The liquid was circulated by a canned type non-seal pump through a previously evacuated loop shown with arrows. Upstream of the non-seal pump is a 440 μm filter which is used to prevent flow block from small particles. The flow rate was measured with a precision vortex flow meter which is located upstream of the test section. Fine adjustment of flow rate was accomplished by regulating the frequency of a three-phase alternating power source to the circulation pump with an inverter. The inlet temperature of the test section was maintained by adjusting the heat input to a preheater and cooling capacity of a cooler.

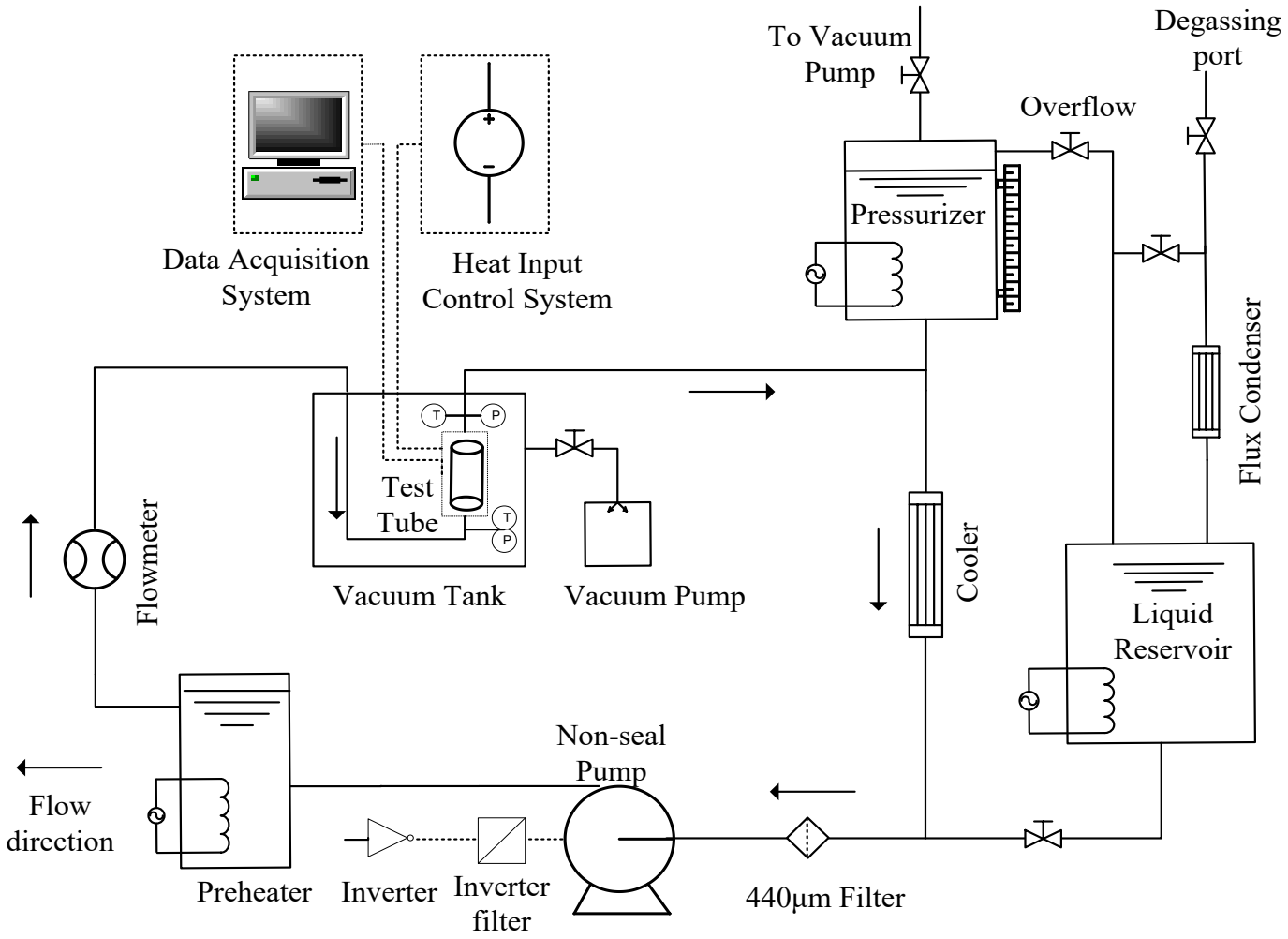

Fig. 2.3 Schematic diagram of single-phase and two-phase flow apparatus

The system pressure was established by saturated vapor in pressurizer and could be maintained within ±1 kPa of a desired value by utilizing the heater controller of the pressurizer. The test section was held in a vacuum tank so that the heat loss from test section to the surroundings could be minimized during adiabatic experiments. Two 1-mm-diameter K-type thermocouples were arranged at the inlet and outlet of the test tube to measure the inlet and outlet liquid temperatures. The inlet and outlet pressures were measured by two high quality strain gauge transducers (Kyowa PG-A), located at positions 40 mm upstream and 40 mm downstream from the tube inlet and outlet points. The pressure transducer has a rated capacity of 2MPa and a measurement accuracy of ±0.02%. The detailed measurement locations are shown in Fig. 2.6.

2.2.1.2 Non-seal pump

A canned type non-seal pump (Nikkiso HT21A) was used to circulate the liquid through the loop. The non-seal pump was employed because the Fluorinert liquid, FC-72, has very low surface tension and viscosity. Considering the very low contact angle on most surfaces, FC-72 will leak very easily through the smallest of passages. Seals which hold back water at 10+ atmospheres may leak generously with a fluorochemical fluid. Canned type pump is preferable because it is much less apt to leak. The pump used in this experiment could withstand high temperature up to 80℃ and

high pressure up to 2 MPa. The pump was cooled by the flow water around the pump chamber during operation. It also has a high head of delivery up to 20 m to accommodate the high pressure loss caused by small diameter flow channels.

2.2.1.3 Flow meter

A precise measurement of flow rate is necessary in this experiment. Gear flow meter and turbine flow meter cannot measure a low flow rate for FC-72 due to very low viscosity and surface tension of FC-72. Magnetic flow meter is also excluded because of dielectric characteristic of FC-72. Coriolis mass flow meter is not proper either because it would cause a relatively high pressure loss. A precision vortex type flowmeter (Kofloc FM01) was selected to measure the flow rate. Straight pipes with the same inner diameter of flow meter located upstream and downstream of the flow meter are required to avoid disturbance into the flow. Therefore, the straight length of 33 pipe diameters prior to the flow meter and a straight length of 10 pipe diameters at downstream of the flow meter were adapted. Meanwhile, those straight pipes were fixed to the pedestal to avoid vibration of flow meter. The volumetric flow meter has a range of 0.5-4 L/min and measurement accuracy of ±3%.

The mass flow rate is a constant through the complete loop. A temperature sensor just upstream from the flowmeter provided a means to determine fluid density and,

subsequently, the mass flow rate of the fluid. Then the inlet flow velocity can be calculated with Eq. (2.5).

$$u = \frac{4Q'\rho_0}{\pi\rho_{in}d^2} \tag{2.5}$$

where, ρ_0 is the density at the flow meter, kg/m^3, ρ_{in} is the density at the entrance of test tube, kg/m^3, Q' is the volumetric flow rate measured by vortex flow meter.

Table 2.2 shows the comparison of actual inlet velocity and velocity measured with vortex flow. The velocity differences caused by different densities at the flow meter position and inlet of test tube due to different temperatures (actual differences are less than 3℃) are less than 0.8% and can be negligible for liquid temperature of 20-70℃ and flow rate range less than 2.7 L/min. Therefore, the velocity measured directly by the vortex flowmeter was adopted as flow velocity in this experiment.

The relation between voltage signal and flow rate for the vortex flow meter was calibrated and the result is shown in Fig. 2.4. The variation of voltage against flow rate shows a perfect linear relation in the range of 0.3 - 2.7 L/min (the desired flow rate range in this experiment). It is expressed as follows:

FC-72						Temp in -corrected	Temp in -corrected		Temp in -corrected
Measured FM	FM	Measured FM	Estimated-TEST in	MASS	DT(FM-TEST)	Measured TEST in	TEST in	Estimated TEST in	TEST	Estimated TEST in
temp(1)	density(kg/m3)	flow(L/min)	velocity(m/s)	kg/s	Temp difference =(1)-(2)	temp(2)	density	flow(L/min)	dia(mm)	velocity(m/s)
20	1720.2	10	23.6	0.28669	5	15	1735.9	9.9	3	23.4
30	1690.5	10	23.6	0.28175	5	25	1705.1	9.9	3	23.4
40	1661.8	10	23.6	0.27696	5	35	1676.1	9.9	3	23.4
50	1632.6	10	23.6	0.27209	5	45	1647.3	9.9	3	23.4
60	1601.6	10	23.6	0.26694	5	55	1617.4	9.9	3	23.3
70	1567.9	10	23.6	0.26132	5	65	1585.2	9.9	3	23.3
20	1720.2	5	11.8	0.14335	5	15	1735.9	5.0	3	11.7
30	1690.5	5	11.8	0.14087	5	25	1705.1	5.0	3	11.7
40	1661.8	5	11.8	0.13848	5	35	1676.1	5.0	3	11.7
50	1632.6	5	11.8	0.13605	5	45	1647.3	5.0	3	11.7
60	1601.6	5	11.8	0.13347	5	55	1617.4	5.0	3	11.7
70	1567.9	5	11.8	0.13066	5	65	1585.2	4.9	3	11.7
20	1720.2	30	70.7	0.86008	5	15	1735.9	29.7	3	70.1
30	1690.5	30	70.7	0.84525	5	25	1705.1	29.7	3	70.1
40	1661.8	30	70.7	0.83089	5	35	1676.1	29.7	3	70.1
50	1632.6	30	70.7	0.81628	5	45	1647.3	29.7	3	70.1
60	1601.6	30	70.7	0.80082	5	55	1617.4	29.7	3	70.0
70	1567.9	30	70.7	0.78397	5	65	1585.2	29.7	3	70.0
20	1720.2	10	23.6	0.28669	10	10	1752.4	9.8	3	23.1
30	1690.5	10	23.6	0.28175	10	20	1720.2	9.8	3	23.2
40	1661.8	10	23.6	0.27696	10	30	1690.5	9.8	3	23.2
50	1632.6	10	23.6	0.27209	10	40	1661.8	9.8	3	23.2
60	1601.6	10	23.6	0.26694	10	50	1632.6	9.8	3	23.1
70	1567.9	10	23.6	0.26132	10	60	1601.6	9.8	3	23.1
20	1720.2	5	11.8	0.14335	10	10	1752.4	4.9	3	11.6
30	1690.5	5	11.8	0.14087	10	20	1720.2	4.9	3	11.6
40	1661.8	5	11.8	0.13848	10	30	1690.5	4.9	3	11.6
50	1632.6	5	11.8	0.13605	10	40	1661.8	4.9	3	11.6
60	1601.6	5	11.8	0.13347	10	50	1632.6	4.9	3	11.6
70	1567.9	5	11.8	0.13066	10	60	1601.6	4.9	3	11.5
20	1720.2	30	70.7	0.86008	10	10	1752.4	29.4	3	69.4
30	1690.5	30	70.7	0.84525	10	20	1720.2	29.5	3	69.5
40	1661.8	30	70.7	0.83089	10	30	1690.5	29.5	3	69.5
50	1632.6	30	70.7	0.81628	10	40	1661.8	29.5	3	69.5
60	1601.6	30	70.7	0.80082	10	50	1632.6	29.4	3	69.4
70	1567.9	30	70.7	0.78397	10	60	1601.6	29.4	3	69.2

Table 2.2 Comparison of inlet velocity and velocity measured with vortex flowmeter

$$V' = (0.79112 + 0.807Q') \times 10^{-3} \quad (2.6)$$

where, V' is the voltage signal, V, and Q' is the flow rate, L/min.

The corresponding voltage signal would be amplified and sent to computer for calculating flow velocity during the experiments.

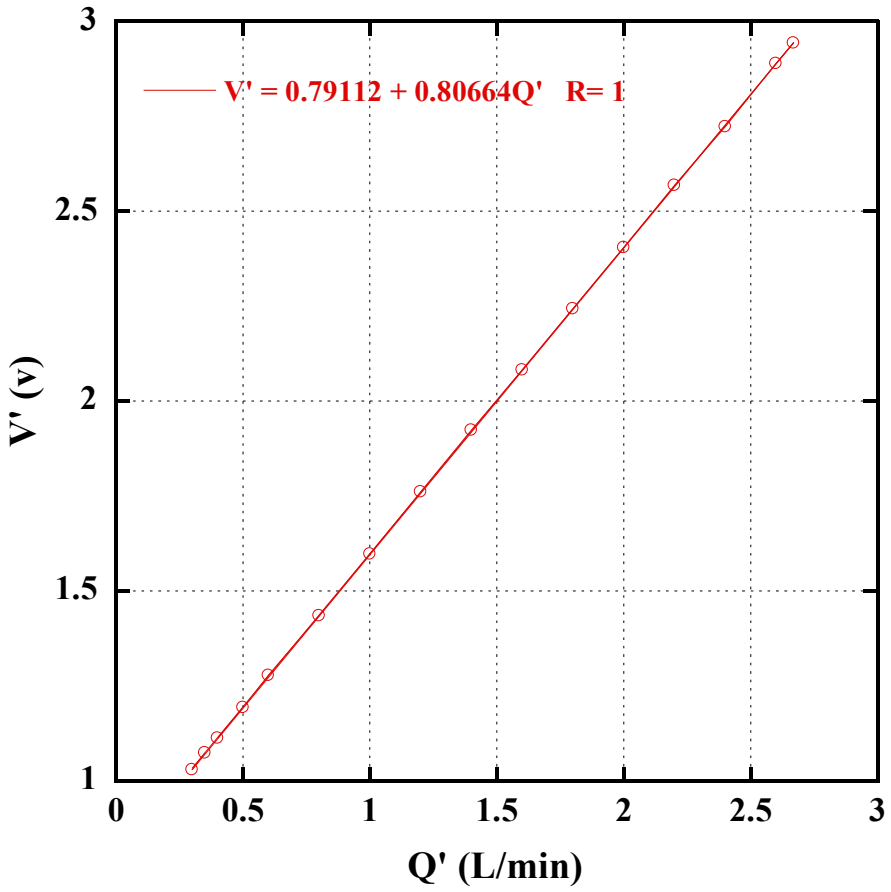

Fig. 2.4 The relation of voltage signal and flow rate for the vortex flow meter

2.2.1.4 Inverter and filter

An inverter (Hitachi, WJ200) was set to regulate the frequency of a three-phase alternating power source to the circulation pump, thereby providing a means for fine

adjustment of flow velocity. The inverter could operate from frequency of 0.5 Hz, which makes a low flow rate condition possible.

However, the inverter caused some noises including conductive noise, inductive noise and radiated noise. There noises would interfere with other sensitive electronic loads, especially the Wheatstone bridge and Kelvin double bridge circuit. Proper grounding was performed to reduce the impact from the noises. In addition, Hitachi NF-L20 filter and ACF-C25 filter were installed at the input and output sides of inverter to minimize noises.

2.2.1.5 Preheater and cooler

The preheater is a liquid vessel with a sheathed heater installed in the lower portion. The vessel was thermally isolated with lagging materials. The liquid temperature in the preheater was adjusted by a PID controller.

The cooler is a double-pipe heat exchanger with counter flow of coolant. The coolant was circulated through a TRL N135 type low temperature cryostat with cooling capacity up to -40°C.

2.2.1.6 Pressurizer

The pressurizer can be activated as follows. Firstly fill liquid in the pressurizer completely. Engage the heater in the lower portion to heat the liquid to the desired

temperature. Then partially drain the liquid and vapor mixture to create a vapor void at the top of the vessel. A liquid level indicator was equipped to determine the liquid level in pressurizer. Liquid temperature determined the pressure developed in the vapor space. The pressure could be adjusted and maintained within ±1 kPa of a desired value.

2.2.1.7 Vacuum pump

A diaphragm vacuum pump (Ulvac, DA-120S) was used to vacuum the flow loop. At the beginning of the experiment, the FC-72 in the storage tank was heated over saturation temperature to establish a high pressure. Meanwhile, the flow loop was evacuated with the pump to -80 kPa. Then the liquid was forced into the loop by the pressure difference between the liquid storage tank and flow loop.

2.2.1.8 Thermocouple

Two1-mm-diameter K-type (NiCr-Al) thermocouples were connected with the test section through standard compression fittings. The type K was selected because it's inexpensive, accurate, reliable, and has a wide temperature range. Before installation, the exact voltage-temperature relation of each thermocouple was calibrated by placing the thermocouple probe in a temperature controlled water bath for better measurement accuracy. A motor fan was used to ensure the bath temperature to be uniform. The bath

temperature was measured by using a precision temperature instrument with a PT 100 sensor (Testo 735-2). It has a measurement accuracy of ±0.05℃. The measured data within 20-100℃ was calibrated together with the JIS reference data of 100-200℃. One of the calibration results is shown in Fig. 2.5.

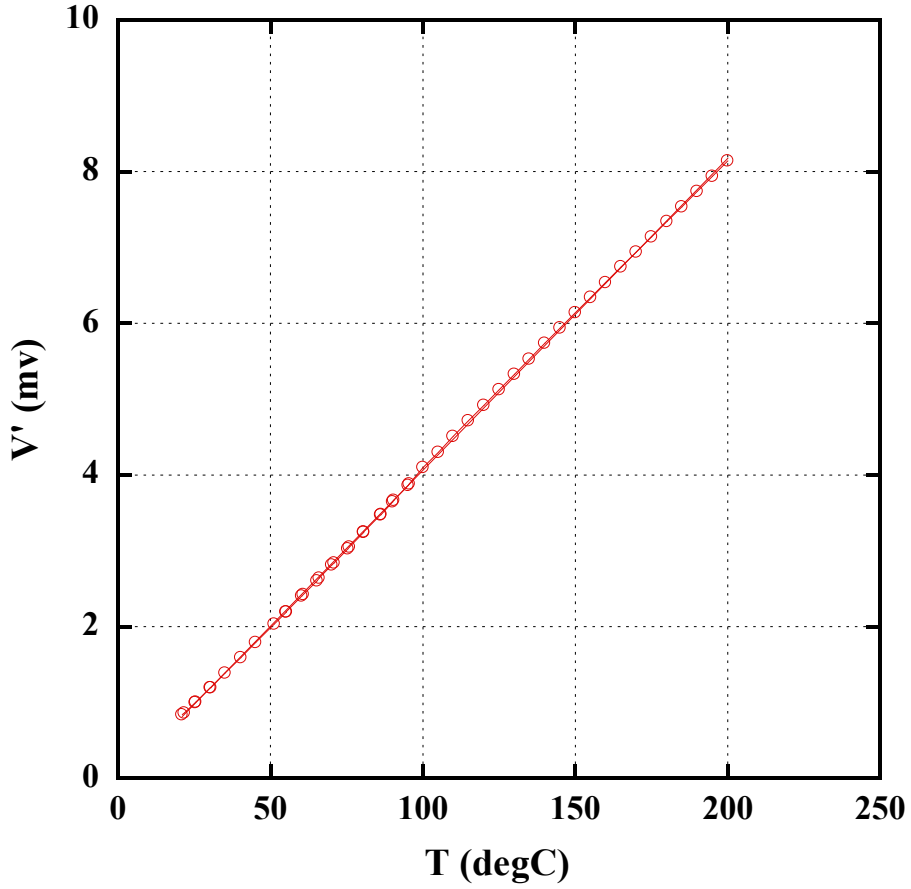

Fig. 2.5 Calibration result of the thermocouple for measuring outlet temperature

The calibration results for thermocouples used to measure inlet and outlet liquid temperature are expressed as Eq. (2.7) and Eq. (2.8), respectively. The computer read

the voltage signals to record corresponding temperatures.

$$V' = -0.0859 \times 10^{-3}(1 - 0.486T + 2.5285 \times 10^{-5} T) \quad (2.7)$$

$$V' = -0.0792 \times 10^{-3}(1 - 0.527T + 3.2745 \times 10^{-5} T) \quad (2.8)$$

where, V' is the voltage signal, V, and T is the temperature, ℃.

2.2.2 Test Section

This section describes the structure and dimension of the test section used in single-phase and two-phase flow boiling experiments. The calibration of test section is also introduced. The entrance effect is discussed for the relatively short test tubes.

2.2.2.1 Structure and dimension of test section

The structure and dimensions of the test section assembly are shown in Fig. 2.6. The test heaters used in this study were circular tubes made of SUS304. The physical properties of SUS304 are listed in Table 2.2. The test tubes have inner diameters, d, of 1, 1.8 and 2.8 mm, wall thickness, δ, of 0.5 mm, heated lengths, L, around 30, 40 and 50 mm, and a commercial finish inner surface condition as tabulated in Table 2.4.

The heated length of the test section is the vertical length between the electrode connections. It was measured using Vernier caliper with accuracy of ±0.01mm. The inner diameter of the investigated tubes, d, was calculated through measuring the outer

diameter, d_o (m), length, L (m), and mass, m (kg) of each tube. The length and outer diameter were measured using a Vernier Caliper with an uncertainty of ± 0.01mm while the mass was measured using an electronic analytical scale (Shimadzu Libror Aeg-320g) with error less than 0.1 mg. The inner diameter was calculated as follows:

$$d = \sqrt{d_o^{\,2} - \frac{4m}{\pi \rho L}} \tag{2.9}$$

The commercial SUS304 tube has a maximum division of 0.5% for d = 2.8 mm, 2.5% for d = 1.8 mm and 3.5% for d = 1 mm from the nominal inner diameter.

The test tube was soldered to copper plates at each end. Solder joints with very low resistance provided a good seal between the test tube and the copper plates under high pressure and high temperature. The copper plates served as electrodes to provide a resistance free path for introducing direct current from the power source to the test tube. Protective Bakelite blocks were used to avoid mechanical vibrations or distortion of the small diameter test tube. The Bakelite plates insulated the test tube from the loop both electrically and thermally. Gaskets were used as a high pressure seal between the copper plates, insulating Bakelite plates and SUS304 instrumentation blocks. All the plates and blocks were clamped together with four steel bolts. In order to secure electrical and thermal isolation between the bolts and copper plates, PTFE sleeves were used to separate them from each other. The SUS304 instrumentation blocks provided a

convenient connection of thermocouples and pressure transducers using standard compression fittings.

Table 2.3 Physical properties of SUS304

Density [g/cm³]	8.03
Melting point [°C]	1399-1454
Specific heat [kJ/(kg·K)]	0.5
Electrical resistivity [mΩ·m] (@20°C)	72
Thermal conductivity [W/(m.K)] (@100°C)	16.2
Thermal expansion coefficient [μm/m°C] (0-315°C)	17.3

Table 2.4 Sizes of test tubes

d (mm)	*L* (mm)	*L*/*d* ratio	*δ* (mm)
1	31.1, 40, 50	31.1, 40, 50	0.5
1.8	30.1, 40.2, 49.9	16.7, 22.3, 27.7	0.5
2.8	31.3, 40.5, 50.2	11.2, 14.5, 17.9	0.5

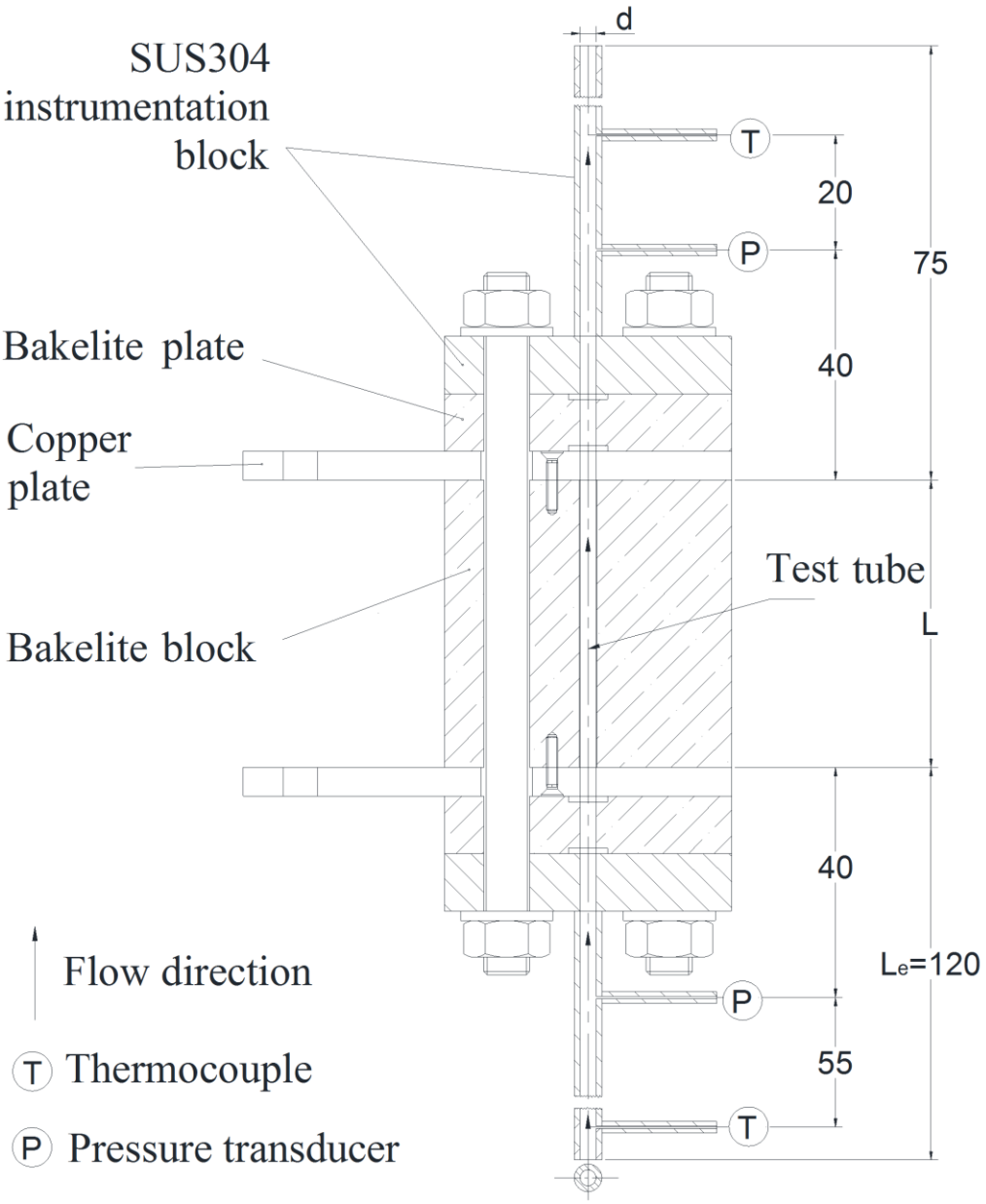

Fig. 2.6 Cross-sectional view of test section

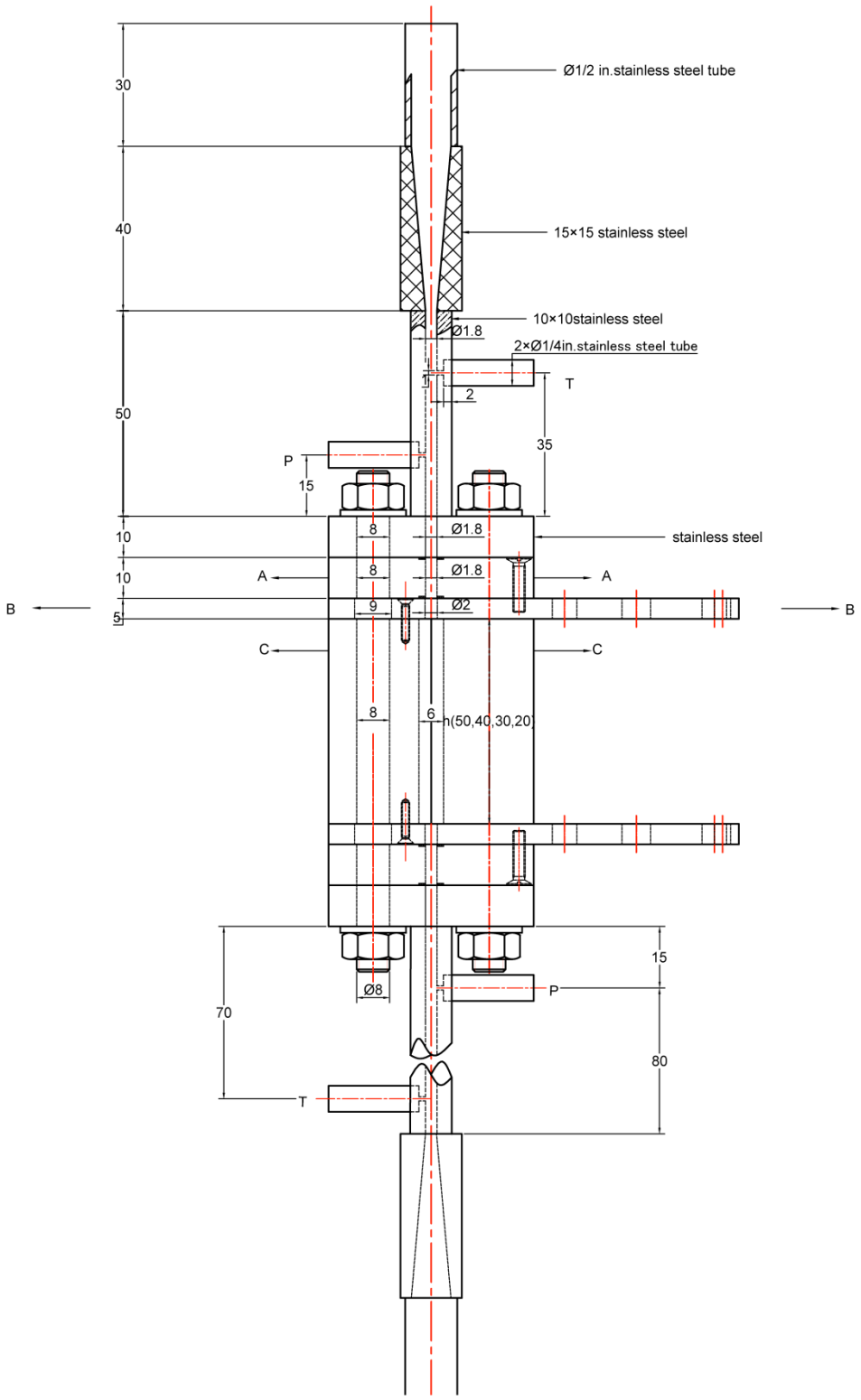

Fig. 2.7 Dimensions of test section (example of d = 1.8 mm)

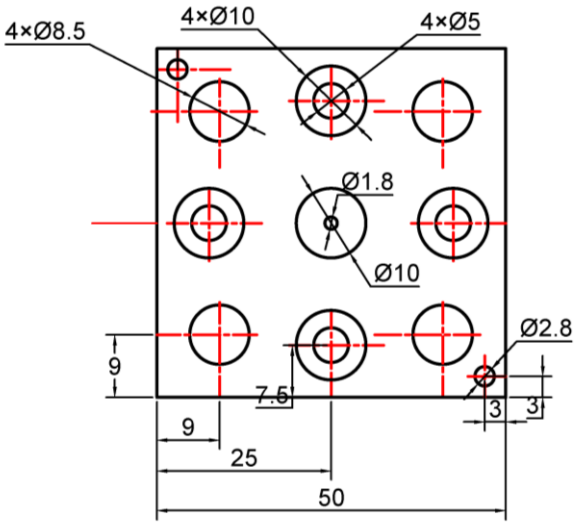

Fig. 2.9 A-A Bakelite plate

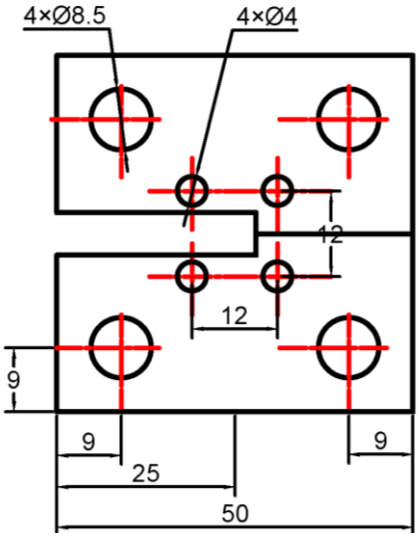

Fig. 2.8 C-C Bakelite block

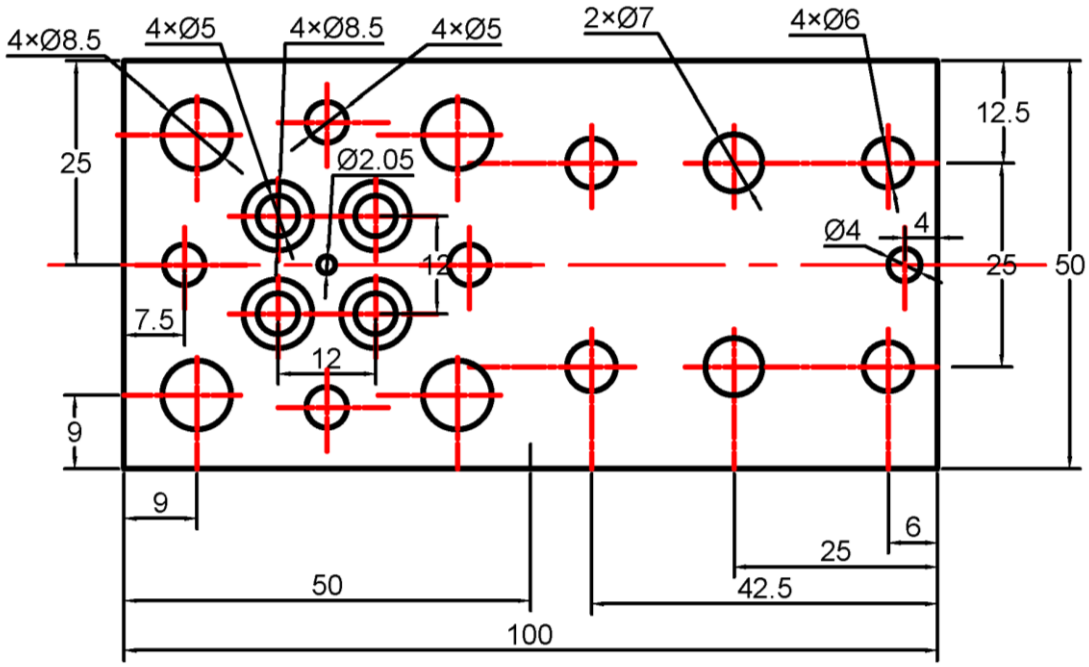

Fig. 2.10 B-B copper plate

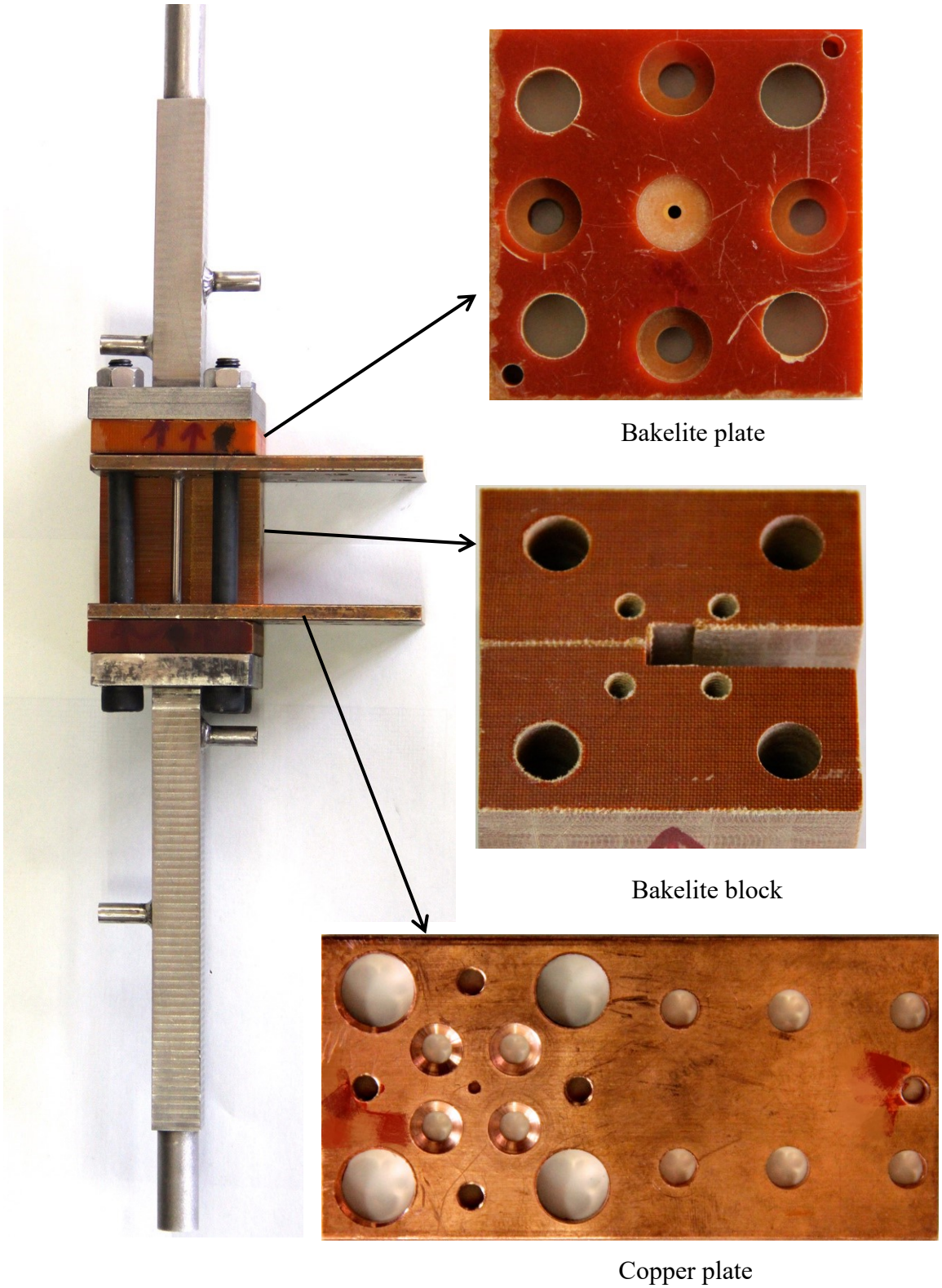

Fig. 2.11 Photos of test section, Bakelite plate, Bakelite block and copper plate

The detailed dimensions of the test section are shown in Fig. 2.7 to Fig. 2.10. Figure 2.11 shows the photos of test section, Bakelite plate, Bakelite block and copper plate. The test section was designed and machined to ensure a fully developed turbulent flow in the test tube without leak, provide a mean of heating the test tube uniformly, and facilitate the installation of measurement instruments.

2.2.2.2 Calibration of test tube

A precision double bridge was used to calibrate the relationship between electric resistance and temperature of the test tube. The relationship is expressed in the following form:

$$R = R_0(1 + aT_a + bT_a^2) \tag{2.10}$$

where, T_a is the average temperature of test tube; R is the measured resistance at temperature of T_a; a and b are temperature coefficients. The resistance-temperature relations for test tube used in the study of steady and transient turbulent heat transfer are shown as follows:

$$R = 6.8244\times(1+1.1468\times10^{-3}T - 5.668\times10^{-7}T^2) \text{ for } d\text{=2.8 mm, } L\text{=50.2 mm} \tag{2.11}$$

$$R = 4.2512\times(1+1.1755\times10^{-3}T - 5.668\times10^{-7}T^2) \text{ for } d\text{= 2.8mm, } L\text{=31.3 mm} \tag{2.12}$$

$$R = 5.4902 \times (1 + 1.1913 \times 10^{-3} T - 5.668 \times 10^{-7} T^2) \text{ for } d\text{= 2.8mm, } L\text{=40.5 mm} \quad (2.13)$$

$$R = 5.86 \times (1 + 1.2353 \times 10^{-3} T - 5.668 \times 10^{-7} T^2) \quad \text{for } d\text{= 1.8mm, } L\text{=30.1 mm} \quad (2.14)$$

$$R = 7.8263 \times (1 + 1.25 \times 10^{-3} T - 5.668 \times 10^{-7} T^2) \text{ for } d\text{= 1.8mm, } L\text{=40.2 mm} \quad (2.15)$$

$$R = 9.7042 \times (1 + 1.2071 \times 10^{-3} T - 5.668 \times 10^{-7} T^2) \text{ for } d\text{= 1.8mm, } L\text{=49.9 mm} \quad (2.16)$$

$$R = 8.5939 \times (1 + 1.3161 \times 10^{-3} T - 5.668 \times 10^{-7} T^2) \text{ for } d\text{= 1 mm, } L\text{=31.1 mm} \quad (2.17)$$

$$R = 11.407 \times (1 + 1.301 \times 10^{-3} T - 5.668 \times 10^{-7} T^2) \text{ for } d\text{= 1 mm, } L\text{=40 mm} \quad (2.18)$$

$$R = 14.278 \times (1 + 1.2838 \times 10^{-3} T - 5.668 \times 10^{-7} T^2) \text{ for } d\text{= 1 mm, } L\text{=50 mm} \quad (2.19)$$

The resistance-temperature relation for test tube used in the study of two-phase flow boiling heat transfer is shown in Eq. (20)

$$R = 5.1027 \times (1 + 1.2579 \times 10^{-3} T - 5.668 \times 10^{-7} T^2) \text{ for } d\text{= 1.8 mm, } L\text{=26.2 mm} \quad (2.20)$$

The case for test tube with *d* of 1.8 mm and *L* of 30.1 mm is plotted in Fig. 2.12. As shown in this figure, the variations of resistance against temperature show a good linear relation in the range of 20-70℃.

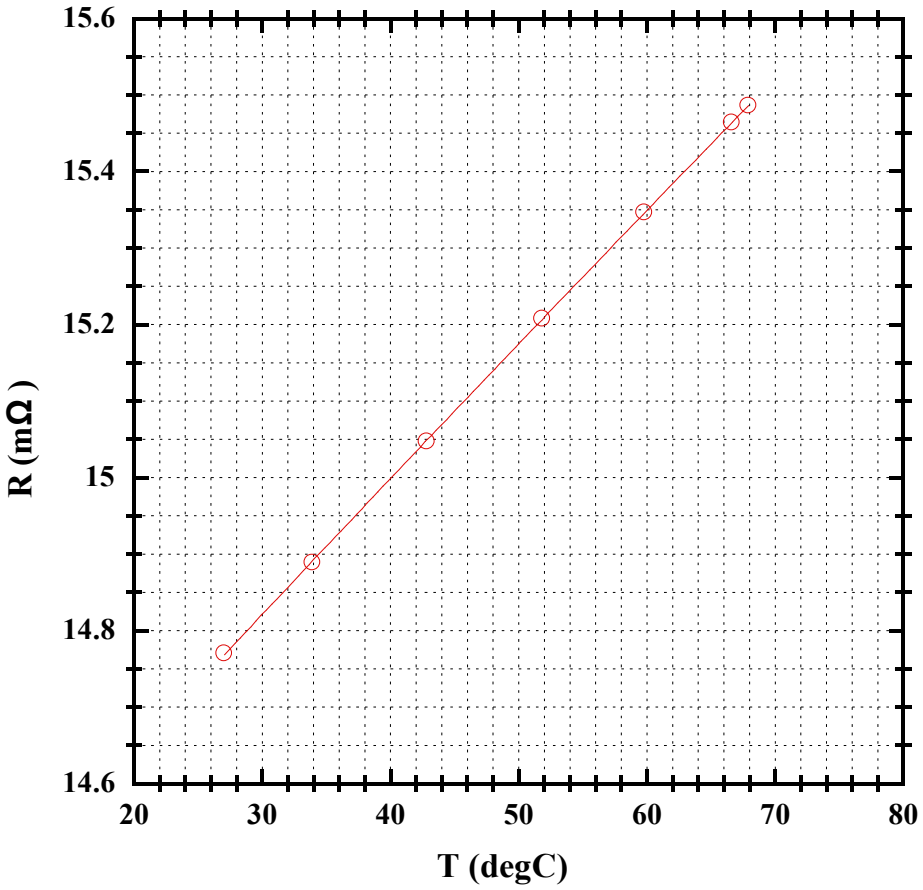

Fig. 2.12 Resistance-temperature relation for tube of *d*=1 mm and *L*=50 mm

2.2.2.3 Entrance effect

Since the lengths of test tube used in this study were relatively short (about 30-50 mm), if the entrance effect has an influence on the turbulent heat transfer process or not should be clarified. In another word, if the liquid flowing in the tube is in fully developed hydrodynamic and thermal conditions should be confirmed.

The test section was vertically oriented along the centerline of the flow channel with liquid flowing upward. Before entering the test tube, the liquid flows through an entrance region which has the same diameter as the inner diameter of the test tube to create a fully developed turbulent flow. In this study, the entrance region length, L_e, was given as 120 mm (L_e/d=120, 66.7 and 42.8 for d=1, 1.8 and 2.8 mm, respectively), which was assumed to be sufficient to secure fully developed hydrodynamic conditions according to the well-accepted correlation [4] as follows:

$$L_e/d = 4.4\,\mathrm{Re}^{1/6} \tag{2.21}$$

On the other hand, Kays [5] proposed that the entrance length only depend on inner diameter as Eq. (2.22). Therefore, the entrance region adopted in the experiment (L_e/d=120, 66.7 and 42.8 for d=1, 1.8 and 2.8 mm, respectively) is enough to ensure a fully developed turbulent flow.

$$10 \le L_e/d \le 60 \tag{2.22}$$

As to the thermal entrance region, Kays [7] has computed the influence of entrance region on turbulent heat transfer for several values of Reynolds number, Re, and Prandtl number, Pr, as shown in Fig. 2.13. The ordinate is the ratio of the local Nusselt number, $Nu_d(x)$, to that for fully developed thermal conditions, $Nu_{d,st}$. In general, the higher the Pr, the shorter the entrance length; the lower the Re, the shorter the entrance length. The

ranges of Re_d and Pr in this experimental study were 23,400 to 81,800 and 8.4 to 10.8, respectively. The L/d ratios for the test tube used in this study were from 11.2 to 50. As shown in this figure, the thermal entrance region will affect the convective heat transfer more or less within the ranges of experimental conditions. Therefore, the thermal entrance effect will be discussed later.

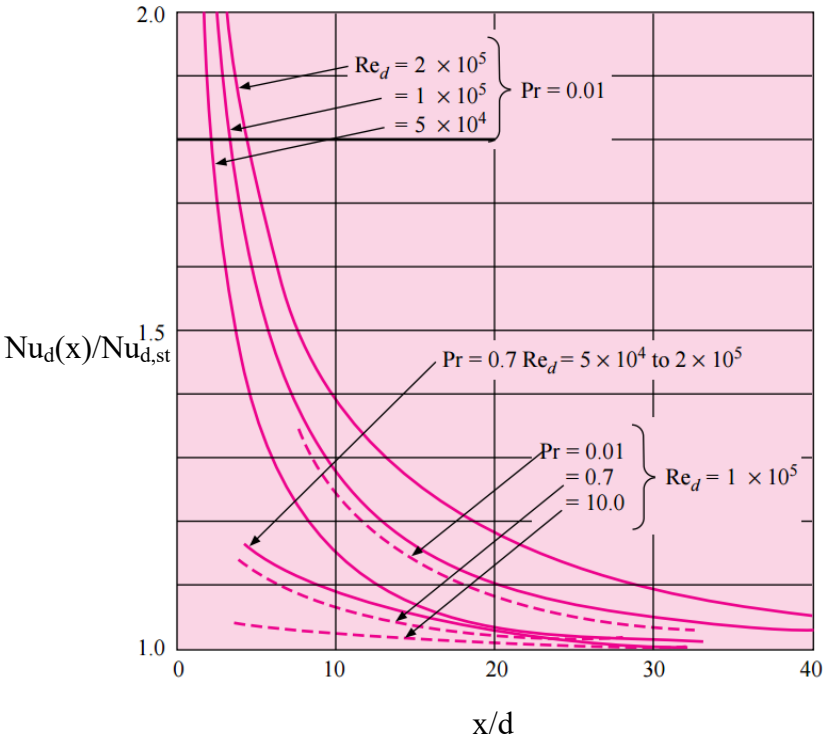

Fig. 2.13 Turbulent Nusselt number at the thermal entrance of circular tube for constant heat flux

2.2.3 Test Fluid – FC-72

3M™ Fluorinert liquid, FC-72, is a clear, colorless, fully-fluorinated liquid. Fluorinert liquid FC-72 is thermally and chemically stable, compatible with sensitive

materials including metal, plastics and elastomers, nonflammable, practically nontoxic and friendly to the environment [7]. The properties of FC-72 are shown in Table 2.1 in comparison with normal coolant, water. FC-72 has high thermal conductivity, high latent heat of vaporization, low viscosity and super dielectric characteristics. The excellent low temperature viscosity makes it works well in low temperature heat transfer applications. Its higher dielectric constant means that it would not damage electronic equipment in case of a leak or other failure. The low viscosity and surface tension are critically required for the single phase and two-phase heat transfer in small sized channels. Those properties make FC-72 ideal for direct contact single and two-phase cooling of many electronics applications, especially the compact and ultra-compact structures. FC-72 is also used in testing of power electronics and other electronic applications.

The following formulas were used to calculate the specific heat, thermal conductivity density and saturation presssure of 3M™ Fluorinert, FC-72 at various temperatures, T(℃).

Specific heat at constant pressure, c_p (J/(kg·℃)):

$$c_p = 1014 + 1.554T \tag{2.23}$$

Thermal conductivity, λ (W/(m·℃)):

$$\lambda = 0.06 - 0.00011T \tag{2.24}$$

Liquid density, ρ (kg/m^3):

$$\rho = 1740 - 2.61T \tag{2.25}$$

Saturation pressure, P_{sat} (pascals):

$$\log_{10} P_{sat} = 9.729 - 1562/(T + 273.15) \tag{2.26}$$

2.2.4 Experimental methods

The heat input and data acquisition system are described in this section. The calculation scheme for the derived quantities is also explained. The associated experimental errors and uncertainties are discussed next. Finally, the experimental procedures are presented in detail.

2.2.4.1 Heat input and data acquisition system

Figure 2.14 illustrates a block diagram of the heat input and data acquisition system which is essentially the same as in experiments performed by Sakurai [8] and Fukuda [9]. Power cables from a fast response DC power supply with capacity of 1100 A and 15 V were connected with copper electrodes to pass direct current to heat the test tube. For the DC power supply, the constant-voltage (CV) mode regulation is 4.75 mV; CV mode ripple is 500 μV r.m.s and the CV mode transient response time is less than 200 μsec.

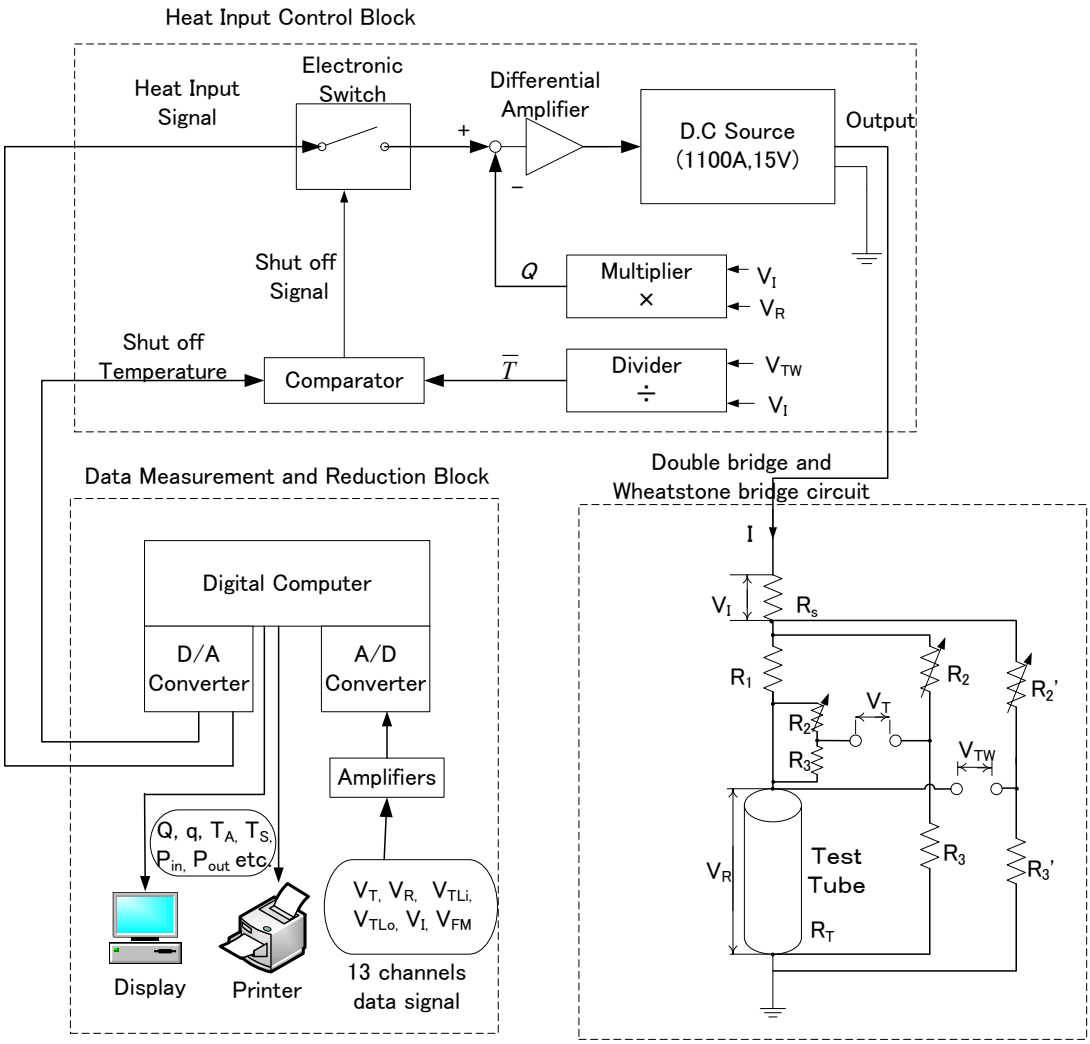

Fig. 2.14 Power supply and data acquisition system

The electrical resistance of the test tube was much smaller than the remainder of the electrical paths. Therefore, the overwhelming majority of the current was used to heat the test tube. The heat generation rate of the test tube was increased with a function of $Q=Q_0 exp(t/\tau)$. The heat input control was achieved as follows.

The signal of exponentially increasing heat input with a certain period (a lower period means a higher heat generation rate) was sent to the heat input control block through digital to analog (D/A) converter. Then the low-voltage power supply was used for heating the test heater. Meanwhile, the voltage signals including voltages of velocity and temperatures and output voltages of Wheatstone bridge and Kelvin double bridge were amplified and fed back to the computer through an analog to digital (A/D) converter. Subsequently, the data including heat flux, heat generation rate, and average temperature of test heater and so on were calculated. The calculated instantaneous heat generation rate in the test tube was always compared with the heat input signal to ensure the two values are equal. Moreover, once the test heater instantaneous average temperature calculated by Wheatstone bridge exceeded the preset value, the heat input is cut off immediately to prevent real burnout of test heater. The working principle of Wheatstone is explained in detail in Appendix A.2.

2.2.4.2 Data reduction

The measured and reduced quantities are the instantaneous heat generation rate, $Q(t)$, the instantaneous average temperature of the test heater, $T_a(t)$, the instantaneous surface heat flux, $q(t)$, the instantaneous tube inner surface temperature, $T_s(t)$, the inlet and outlet pressures for the test tube, P_{in} and P_{out}, and the bulk liquid temperature, T_L. The

calculation scheme for the above quantities is described as follows.

a) the instantaneous heat generation rate, $Q(t)$

Since R_1=8.5115mΩ, R_T≈12mΩ, R_2=R_3=2000Ω, the branch current through R_2 and R_3 could be negligible. The current through test tube is almost the same with the total current, I (=V_I/R_s) measured with standard resistance. Therefore, the instantaneous heat generation rate, $Q(t)$, for the test tube was calculated from the measured voltage differences between the two ends of the test tube and the current measured using Manganin standard resistance as shown by the next expression.

$$Q(t) = V_R(t)\frac{V_I(t)}{R_S} \tag{2.27}$$

b) the instantaneous average temperature of the test heater, $T_a(t)$

The instantaneous average temperature of the test heater, $T_a(t)$, was measured by means of resistance thermometry using the test tube itself as a branch of a double bridge circuit. A Kelvin double bridge is a variant of the Wheatstone bridge used for measuring very low resistances. It is employed for avoiding errors otherwise incurred by stray resistances along the current path between the low-resistance standard and the resistance

being measured. The working principle of the Kelvin double bridge is described in Appendix A.2.

The unbalanced voltage of the double bridge circuit, $V_T(t)$, was generated by change of the tube resistance due to its temperature variation. $V_T(t)$ is expressed as follows.

$$V_T(t) = \frac{I(t)\left[R_2 R_T(t) - R_1 R_3\right]}{R_2 + R_3} \tag{2.28}$$

The unbalanced voltages of the double bridge circuit, $V_T(t)$, together with the voltage drops across the electrodes of the test section, $V_R(t)$, and that across a standard resistance, $V_I(t)$, were amplified and sent to a digital computer through a 16 bit analog to digital (A/D) converter. All these voltage signals were simultaneously sampled at a desired time interval by the A/D converter. The fastest sampling speed was 1 μs/channel. The average temperature was obtained by means of the previously calibrated resistance-temperature relation in the following form.

$$R_T(t) = a(1 + bT_a(t) + cT_a(t)^2) \tag{2.29}$$

c) the instantaneous surface heat flux, $q(t)$

The instantaneous surface heat flux, $q(t)$, was then obtained from the following heat balance equation for a given heat generation rate. $q(t)$ means the difference between the heat generation rate per unit surface area and the change rate of energy storage in the

test tube obtained from the faired average temperature versus time curve.

$$q(t)=\frac{V}{S}\left[Q(t)-\rho c\frac{dT_a(t)}{dt}\right] \tag{2.30}$$

where, ρ, c, V and S are the density (kg/m^3), specific heat (J/(kg· K)), volume (m^3) and inner surface area (m^2) of the test tube, respectively.

d) the instantaneous tube inner surface temperature, $T_s(t)$

With the measured instantaneous average temperature and instantaneous surface heat flux of the test tube as conditions, the instantaneous tube inner surface temperature, $T_s(t)$, was calculated by solving the following unsteady heat conduction equation assuming the inner surface temperature to be distributed evenly.

$$\rho c\frac{\partial T}{\partial t}=\frac{1}{r}\frac{\partial}{\partial r}(r\lambda\frac{\partial T}{\partial t})+\frac{1}{r}\frac{\partial}{\partial \theta}(\frac{\lambda}{r}\frac{\partial T}{\partial \theta})+Q(t) \tag{2.31}$$

Calculation of Eq. (2.31) was carried out with PHOENICS code (version.2013) [10] using a digital computer. The boundary conditions are as follows:

$$q(t)=-\lambda\frac{\partial T}{\partial r}\Big|_{r=r_i} \tag{2.32}$$

$$\frac{\partial T}{\partial r}\Big|_{r=r_o}=0 \tag{2.33}$$

When the period of exponentially increasing heat input is larger than about 5s, the heat transfer process is practically considered as steady state, which will be explained later. The solution for the inner surface temperature of the test heater, T_s, is given by the

steady state one-dimensional heat conduction equation. The basic equation is as follows:

$$\frac{d^2T}{dr^2}+\frac{1}{r}\frac{dT}{dr}+\frac{Q}{\lambda}=0 \tag{2.34}$$

Then the average temperature of the test tube is obtained.

$$T(r)=-\frac{Qr^2}{4\lambda}+\frac{Qr_0{}^2}{2\lambda}\ln r+C \tag{2.35}$$

$$\overline{T}=\frac{1}{\pi(r_0{}^2-r_i{}^2)}\int_{r^i}^{r^o}2\pi rT(r)dr \tag{2.36}$$

The boundary conditions are as follows:

$$q=-\lambda\left.\frac{dT}{dr}\right|_{r=r_i}=\frac{(r_0{}^2-r_i{}^2)Q}{2r_i} \tag{2.37}$$

$$\left.\frac{dT}{dr}\right|_{r=r_0}=0 \tag{2.38}$$

The inner temperature of the test heater, T_s and C in Eq. (2.35) can be described as follows [11]:

$$T_s=T(r_i)=\overline{T}-\frac{qr_i}{4(r_o{}^2-r_i{}^2)^2\lambda}\times\left[4r_o{}^2\left\{r_o{}^2(\ln r_o-\frac{1}{2})-r_i{}^2(\ln r_i-\frac{1}{2})\right\}-(r_o{}^4-r_i{}^4)\right]-\frac{qr_i}{2(r_o{}^2-r_i{}^2)\lambda}(r_i{}^2-2r_o{}^2\ln r_i) \tag{2.39}$$

$$C=\overline{T}-\frac{qr_i}{4(r_o{}^2-r_i{}^2)^2\lambda}\times\left[4r_o{}^2\left\{r_o{}^2(\ln r_o-\frac{1}{2})-r_i{}^2(\ln r_i-\frac{1}{2})\right\}-(r_o{}^4-r_i{}^4)\right] \tag{2.40}$$

e) heat transfer coefficient, *h*

The heat transfer coefficient, h, is expressed as follows:

$$h = q / \Delta T_L = q / (T_s - T_L) \tag{2.41}$$

where T_L is the average bulk liquid temperature, K. T_s is the tube inner surface temperature, K.

f) Nusselt number, Nu_d

The Nusselt number, Nu_d, was calculated by the following equation:

$$Nu_d = hd / \lambda \tag{2.42}$$

where h is the heat transfer coefficient, W/(m^2·K); d is the tube inner diameter, m, and λ is the thermal conductivity, W/(m·K).

g) the inlet and outlet pressures for the test tube, P_{in} and P_{out}

The inlet and outlet pressures for the test tube, P_{in} and P_{out} were calculated from the pressures measured with inlet and outlet pressure transducers as follows:

$$P_{in} = P_{ipt} - (P_{ipt} - P_{opt}) \times \frac{0.04}{L + 0.08} \tag{2.43}$$

$$P_{out} = P_{in} - (P_{in} - P_{opt}) \times \frac{L}{L + 0.04} \tag{2.44}$$

h) the average bulk liquid temperature, T_L

All thermal physical properties were evaluated at the average bulk liquid temperature, T_L, except μ_w (viscosity of fluid next to the inner surface), which is evaluated at the tube inner surface temperature.

$$T_L = \left(T_{in} + \left(T_{out}\right)_{cal}\right)/2 \tag{2.45}$$

Since the outlet temperature is measured at 60 mm downstream of the tube outlet, the measured temperature is slightly lower than the actual one due to heat loss caused by heat conduction. For better accuracy, the outlet liquid temperature, $(T_{out})_{cal}$, was calculated by the energy balance as follows:

$$(T_{out})_{cal} = T_{in} + \frac{4Lq}{uc_{p,l}\rho_l d} \tag{2.46}$$

2.2.4.3 Measurement accuracies and experimental uncertainties

The flow meter was calibrated and its accuracy is ±3%. The thermocouples were well calibrated with an accuracy of ±0.05 K. But the inlet liquid temperature was kept within ±1 K of a desired value. Although the accuracy of pressure transducer is ±0.02%, the pressurizer can only maintain the system pressure within ±1 kPa of a desired value. The accuracies of the measured parameters including inlet flow velocity (u), inlet and outlet temperatures (T), inlet and outlet pressure (P), and exponential period (τ) are ±3%, ±1 K, ±1 kPa and ±2%, respectively.

The experimental uncertainties of the derived values were calculated using the ANSI/ASME PTC 19.1-1985 [12]. The maximum uncertainties of the heat generation rate (Q), heat flux (q), heat transfer coefficient (h) and Nusselt number (Nu_d) can be calculated as follows:

$$\frac{U_{RSS,Q}}{Q} = \sqrt{\left(\frac{B_Q}{Q}\right)^2 + t_{95}\left(\frac{S_Q}{Q}\right)^2} \tag{2.47}$$

where, B_Q, S_Q and t_{95} are the basis of the heat generation rate, the precision index of the heat generation rate, and confidence level, respectively

$$\frac{U_{RSS,q}}{q} = \sqrt{\left(\frac{B_q}{q}\right)^2 + t_{95}\left(\frac{S_q}{q}\right)^2} \tag{2.48}$$

$$\frac{U_{RSS,h}}{h} = \sqrt{\left(\frac{B_h}{h}\right)^2 + t_{95}\left(\frac{S_h}{h}\right)^2} \tag{2.49}$$

$$\frac{U_{RSS,Nu_d}}{Nu_d} = \sqrt{\left(\frac{B_{Nu_d}}{Nu_d}\right)^2 + t_{95}\left(\frac{S_{Nu_d}}{Nu_d}\right)^2} \tag{2.50}$$

where, B_q and S_q are the basis and the precision index of the heat flux, respectively; B_h and S_h are the basis and the precision index of the heat transfer coefficient, respectively; B_{Nud} and S_{Nud} are the basis and the precision index of the Nusselt number, respectively.

All the measurement accuracies and experimental uncertainties are summarized in Table 2.5. The maximum uncertainties of heat generation rate, heat flux, and heat transfer coefficient, Nusselt number, average temperature and inner surface temperature

of test tube were estimated to be ±2.0%, ±2.4%, ±4.4 %, ±4.4 %, ±1 K and ±1 K , respectively.

Table 2.5 Summary of experimental errors and uncertainties

Primary measurements		Derived quantities	
u	±3%	Q	±2.0%
T	±1.5 K	q	±2.4%
P	±1 kPa	h	±4.4%
τ	±2%	Nu_d	±4.4%
		T_a, T_s	±1 K

2.2.4.4 Experimental procedure

The experiments were performed as in the following procedure. Experiments were conducted over several years and it showed excellent repeatability.

1) After treatment with acetone to remove oil or dust, the test tube was soldered and set up to the test section assembly. Airtight test for the flow loop was conducted after installation of test section assembly.
2) FC-72 was heated to boil vigorously for 30 minutes to get rid of any gases. Then FC-72 in storage tank was heated to increase temperature and pressure. Meanwhile, the flow loop was evacuated by a vacuum pump. Then the liquid was

charged into the flow loop by the pressure difference.

3) The resistance-temperature relation of the test heater was calibrated with flowing liquid. Relevant data was input to the computer.

4) The desired system pressure was established and kept by the pressurizer. The inlet liquid temperature was adjusted by using the heater and cooler. The flow velocity was controlled by regulating the inverter.

5) After the required experimental conditions became stable, balancing of the double bridge and Wheatstone bridge from the bulk liquid temperature was taken with a small current input from DC power supply.

6) The experimental run was executed from the personal computer. The heat input was then increased exponentially with a certain exponential period. For each run, the inlet and outlet temperatures, T_{in} and T_{out}, the inlet and outlet pressures, P_{in} and P_{out}, the flow velocity, u, and other voltage signals accompanying the passage of time were recorded by the data acquisition system. The heat input would be cut off once the average temperature of test heater reached the preset shut off temperature.

7) After the experiment, the FC-72 was pushed back to the storage tank by high-pressure nitrogen gas.

References

[1] Sakurai, A., and Shiotsu, M., Transient Pool Boiling Heat Transfer, Part 2, Boiling Heat Transfer And Burnout, ASME J. Heat Transfer, Vol. 99, (1977), 554–560.

[2] Y. Li, K. Fukuda and Q. Liu, Steady and Transient Critical Heat Fluxes under Sub-atmospheric Pressures, Proceedings of International Symposium on Marine Engineering,17-21 Oct 2011 Kobe, Japan,(2011).

[3] Y. Li, K. Fukuda and Q. Liu, Steady and Transient pool Boiling CHF at Various Pressures in a Pool of Water, 4th Proceedings of International Symposium on Heat Transfer and Energy Conservation, 6-9 Jan 2012, Guangzhou, China,(2012).

[4] Frank M. White. Fluid Mechanics, 8th Edition. McGraw-Hill Education, (2015) 31.

[5] W. M. Kays and M. E. Crawford. Convective Heat and Mass Transfer, McGraw-Hill, Second Edition, New York, (1980).

[6] W. M. Kays, Convective Heat and Mass Transfer, pp. 187–90. New York: McGraw-Hill, (1966).

[7] Fluorinert™ Electronic Liquid FC-72 Product Information, http://multimedia.3m.com/mws/media/648920/fluorinert-electronic-liquid-fc-72.pdf, (2000).

[8] A. Sakurai, and M. Shiotsu, Transient pool boiling heat transfer, Part 1: incipient

boiling superheat", ASME J. Heat Transfer, (1977) 547-553.

[9] K. Fukuda, Q. Liu, Steady and transient critical heat fluxes on a horizontal cylinder in a pool of Freon-113, Int. J. Trans Phenom. 7 (2006) 71–83.

[10] D.B. Spalding,, The PHOENICS Beginner's Guide, CHAM Ltd., London, United Kingdom, (2013).

[11] K. Hata, N. Kai, Y. Shirai, S. Masuzaki, Transient turbulent heat transfer for heating of water in a short vertical tube, J. Power Energy Syst. 5, (2011) 414–428.

[12] ANSI/ASME PTC 19.1-1985, Measurement Uncertainty, Supplement on Instruments and Apparatus, Part 1, (1985).

CHAPTER 3

Pool Boiling Heat Transfer

Kandlikar [1] pointed out that there exist similarity between pool boiling CHF and flow boiling CHF, especially at low flow rate. Pool boiling heat transfer could be regarded as a kind of flow boiling when velocity equals zero. Therefore, the essential characteristics of the pool boiling CHF are retained in flow boiling CHF. The study on physical mechanism of pool boiling and its CHF is necessary for better understanding of flow boiling and its CHF.

This chapter presents and discusses the obtained steady state and transient pool boiling heat transfer data under one atmosphere and sub-atmospheric pressures for the subcoolings ranging from zero up to 40 K. The typical pool boiling curve has been described together with the bubble behaviors recorded by high speed video camera. The steady state and transient pool boiling CHF results are also presented and discussed.

3.1 Experimental Conditions

Heat pipes, thermosyphons and some heat pump cycles need to keep low in the working temperature for boiling phenomena, which can be achieved by keeping low

saturation pressure. A reduction in the saturation pressure can lead to lower saturation temperature, providing given superheat at low temperature surface. Therefore the present work set the experimental conditions under low pressures ranging from 101.6 kPa down to 10 kPa.

The exponentially increasing heat input, $Q_0 exp(t/\tau)$, is a function of period, τ. In this study, the exponential periods were ranged from 10 ms up to 20 s. Besides, the subcooling parameter was ranged from saturated condition up to 40K.

Ion-exchange-distilled water was used as the working liquid in pool boiling experiments. The physical properties of water are listed in Table 2.1.

All requirements of the experimental conditions are summarized in Table 3.1.

Table 3.1 Experimental conditions of pool boiling

Working liquid	Pure water
Cylinder diameter (d)	1 mm
Effective length (L)	49.8 mm
System pressure (P)	10 -101.6 kPa
Period (τ)	10 ms-20 s
Liquid subcooling (ΔT_{sub})	0-40 K

3.2 Time Dependence of Pool Boiling Characteristics

Figure 3.1 shows typical changes in the heater surface superheat, ΔT_{sat}, and the heat flux, q, with time for the exponentially increasing heat input, Q. The heat input to

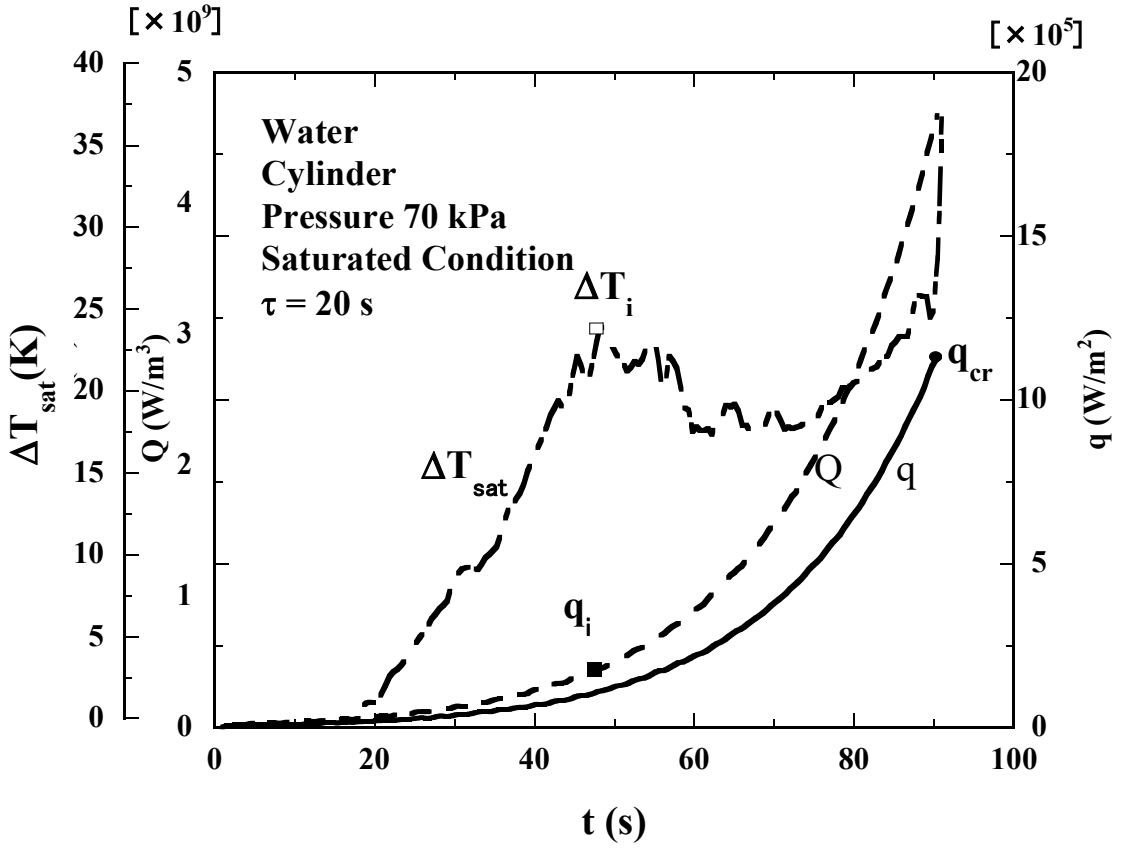

Fig. 3.1 Typical changes of heat generation rate, heat flux and surface superheat relating to elapsed time (τ＝20 s)

the test heater was increased quasi-steadily as an exponential time function with period of 20 s. This figure shows a typical transition to film boiling through fully developed nucleate boiling or FDNB. The heater surface temperature firstly increases with an

increase in the heat input. Boiling starts at T_i beyond saturation temperature, T_{sat}. The temperature differences of $\Delta T_i = T_i - T_{sat}$ is called the incipient boiling surface superheat. The heater surface temperature increases up to maximum temperature overshoot, then decreases due to incipient boiling and again increases with lower rate in the nucleate boiling process. When the heat flux reaches a certain value, q_{cr}, which is named as critical heat flux (CHF), the heater temperature rapidly increases along the transition region to film boiling. The heat flux q always increases with the increase of heat input Q. It should be noted that the heat flux rapidly increases after the incipient boiling heat flux point. During nucleate boiling process, a steep increase in heat flux up to CHF under small temperature difference is shown.

Figure 3.2 shows the case that heat input to the test heater was increased as an exponential time function with period of 10 ms. Heater surface temperature always increases with the increase of heat input. After reaching the CHF point shown with circle mark, the heater temperature increases sharply. At first the heat flux increases as the increase of Q, then increases sharply in a very short time to the critical heat flux q_{cr} after reaching the incipient boiling heat flux, q_i. After CHF point, the transition boiling occurs with the decrease in heat flux and the unsteady increase in surface temperature and then reaches minimum heat flux. This figure shows a typical direct transition to film

boiling without occurrence of nucleate boiling. The direct transition refers to a simultaneous process of CHF after boiling incipience. It is assumed to be caused by the explosive-like heterogeneous spontaneous nucleation (HSN) [4].

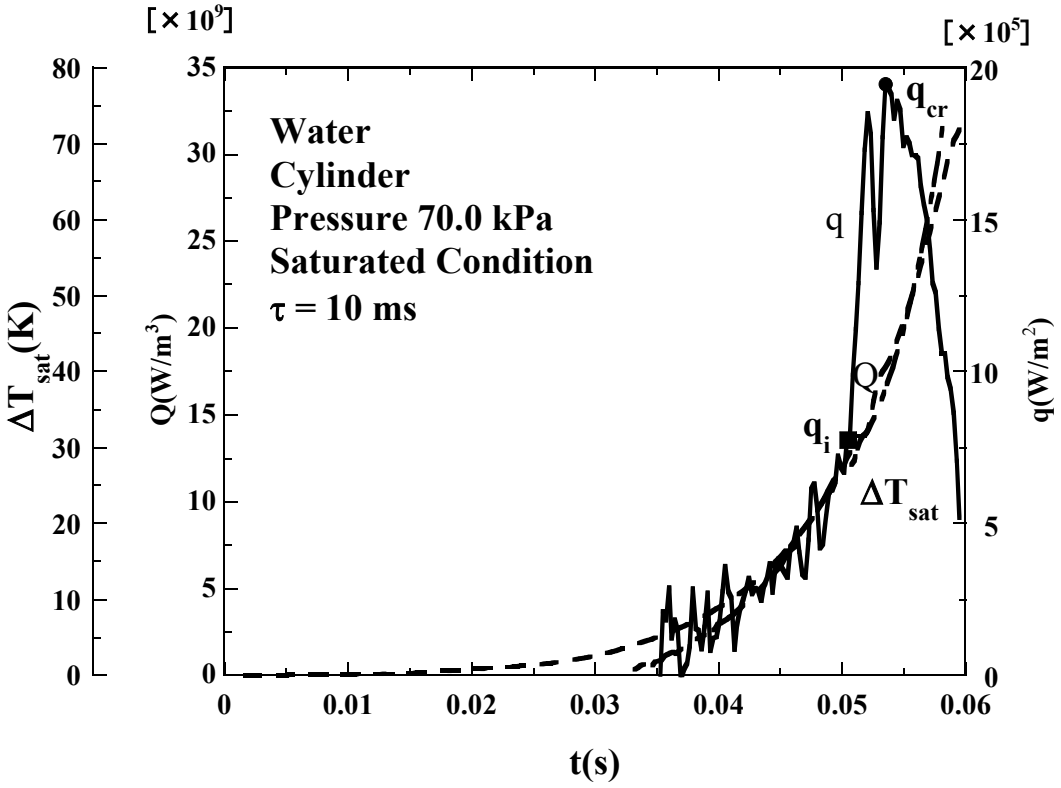

Fig. 3.2 Typical changes of heat generation rate, heat flux and surface superheat relating to elapsed time (τ＝10 ms)

3.3 Heat Transfer in the Non-boiling Region

The heat transfer coefficients in the non-boiling region were measured for the exponential periods ranging from 20 s to 10 ms. The typical heat transfer coefficients at Ts=383 K for $\Delta T_L(T_S\text{-}T_L)$=20 K are shown versus exponential periods in Fig. 3.3. The

experimental data of heat transfer coefficient versus exponential period match basically with the conventional correlations. For the shorter periods, the heat transfer coefficients increase with a decrease in the period along the transient conduction curve, h_c, obtained by Sakurai et al [2]. These heat transfer coefficients are higher than h_n due to the transient conductive heat transfer contribution. The experiment runs under shorter periods are taken as transient state. For the longer periods, the heat transfer coefficients approach an asymptotic value, h_n, which is estimated by conventional natural convection correlation obtained by Takeuchi et al. [3]. Due to the heat transfer coefficients agree with those for steady state, the experiment runs under longer periods are considered as steady state. The heat transfer coefficients for intermediate periods match the curve, h_m, derived by Sakurai et al [2].

The natural convection heat transfer coefficient correlation is given as follows:

$$h_n = \frac{k}{H}\left[C\left(Gr_H \,\mathrm{Pr}\right)^{1/5}\right] \tag{3.1}$$

where

$$C = \left[\frac{\mathrm{Pr}}{4 + 9\,\mathrm{Pr}^{1/2} + 10pr}\right]^{1/5} \tag{3.2}$$

$$Gr_H = \frac{H^4 g\beta q}{kv^2} \tag{3.3}$$

The combination of natural convection and transient conduction is given as follows:

$$h_m = \left[h_c^{\,4} + h_n^{\,4} \right]^{1/4} \tag{3.4}$$

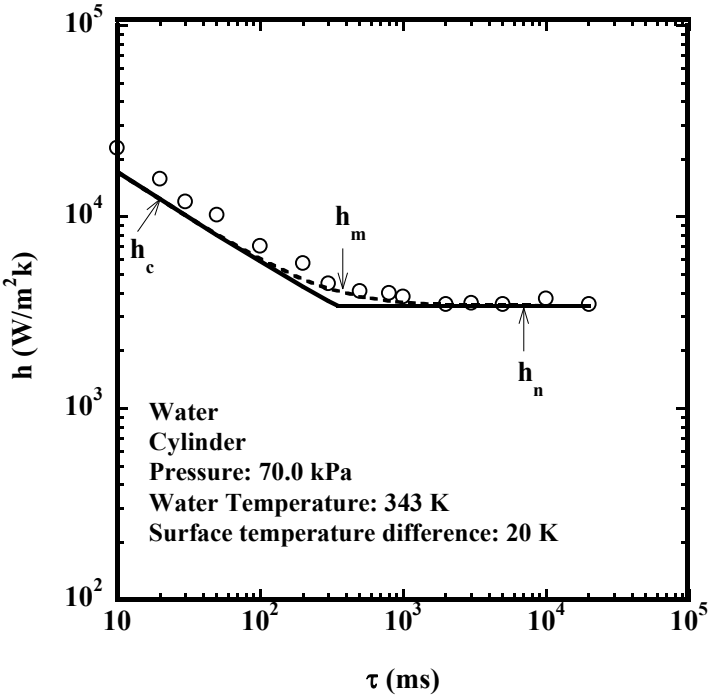

Fig. 3.3 Non-boiling heat transfer coefficient versus exponential period at ΔT_L=20 K

3.4 Steady State Pool Boiling Curve and Vapor Behaviors

Figure 3.4 shows the typical steady state boiling heat transfer process up to the CHF for exponential period of 20 s at the pressure of 70 kPa for saturation condition. In addition to the boiling process, the natural convection curve obtained from the correlation given by Sakurai et al. [2] is shown in this figure. Fig. 3.5 shows the photographs which were taken at six points shown on the graph in Fig. 3.4 for the vapor and bubble behaviors on a horizontal cylinder.

The photos (a) to (f) show the vapor and bubble behaviors caused by quasi-steadily

increasing heat input with period of 20 s. At first, the heat flux increase along natural convection curve to the incipient boiling point (a). Figure 3.5(a) shows that an isolated bubble generates from active cavities. Then subsequent bubble growth is observed in Fig. 3.5(b). More and more nucleation sites are activated as heat flux, q, and surface superheat increase.

The onset of fully developed nucleate boiling is at point (c). Fig. 3.5(c) shows the detachment of large bubbles induced by unstable Taylor wave which exists on the vapor-liquid interface. The large vapor bubbles collapse from the top of thin vapor film covering the cylinder surface. Several points on the top of vapor-liquid interface of thin vapor film were connected with the bottoms of large vapor bubbles. When active sites become very numerous, the bubbles start to merge with one another immediately and make a different kind of vapor escape path. A photograph of slug and column regime is shown in Fig. 3.5(d). Then the heat flux increases along nucleate boiling to the point (e) of the CHF point, q_{cr}, which is marked with a circle. At point (e), the heater surface was blanketed with a large vapor film as shown in Fig. 3.5(e). After CHF, the process continues to the transition boiling, whose typical vapor behavior was shown in Fig. 3.5(f).

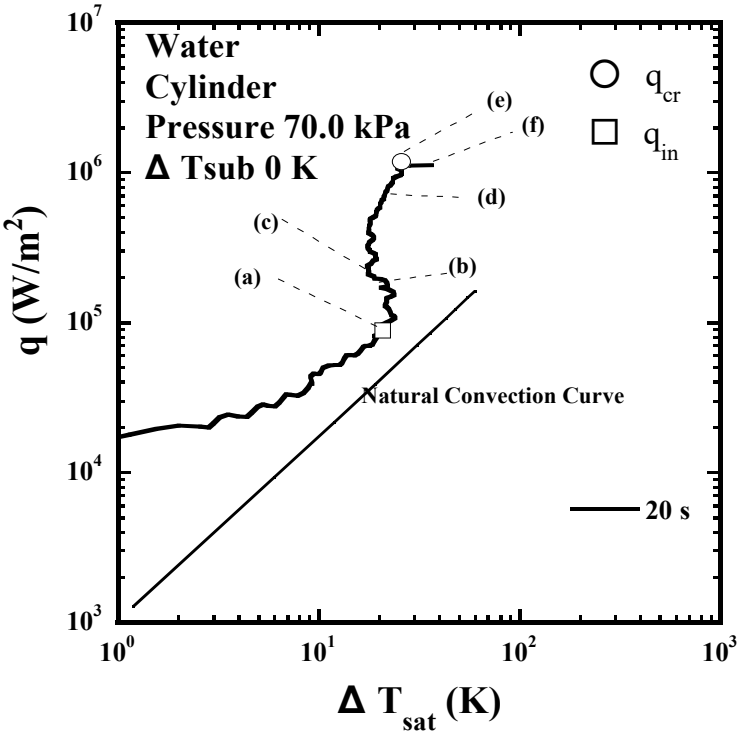

Fig. 3.4 Typical steady state boiling curve and critical heat flux due to quasi-steadily increasing heat input with a period of 20 s

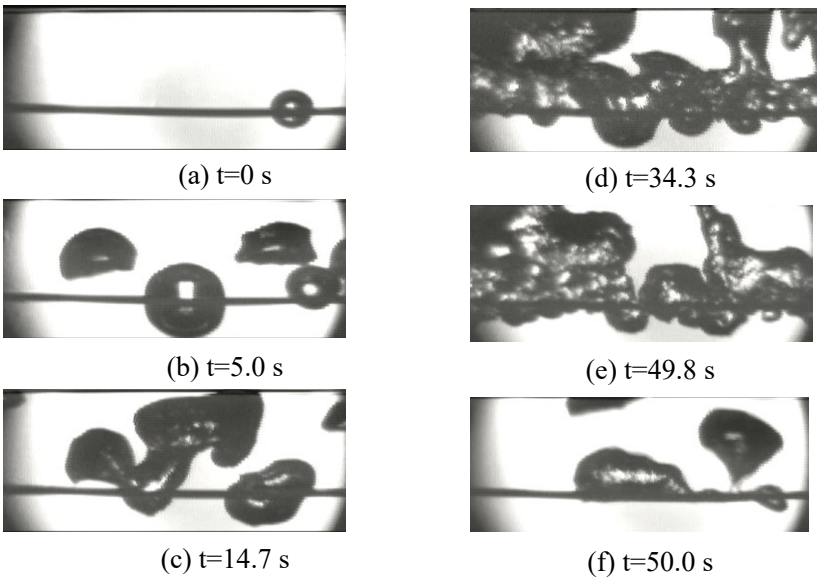

Fig. 3.5 Vapor behaviors on a horizontal cylinder caused by quasi-steady heat input with a period of 20s

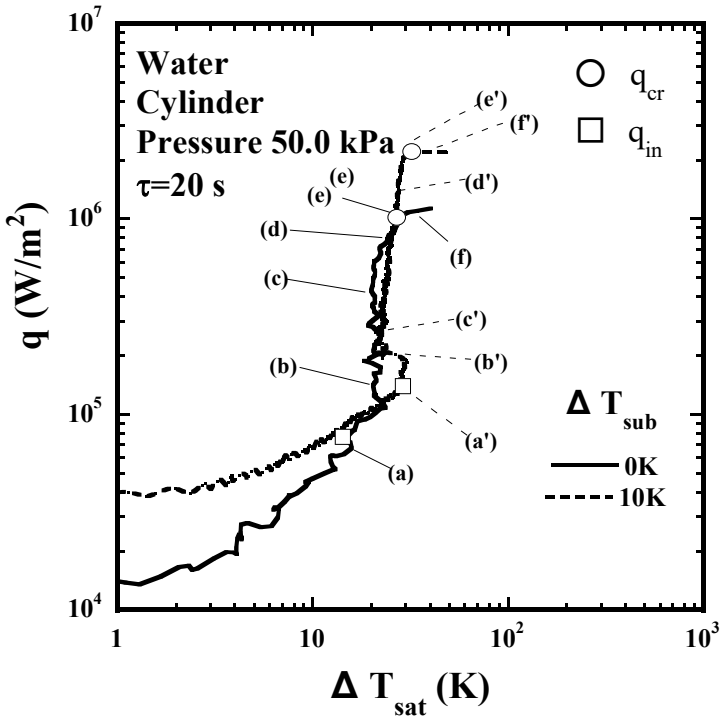

Fig. 3.6 Pool boiling heat transfer process for subcooling of 0 K and 10 K at a pressure of 50 kPa.

Figure 3.6 shows typical pool boiling heat transfer process for subcooling of 0 K and 10 K at a pressure of 50 kPa. A comparison of the vapor and bubble behaviors was made in Fig. 3.7. As shown in Fig. 3.6, CHFs increase with the increase of subcooling, which can be explained by the vapor behaviors as shown in Fig. 3.7. In the subcooled pool boiling heat transfer process, the bubbles contact the subcooled liquid core causing condensation at the liquid-vapor interface, or even without leaving the heated surface. The higher level of subcooling in the liquid requires a higher heat flux to initiate and sustain bubble activity. Fig. 3.7(a') to Fig. 3.7(f') shows the similar phenomena as the case in saturation condition, except much smaller vapor bubbles due to the effect of

subcooling.

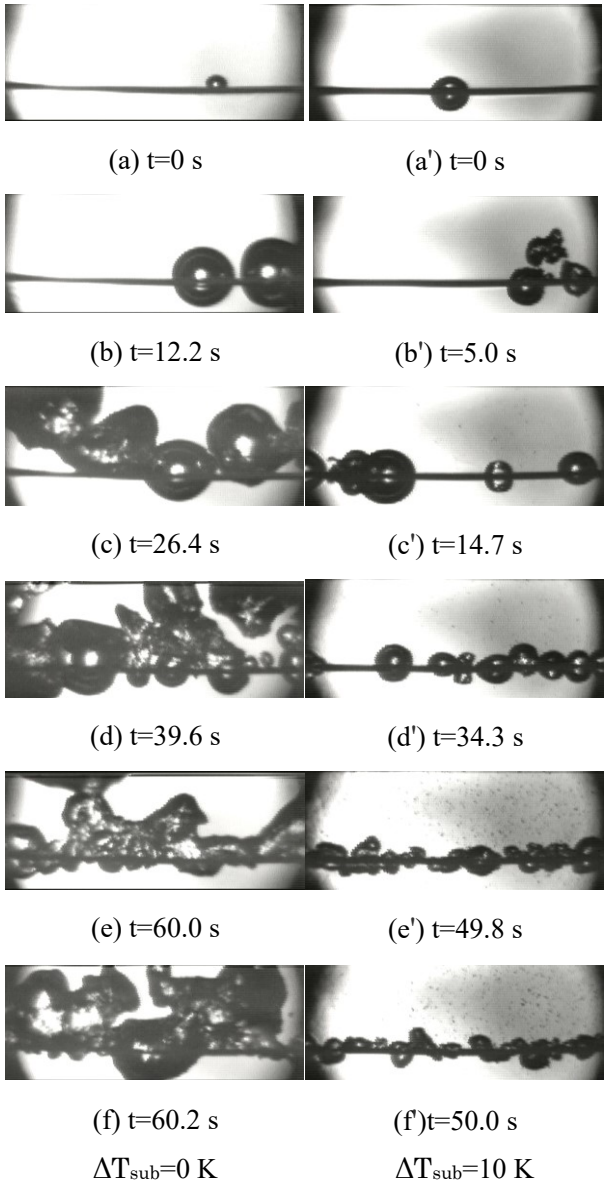

Fig. 3.7 Comparison of bubble behavior of typical heat transfer process for subcooling of 0 K and10 K at a pressure of 50 kPa

3.5 Transient Pool Boiling Curve and Vapor Behaviors

The heat transfer process for exponential period of 10 ms at a pressure of 70 kPa is shown in Fig. 3.8. The boiling curve reaches to the CHF directly by the rapid increasing

heat input. The direct transition occurs from non-boiling regime to film boiling without nucleate boiling. Figure 3.9 shows bubbles behaviors in the direct transition process. After the incipient vapor bubble at point (a), the cylinder was rapidly covered with large vapor film as shown in Fig. 3.9(b) to (d). It should be noted that the vapor film fully blankets the cylinder surface in only 5 ms after the incipient boiling. It was assumed that the vapor bubbles due to an explosive-like HSN in originally flooded cavities on the whole cylinder surface form the vapor tube concentrically covering the cylinder [4]. Figure 3.9(e) shows the detachment of bubbles from top of vapor tube which moves upward by buoyancy force from the position shown in the former photograph.

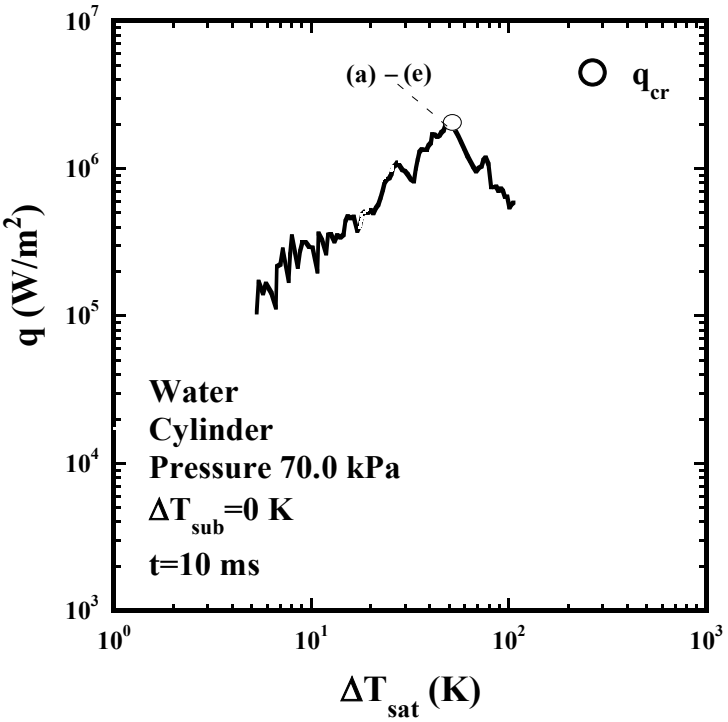

Fig. 3.8 Typical transient boiling heat transfer process and critical heat flux due to rapidly increasing heat input.

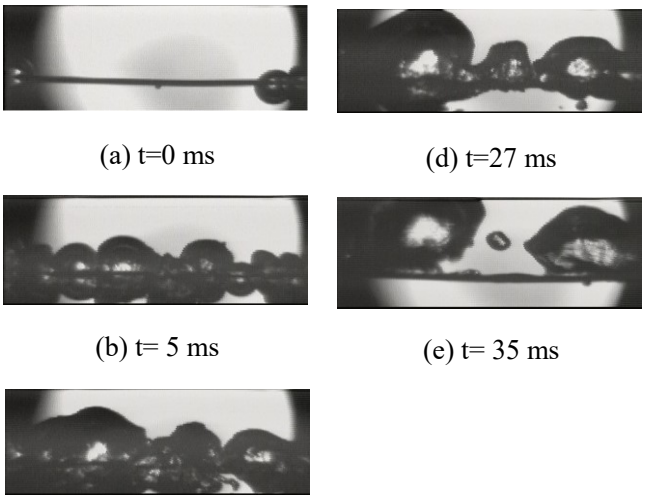

Fig. 3.9 Vapor behaviors of transient boiling under the pressure of 70 kPa

3.6 Steady State Pool Boiling CHF

The steady state CHF data under pressures of 101.6 kPa and 30 kPa for the subcoolings ranging from 0 to 40 K are shown in the Fig. 3.10 and Fig. 3.11 in comparison with correlations proposed by Kutateladze [5], Zuber [6], Ivey and Morris [7], and Sakurai [8]. The steady state CHF increases with the increase of subcoolings, which can be explained with vapor behaviors. In the subcooled pool boiling heat transfer process, the higher level of liquid subcooling requires a higher heat flux to initiate and sustain bubble activity. As the bubbles grow, they contact the subcooled bulk liquid causing condensation at the liquid-vapor interface, or even without leaving the heated surface. Therefore, higher heat flux is required to generate and sustain bubble

behavirs.

The saturated and subcooled pool boiling CHF correlations representing the CHF values resulting from the hydrodynamic instability are developed by Sakurai and Fukuda [8] as follows:

$$q_{cr,sat} = K_1 h_{lv} \rho_v \left[\frac{\sigma g(\rho_l - \rho_v)}{\rho_v^2} \right]^{\frac{1}{4}} \tag{3.5}$$

$$q_{cr,sub} = q_{cr,sat} \left[1 + K_2 (\rho_l / \rho_v)^{0.69} \left(C_{pl} \Delta T_{sub} / h_{lv} \right)^{1.5} \right] \tag{3.6}$$

where,

$$K_2 = 0.39 / L'^{0.6} \tag{3.7}$$

$$L' = \frac{d/2}{\sqrt{\sigma / g(\rho_l - \rho_v)}} \tag{3.8}$$

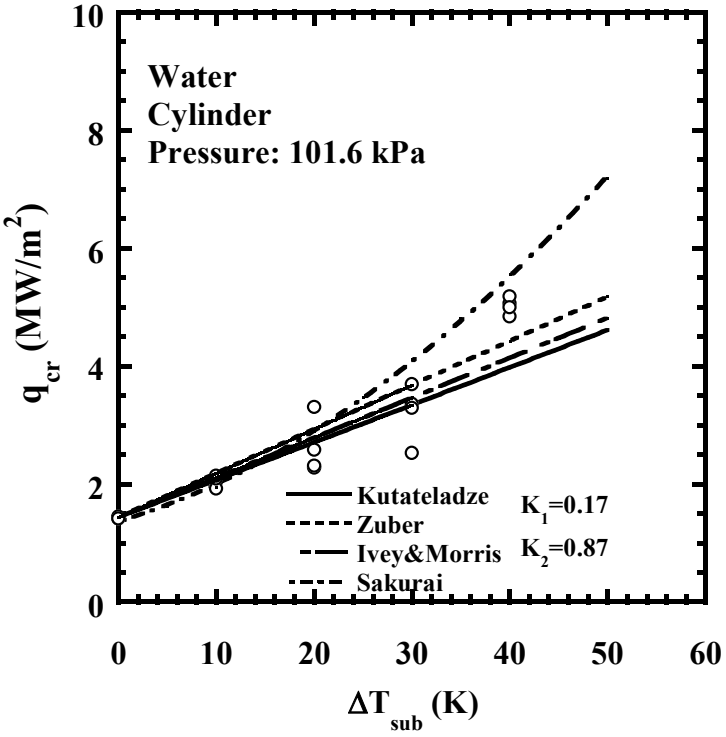

Fig. 3.10 Change of steady CHF relating to subcoolings at 101.6 kPa

As shown in Fig. 3.10, those CHF data for one atmosphere are in agreement with those conventional correlations. However, the CHF data for pressure of 30 kPa show higher values compared with the conventional correlations as shown in Fig. 3.11. The CHF values for other sub-atmospheric pressures of 20 to 70 kPa were also found to be higher than predicted by the conventional correlations.

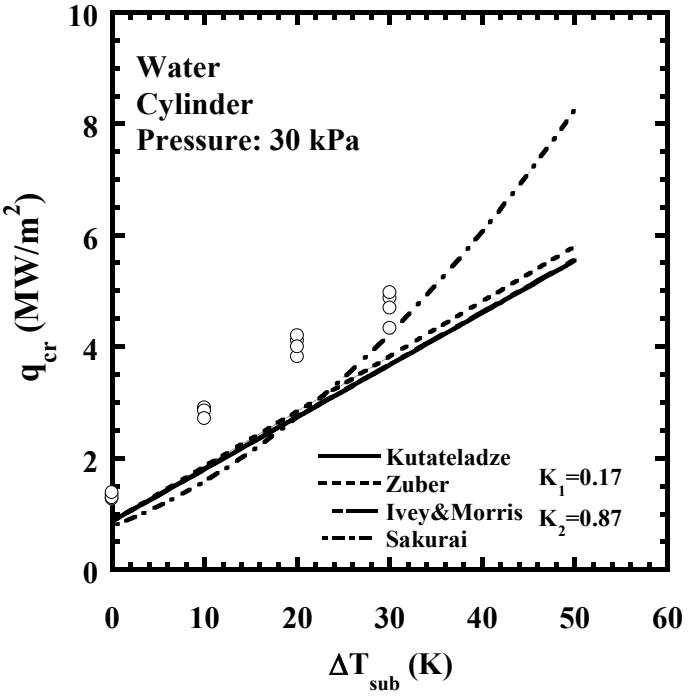

Fig. 3.11 Change of steady CHF relating to subcoolings at 30 kPa

The steady state CHF against pressures with the subcooling as a parameter is shown in Fig. 3.12. For comparison, the CHF data obtained by Sakurai and Fukuda [8] for the pressures higher than 200 kPa were also plotted with their empirical correlations shown in solid lines in this figure. Sakurai and Fukudas' CHF data for pressures higher than

atmospheric pressure increase with an increase of pressure. However, the authors' CHF data for sub-atmospheric pressures are not in agreement with Sakurai and Fukuda's correlations. Those CHF values increase with decrease of pressure.

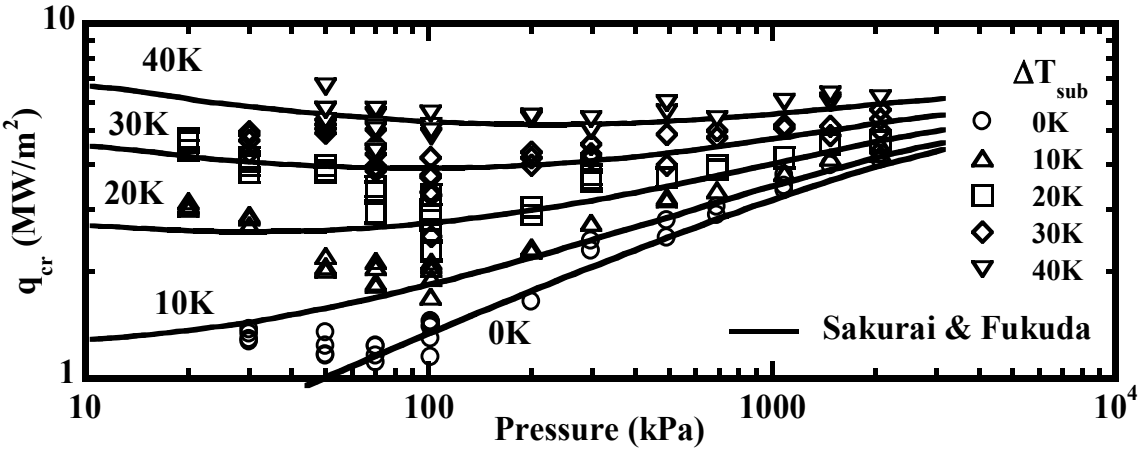

Fig. 3.12 Steady state CHF versus pressures with liquid subcooling as a parameter

3.7 Transient Pool Boiling CHF

The transient CHF data measured in saturated condition at pressure of 50 kPa are plotted in Fig. 3.12 against exponential periods. The transient pool boiling CHF values first increase with a decrease in exponential periods up to a maximum CHF, then those decrease down to a minimum one and again increase with a decrease in exponential period. The transient CHF values under sub-atmospheric pressures can be separated into two groups based on the exponential periods. The first group data correspond to long period region. The corresponding heat transfer process is transition from non-boiling to

film boiling through fully developed nucleate boiling. The second group data correspond to short period region. The corresponding heat transfer process is transition from non-boiling to film boiling without nucleate boiling or direct transition.

Figure 3.13 shows CHF measured for subcooling ranging from 0 to 40 K at a pressure of 50 kPa versus exponential periods. For the transient CHF of the first group, the corresponding heat transfer process is transition from non-boiling region to fully developed nucleate boiling. The CHF values slightly increase as periods shortens from steady state one. The transient CHF of first group for low subcoolings were plotted in comparison with the following empirical correlation obtained by Fukuda et al. [9] as shown in solid line.

$$q_{cr} = q_{st,sub}\left(1 + 0.21\tau^{-0.5}\right) \tag{3.9}$$

The transient CHF of first group for higher subcoolings are expressed in comparison with the following empirical correlation [9] as shown in dashed lines.

$$q_{cr} = q_{st,sub}\left(1 + 2.3\times10^{-2}\tau^{-0.7}\right) \tag{3.10}$$

The second group represents the transient CHF that mainly occur within short periods. It was assumed the direct transition would occur from non-boiling region to film boiling due to the instantaneous levitation of the liquid from the cylinder surface by the explosive-like HSN as suggested by Sakurai et al [10]. The heterogeneous spontaneous

nucleation occurs easily at 0 K. However, with an increase of subcooling, a much higher wall superheat may be required for nucleation from cavities, which means a higher heat generation rate or a shorter exponential period of heat input. It is assumed that the heterogeneous spontaneous nucleation would take place with further decrease of exponential period for subcooling of 10 to 40 K. The CHF data belonging to the second group under lower subcooling were plotted in comparison with the following correlation [9] as shown in dot-dash lines.

$$q_{cr} = h_c\left(\Delta T_i + \Delta T_{sub}\right) \tag{3.11}$$

$$h_c = \left(k_l \rho_l c_{pl} / \tau\right)^{1/2} \tag{3.12}$$

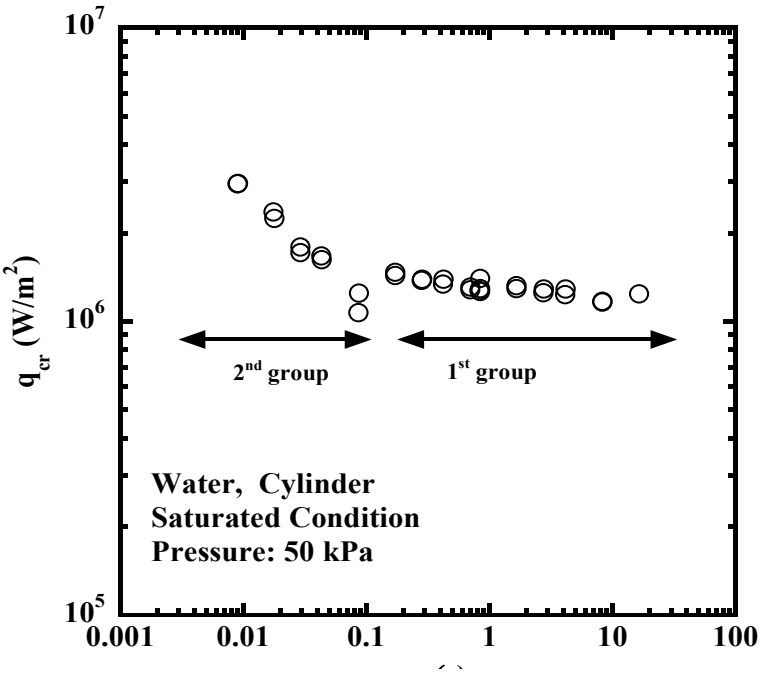

Fig. 3.13 Two groups of q_{cr} in relation to exponential periods in saturated condition at 50 kPa.

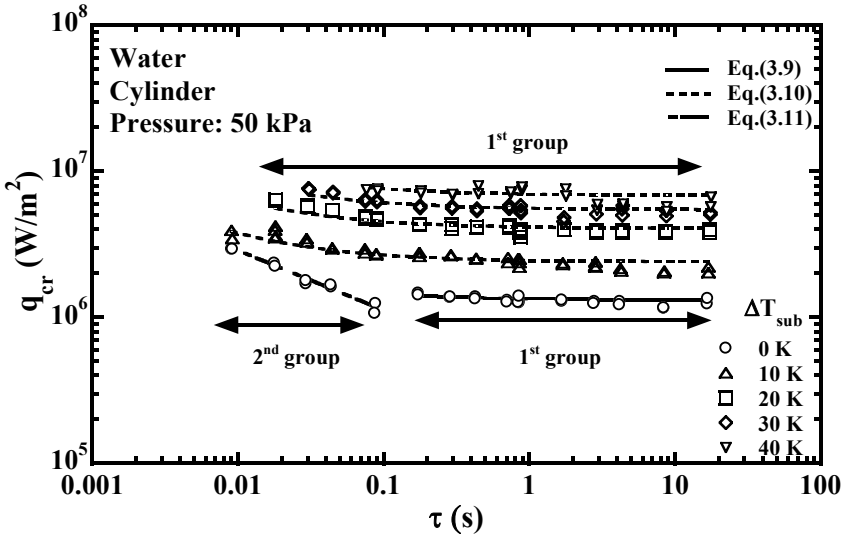

Fig. 3.14 Relation between q_{cr} and τ for subcooling ranging from 0 to 40 K at a pressure of 50 kPa

As shown in Fig. 3.14, the first and second groups of transient CHF data measured for saturation and subcooling conditions at sub-atmospheric pressure of 20 kPa match well with Fukuda's empirical correlations which derived at pressures of 103 to 2063 kPa. Similar trend was also found for other CHF data measured for pressures of 20 to 101.6 kPa.

3.8 Summary

The steady and transient CHF data for the wide ranges of exponential periods of heat generation, system pressures and liquid subcoolings were measured and studied. The following conclusions were obtained:

(1) For short periods of heat generation, the non-boiling heat transfer coefficients increase with a decrease of periods caused by transient heat conduction contribution. However, in the long period region, the heat transfer coefficients approach an asymptotic value which is predicted by natural convection correlation.

(2) It was found that the steady state CHF increase with the increase of subcoolings. And although the steady CHF data for one atmosphere are in agreement with conventional correlations, the CHF data for sub-atmospheric pressures show higher values.

(3) The steady state CHF data for sub-atmospheric pressures are not in agreement with conventional correlations. Those CHF values within sub-atmospheric pressures increase with a decrease in pressure.

(4) The transient CHF values under sub-atmospheric pressures could be divided into two groups based on the exponential periods, corresponding to short period region and long period region.

Reference

[1] S.G. Kandlikar, Critical heat flux in subcooled flow boiling-an assessment of current understanding and future directions for research, Multiph. Sci. Technol. 13 (2001).

[2] Sakurai, A. and Shiotsu, Transient Pool Boiling Heat Transfer, Part 1:Incipient Boiling Superheat,", M.,ASME J. Heat Transfer, (1977), 547-553,.

[3] Takeuchi Y., Hata K., Shiotsu M. and Sakurai A., A general correlation for laminar natural convection heat transfer from single horizontal cylinders in liquids and gases with all possible Prandtl numbers", International Mechanical Engineering Congress and Exposition, ASME HTD-Vol. 317-1, (1995) 259-270.

[4] Sakurai, A. "Mechanism of Transitions to Film Boiling at CHFs in Subcooled and Pressurized Liquids Due To Steady and Increasing Heat Inputs", Nuclear Engineering and Design, Vol. 197, (2000) 301-356.

[5] Kutateladze S. S., Heat Transfer in Condensation and Boiling, AEC-tr-3770, USAEC (1959).

[6] Zuber N., , Hydrodynamic Aspects of Boiling Heat Transfer, AECU-4439, USAEC(1959).

[7] Ivey, H. J. and Morris, D. J., UKAEA, On the Relevance of the Vapor-Liquid

Exchange Mechanism for Subcooled Boiling Heat Transfer at High Pressures, AEEW-R 137 (1962).

[8] Sakurai, A and Fukuda, K., Mechanisms of Subcooled Pool Boiling CHFs depending on Subcooling, Pressure, and Test Heater Configurations and Surface Conditions in Liquids, Proc. of ASME IMECE 2002, IMECE 2002-39066 (2002).

[9] Fukuda, K., Shiotsu, M. and Sakurai, A., Transient Pool Boiling Heat Transfer due to Increasing Heat Inputs in Subcooled Water at High Pressures, Proc. of 7th International Topical Meeting on Nuclear Reactor Thermal Hydraulics (NURETH-7), Saratoga Springs, NY, NUREG/CP-0142, pp.554-573, (1995).

[10] Sakurai, A., Mechanism of Transitions to Film Boiling at CHFs in Subcooled and Pressurized Liquids Due to Steady and Increasing heat Inputs, Nuclear Engineering and Design, Vol.197, pp. 301-356, (2000).

CHAPTER 4

Single-phase Heat Transfer in Vertical Small Diameter Tubes

This chapter presents and discusses the experimental results on steady state and transient single-phase heat transfer for turbulent flow in small diameter tubes. The experimental study was conducted for different combinations of parameters such as flow velocity, inlet liquid temperature and period of exponentially increasing heat inputs using small diameter tubes with different inner diameters and heated lengths. Single-phase heat transfer tests were performed to check the validation of the experimental apparatus and experimental procedures. The study on single-phase heat transfer is also necessary to explore the mechanism of flow boiling heat transfer in small diameter tubes.

4.1 Steady State Turbulent Heat Transfer

Prior to study of transient turbulent heat transfer, it is important to know the steady state heat transfer characteristics in vertical small diameter tubes. Steady state

experiments were therefore performed before the transient experiments.

Section 4.1 presents and discusses the experimental results of steady state turbulent heat transfer characteristics with FC-72 flowing upward in vertical small diameter tubes. The experimental conditions are described before presenting the experimental results. Then the effects of ratio of heated length to inner diameter, ratio of viscosity of liquid in bulk to that at the walls, Prandtl number and Reynold number are discussed in detail. The experimental data are also compared with the values calculated by classical correlations for conventional sized channels and the correlation for prediction of heat transfer in small channels. Finally the steady state turbulent heat transfer correlations have been developed for the vertical small diameter tubes based on the experimental data.

4.1.1 Experimental conditions

As shown in Fig. 2.6, the test tube was vertically oriented along the centerline of the flow channel with liquid flowing upward. In this study, SUS304 circular tubes with heated lengths around 30 mm, 40 mm and 50 mm and inner diameters of 1 mm, 1.8 mm and 2.8 mm were used as the test heater. The details of the test tube are also shown in Table 2.4.

Table 4.1 Experimental conditions

Test fluid	FC-72
Inner diameter (d)	1, 1.8 and 2.8 mm
Heated length (L)	31.1, 40 and 50 mm for d =1 mm 30.1, 40.2 and 49.9 mm for d =1.8 mm 31.3, 40.5 and 50.2 mm for d =2.8 mm
L/d ratio	31.1, 40 and 50 for d =1 mm 16.7, 22.3 and 27.7 for d =1.8 mm 11.2, 14.5 and 17.9 for d =2.8 mm
Wall thickness (δ)	0.5 mm
Surface condition	Commercial finish of inner surface
Inlet flow velocity (u)	8, 9, 10 and 11 m/s for d =1 mm 3, 4, 5 and 6 m/s for d =1.8 mm 3, 5 and 7 m/s for d =2.8 mm
Reynold number (Re_d)	23,400 – 45,900 for d =1 mm 16,200 – 44,800 for d =1.8 mm 25,200 – 81,800 for d =2.8 mm
Prandtl number (Pr)	8.4 – 10.8
Inlet temperature (T_{in})	303, 323 and 343K
Exponential period (τ)	6.38-15.48 s
System pressure (P)	400 kPa

FC-72 was selected as the test liquid. The details of the relevant properties are described in section 2.2.3. The experiments were conducted at the flow velocities, u,

changing from 8 to 11 m/s with corresponding Reynold number, Re_d, in the range of 23,400 to 45,900 for d = 1 mm, u changing from 3 to 6 m/s with corresponding Re_d in the range of 16,200 to 44,800 for d = 1.8 mm and u changing from 3 to 7 m/s with corresponding Re_d in the range of 25,200 to 81,800 for d = 2.8 mm. The range of Prandtl number, Pr, was from 8.4 to 10.8. Heat inputs to the test heater were exponentially increased with various exponential periods, τ. The inlet liquid temperatures, T_{in}, were maintained at 303, 323 and 343 K. The system pressure, P, was kept around 400 kPa for all experiment runs. The ranges of all experimental parameters covered in this study are listed in Table 4.1.

Among these parameters, exponential period of exponentially increasing heat input is a key factor because it determines if the heat transfer process is steady state or transient state. Figure 4.1 shows the heat transfer coefficients, h, at various exponential periods, τ, with an inner diameter of 1.8 mm, a heated length of 49.9 mm and flow velocities of 3, 4, 5, and 6 m/s for surface temperature difference (temperature differences between the heater inner surface temperature and the average bulk liquid temperature), ΔT_L, of 30 K. With the increase of exponential periods, the heat transfer coefficients gradually decrease and approach an asymptotic value at each velocity. This trend is similar to observations by other researchers [1-3].

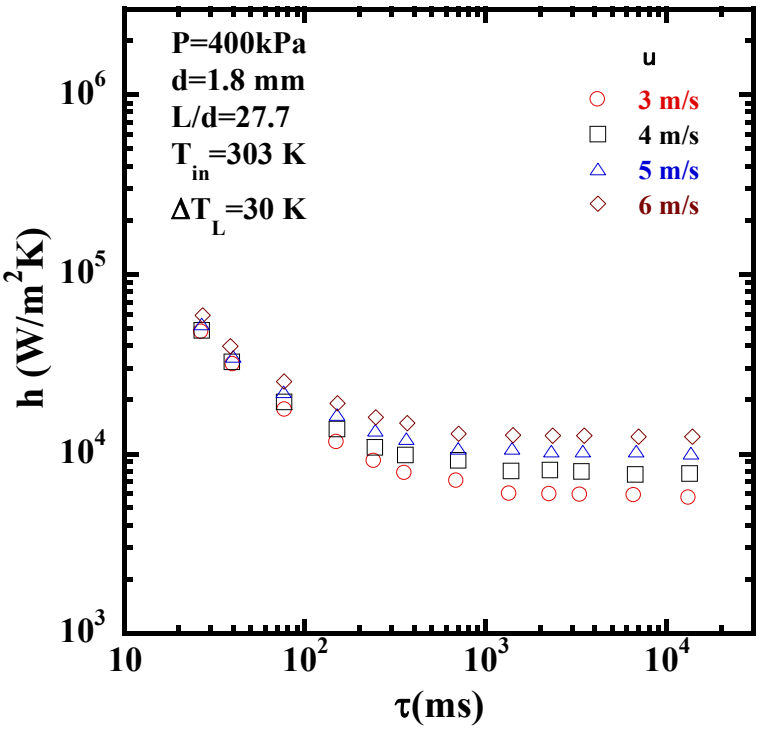

Fig. 4.1 Relationship between h and τ for d=1.8 mm

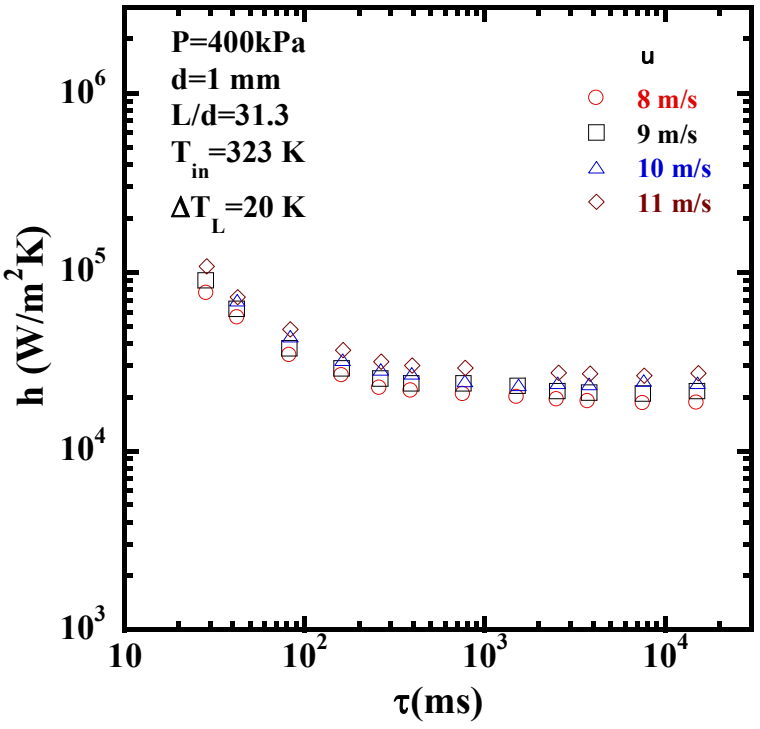

Fig. 4.2 Relationship between h and τ for d=1 mm

For shorter periods，τ , the h increases with a decrease in τ. The conductive heat transfer comes to govern the heat transfer process, and this is defined as transient state. For longer periods, the usual convective heat transfer begins to predominate and the h almost approaches to a constant despite changes in τ. For periods larger than about 5 s, the increase of heat generation rate was so slow that the thermal boundary layer next to the tube inner surface was fully developed. The heat transfer coefficients did not depend upon the exponential periods. Therefore, the experiments with exponential periods larger than 5 s can be practically regarded as steady state. The range of relevant exponential periods is 6.38-15.48 s in the steady state experiments.

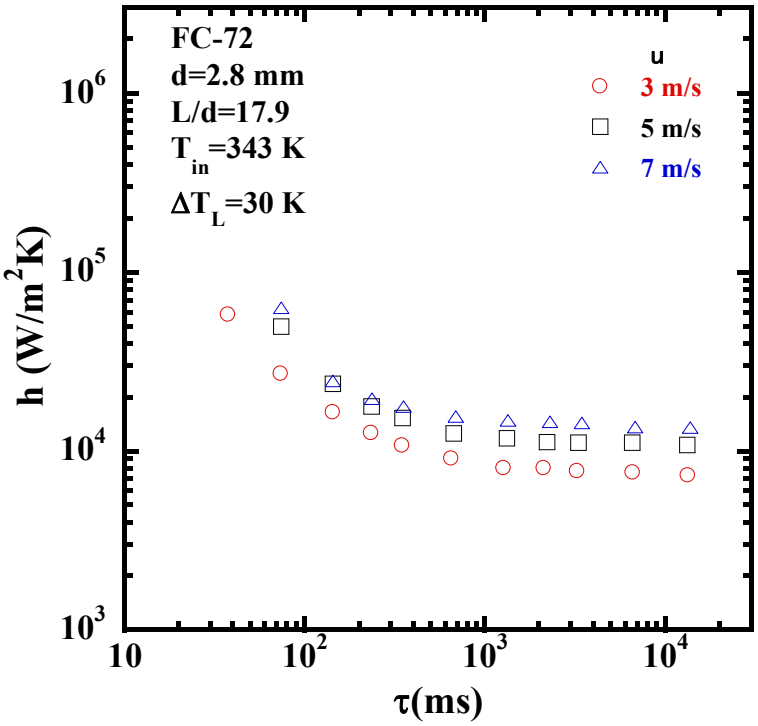

Fig. 4.3 Relationship between h and τ for d=2.8 mm

The same results were also found for all other flow velocities and inlet liquid temperatures using the tubes with different inner diameters and heated lengths. Fig. 4.2 and Fig. 4.3 shows cases for d = 1 mm and d = 2.8 mm.

4.1.2 Experimental data of heat generation rate, surface temperature difference and heat flux

Figures 4.4a and 4.4b show typical experimental data of the time-dependence of heat generation rate, Q, surface temperature, ΔT_L ($\Delta T = T_s - T_L$), and heat flux, q, at the liquid temperature of 303 K and liquid flow velocity of 9 m/s for the exponential periods of heat generation rate of 7.25 s and 14.25 s, respectively. The tube inner diameter is 1 mm and the heated length is 40 mm. As shown in this figure, surface superheat and heat flux increase exponentially as the heat generation rate increases with exponential function ($Q = Q_0 exp(t/\tau)$).

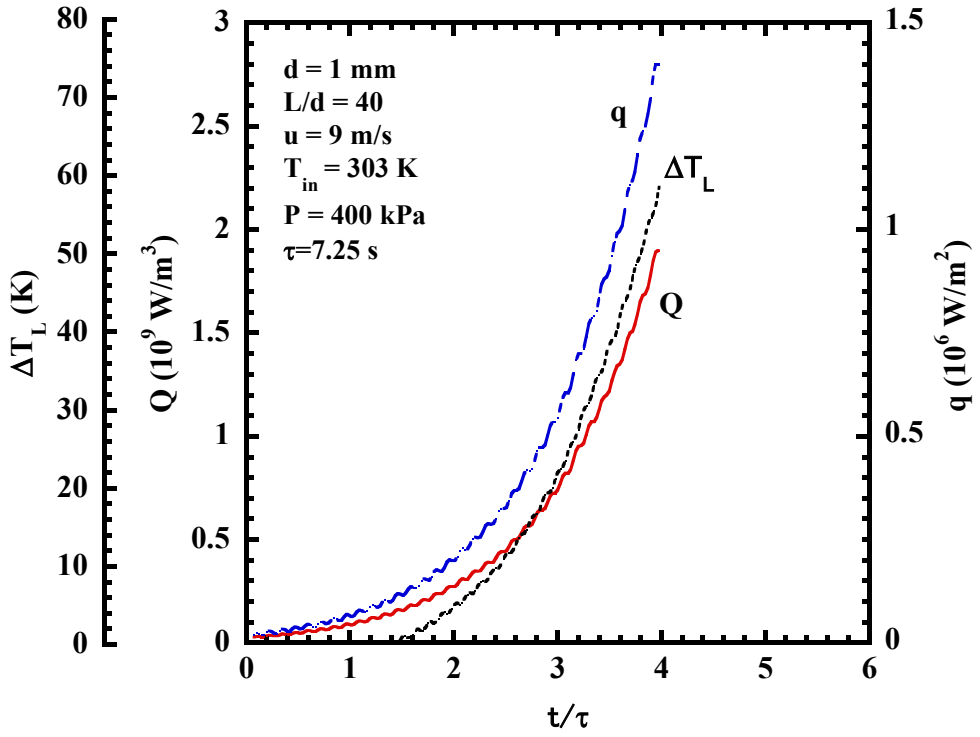

(a)

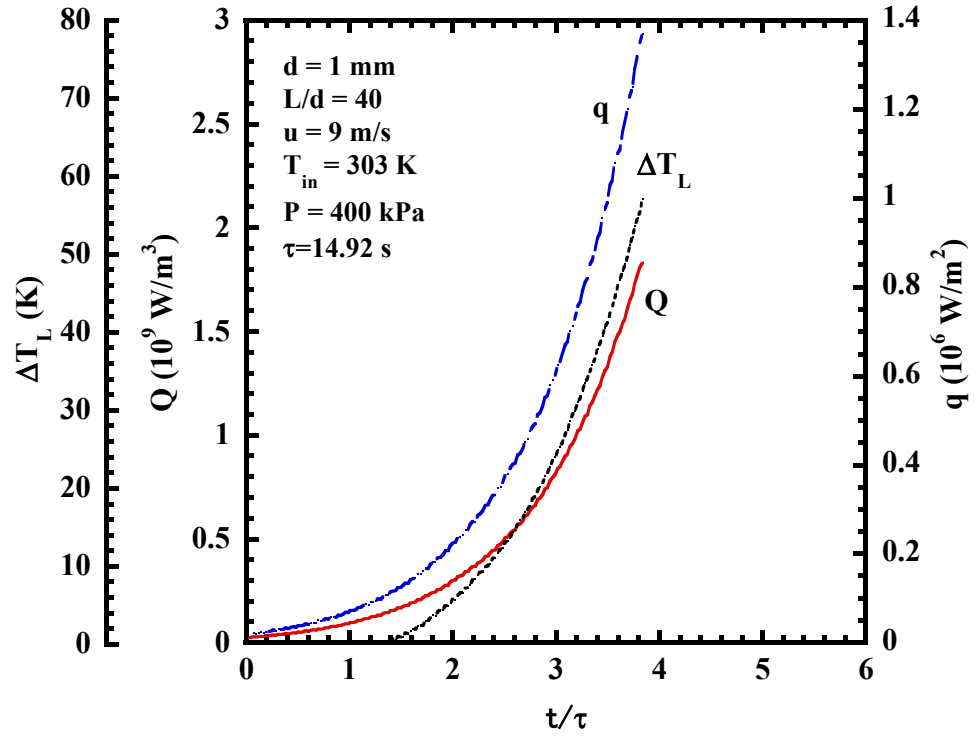

(b)

Fig. 4.4 The relation of Q, ΔT_L, q with time at period of 7.25 s (a) and 14.92 s (b)

4.1.3 Effect of u, L/d, μ/μ_w, Pr and Re

This section qualitatively and quantitatively discusses the effects of flow velocity, u, the ratio of heated length to inner diameter, L/d, viscosity ratio, μ/μ_w (μ is the viscosity of the fluid evaluated at its mainstream temperature and μ_w is the viscosity evaluated at the wall temperature), Prandtl number, Pr, and Reynolds number, Re, on the steady state turbulent heat transfer process.

4.1.3.1 Effect of u

Figure 4.5 gives a clear indication how the flow velocity, u, affects the heat transfer coefficient, h. The heat transfer coefficients for an inner diameter of 1.8 mm, a heated length of 40.2 mm, ΔT_L of 30, 40, 50, 60 K and inlet liquid temperature of 303 K were shown versus the flow velocity. The heat transfer coefficient linearly increases with the increase of flow velocity. The heat transfer coefficient anywhere along the surface is directly related to the temperature gradient at that location. Flow velocity will have a strong effect on the temperature profile, thereby influencing the convective heat transfer process.

The slope, n, on the log-log coordinate system was obtained by the least-squares method. It is about 1.2 for both d = 1.8 mm and d = 1 mm as shown in Fig. 4.5 and Fig. 4.6, respectively. However, in the case of d=2.8 mm, the slope is determined as 0.8 as

shown in Fig. 4.7. This shows that the dependency of heat transfer coefficients on flow velocity is affected by the tube inner diameter somewhat. The dependency of heat transfer coefficients on flow velocity for d = 2.8 mm coincides with conventional correlations proposed by Dittus & Boelter [4] and Nusselt [5]. The cases of d = 1 and 1.8 m show different trend. It seems that the small inner diameter could affect the convective heat transfer process.

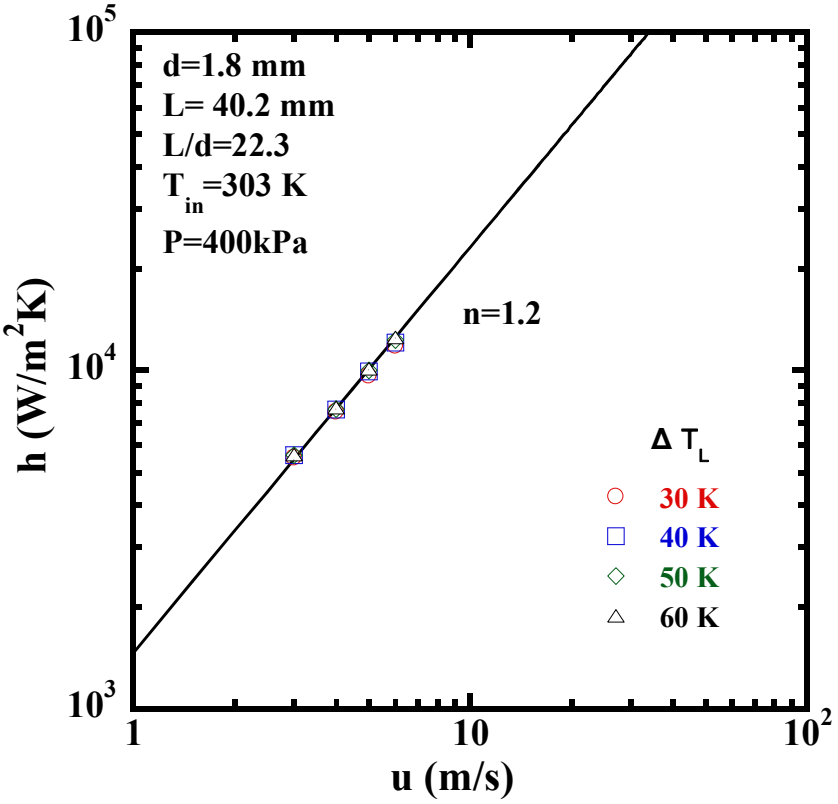

Fig. 4.5 h varies with u at different ΔT_L for d=1.8 mm

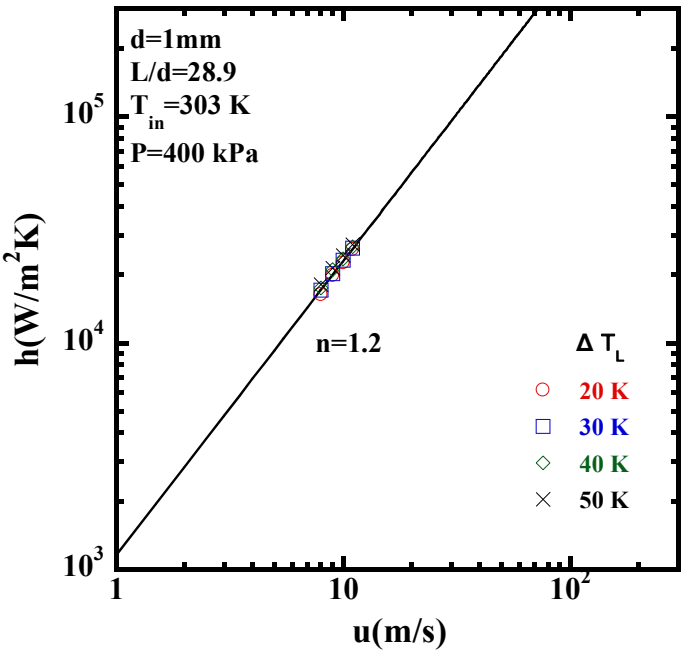

Fig. 4.6 h varies with u at different ΔT_L for d=1 mm

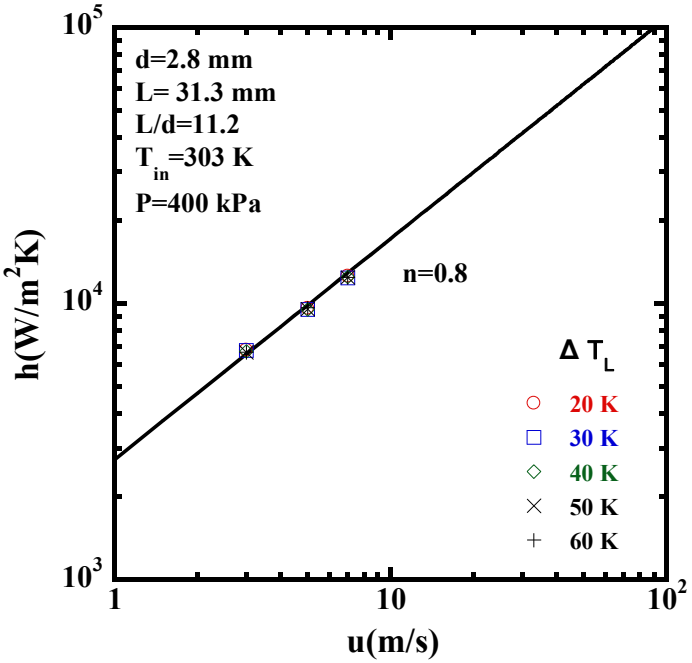

Fig. 4.7 h varies with u at different ΔT_L for d=2.8 mm

4.1.3.2 Effect of L/d

The effect of L/d on the heat transfer coefficient is shown in Fig. 4.8 at flow velocity of 5 m/s and inlet liquid temperature of 303 K for ΔT_L of 30, 40, 50 and 60 K. The heat transfer coefficient in the thermally fully developed region is much lower than that in the thermal entrance region. Thus, the heat transfer coefficient decreases with an increase in the L/d. The slope, n, on this log-log graph was determined as -0.08. The thermal entrance region effects were taken into account through the term $(L/d)^{-0.08}$. The thermal entrance effects tend to increase heat transfer coefficient, especially for relatively short tubes. The variation of the heat transfer coefficient with L/d for inner diameters of 1 mm and 2.8 mm shows the same trend as shown in Fig. 4.9 and Fig. 4.10, respectively.

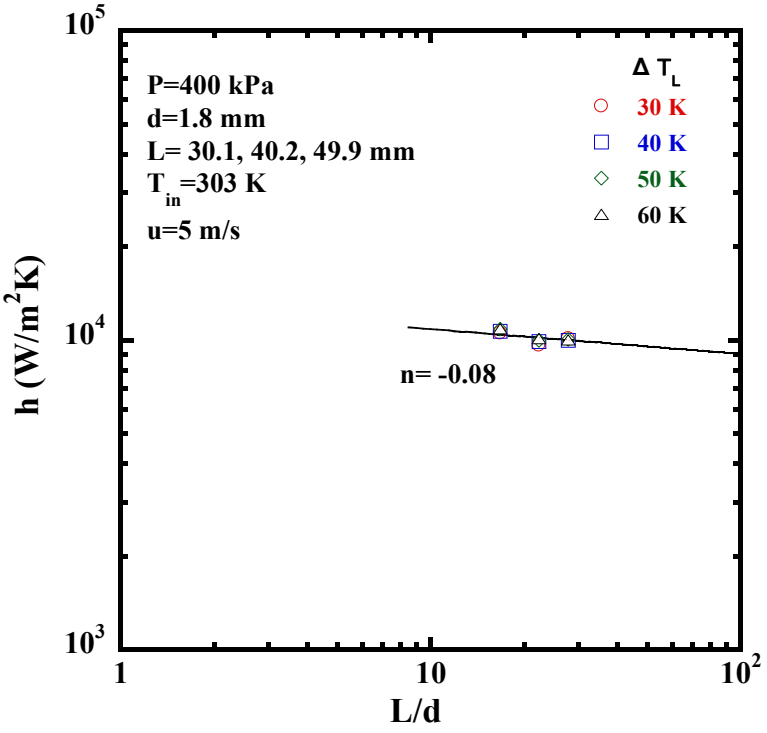

Fig. 4.8 Effect of L/d on h for d=1.8 mm

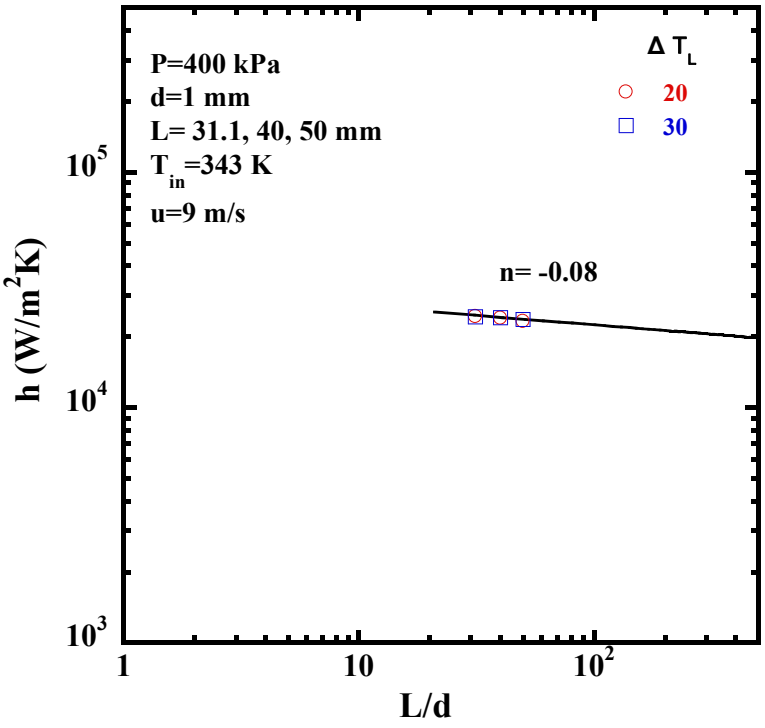

Fig. 4.9 Effect of *L/d* on *h* for *d*=1 mm

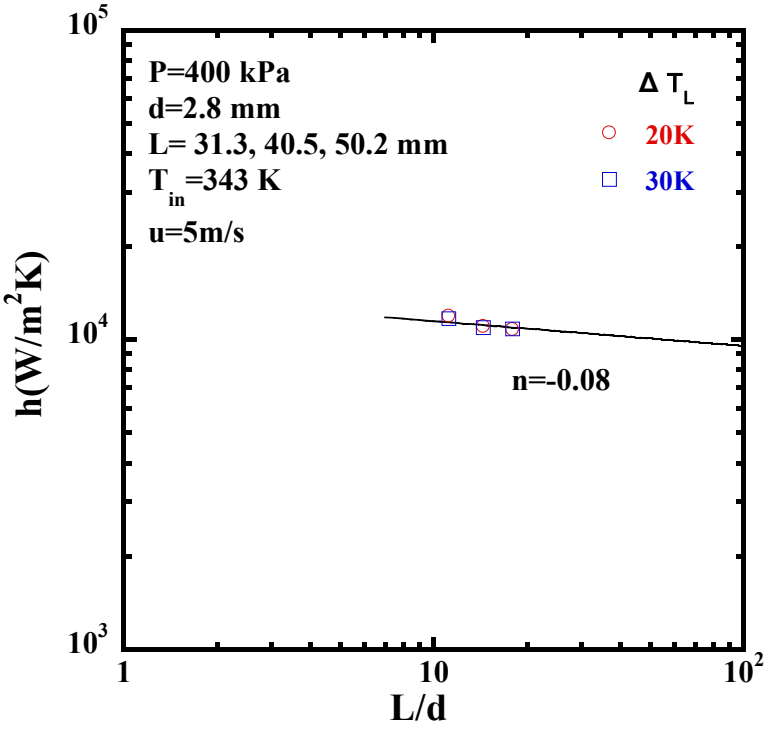

Fig. 4.10 Effect of *L/d* on *h* for *d*=2.8 mm

4.1.3.3 Effect of μ/μ_w

Figure 4.11 describes the dependence of dynamic viscosity on temperature for FC-72 and water. For both of them, the dynamic viscosity decreases obviously with increase of temperature. Hata et al [6] confirmed the effect of dynamic viscosity of water on heat transfer coefficient. Considering the viscosity variation upon temperature of FC-72, it is reasonable to assume that viscosity of FC-72 would also impose effect on heat transfer process. The results are shown in Fig. 4.12 to Fig. 4.14.

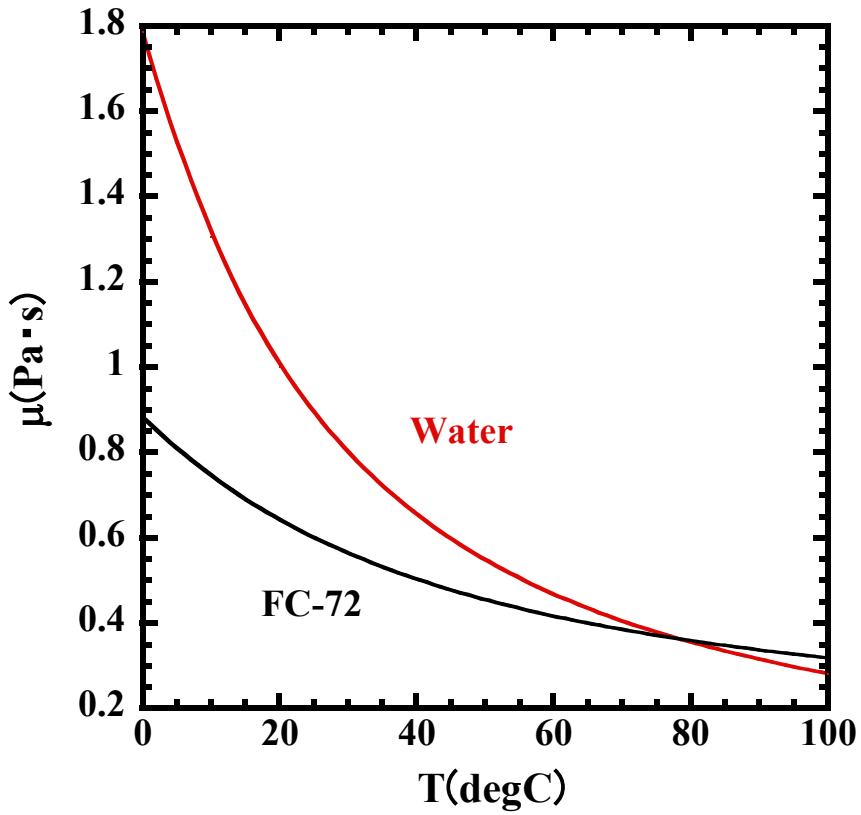

Fig. 4.11 Dynamic viscosity over temperature for FC-72 and water

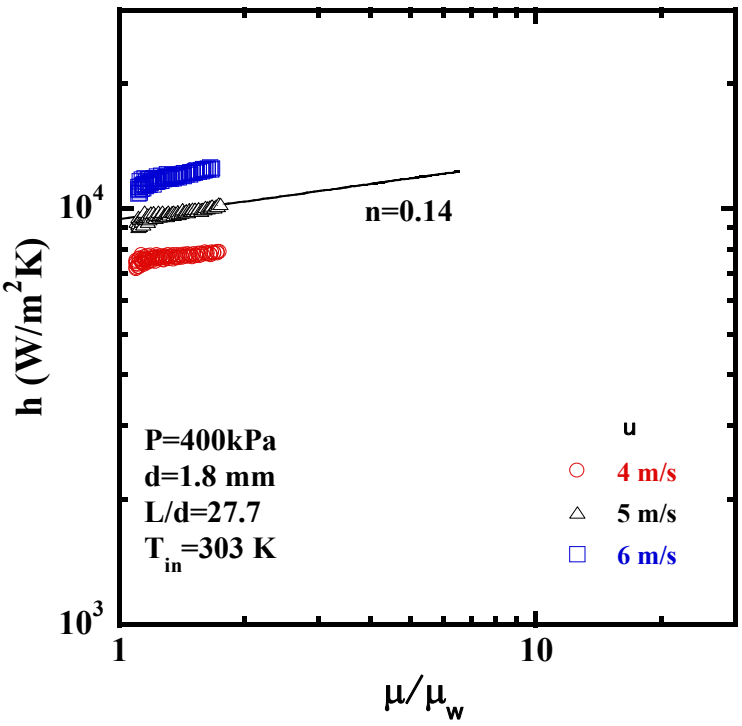

Fig. 4.12 Effect of μ/μ_w on h for d=1.8 mm

The ratio of μ/μ_w was introduced to take into account the variation between the viscosities of the fluid near the wall and that in the bulk of the liquid for high surface temperature difference, ΔT_L. Where, μ is the viscosity of the fluid evaluated at its mainstream temperature and μ_w is the viscosity evaluated at the wall temperature. Figure 4.12 shows the variation of heat transfer coefficient as a function of μ/μ_w for an inner diameter of 1.8 mm, a heated length of 49.9 mm and inlet temperature of 303 K at flow velocities of 4, 5, and 6 m/s. Because the tube wall is hot, the viscosity of the fluid near the wall will be smaller than that of the fluid in the bulk. This increases the velocity gradient near the wall. Therefore, the heat transfer coefficient becomes higher compared

with that obtained by assuming that the fluid is at an evenly distributed bulk liquid temperature. Moreover, in small sized channels the difference between inner surface temperature and average bulk liquid temperature can be larger than in conventional tubes. The heat transfer coefficient becomes linearly higher with the increase of μ/μ_w with a slope, n, of 0.14 for d = 1, 1.8 and 2.8 mm as shown in Fig. 4.12 to Fig. 4.14. This trend is the same with Sider and Tate' correlation [7].

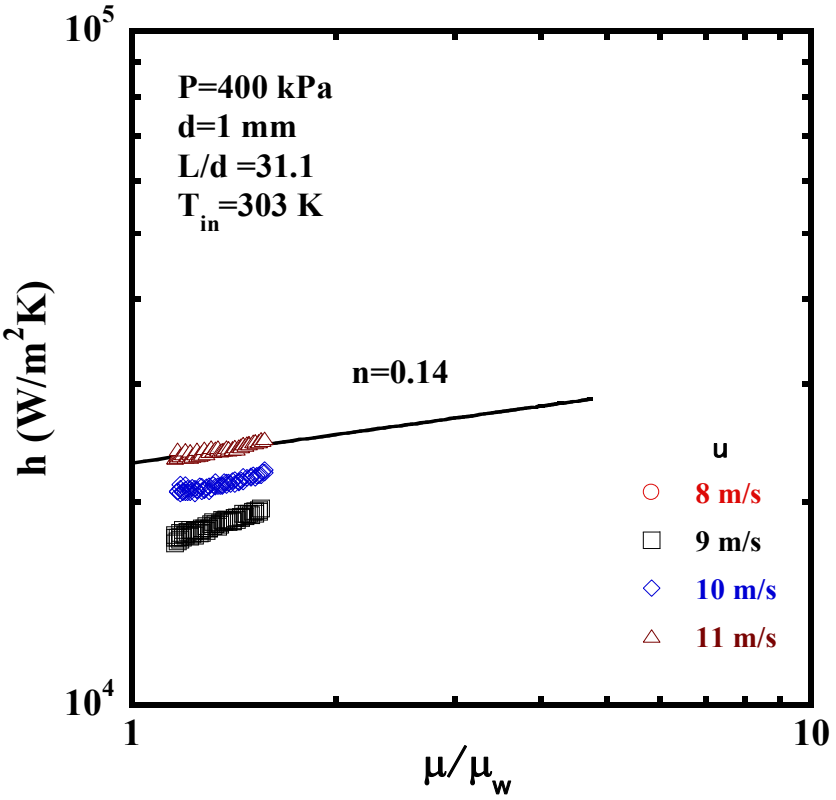

Fig. 4.13 Effect of μ/μ_w on h for d=1mm

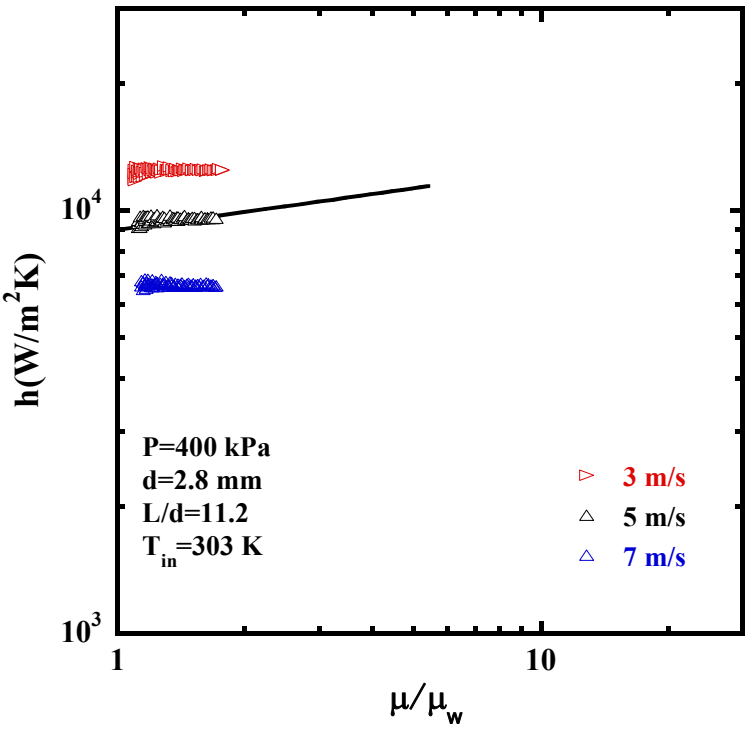

Fig. 4.14 Effect of μ/μ_w on h for d=2.8 mm

4.1.3.4 Effect of *Pr*

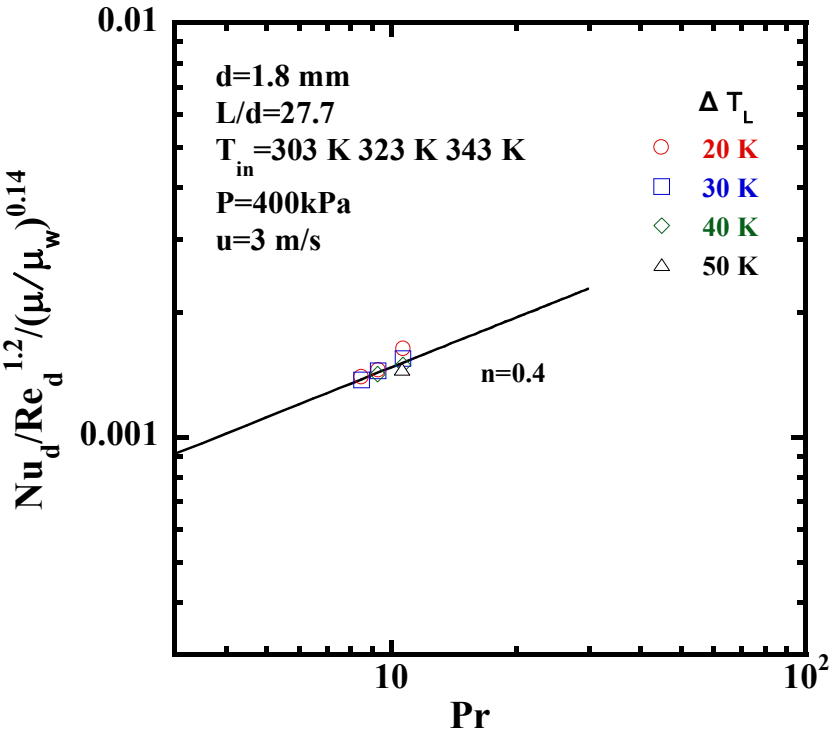

Fig. 4.15 Relation between $Nu_d/Re_d^{1.2}/(\mu/\mu_w)^{0.14}$ and Pr for d=1.8 mm

It has been clarified that the heat transfer coefficients, h, for d = 1 and 1.8 mm are proportional to $u^{1.2}$, $(L/d)^{-0.08}$ and $(\mu/\mu_w)^{0.14}$ and the heat transfer coefficients, h, for d =2.8 mm are proportional to $u^{0.8}$, $(L/d)^{-0.08}$ and $(\mu/\mu_w)^{0.14}$ based on the experimental data. The dependence of heat transfer on the Pr is shown in Fig. 4.15 in the form of $\log[Nu_d/Re_d^{1.2}/(\mu/\mu_w)^{0.14}]$ versus $\log(Pr)$ for an inner diameter of 1.8 mm, a heated length of 49.9 mm and inlet temperatures of 303, 323, 343 K at flow velocity of 3 m/s. The values of $Nu_d/Re_d^{1.2}/(\mu/\mu_w)^{0.14}$ linearly increase with the increase of Pr and the slope, n, is determined as 0.4. As shown in Fig. 4.16, the values of $Nu_d/Re_d^{0.8}/(\mu/\mu_w)^{0.14}$ also increase with the increase of Pr with slope of 0.4 for d = 2.8 mm. The trend of $Pr^{0.4}$ dependence accords with other well-known correlations [6,7].

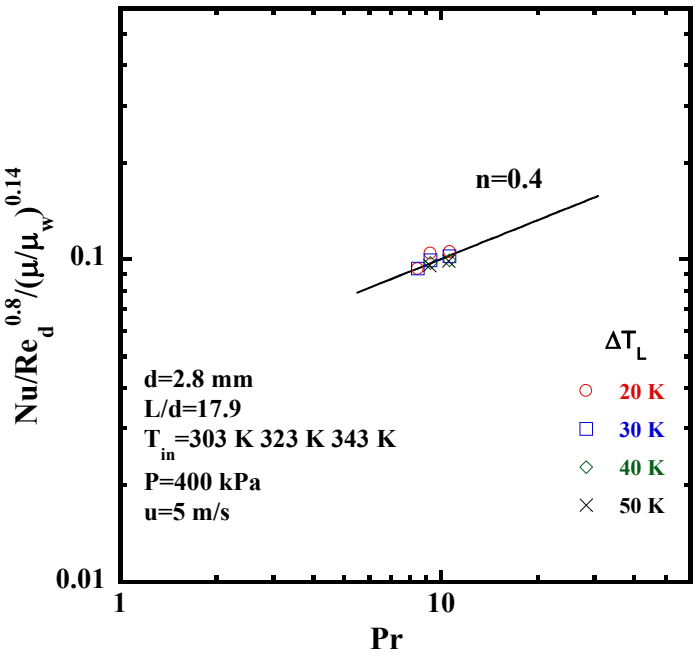

Fig. 4.16 Relation between $Nu_d/Re_d^{1.2}/(\mu/\mu_w)^{0.14}$ and Pr for d=2.8 mm

4.1.3.5 Effect of *Re*

To estimate the dependence of the heat transfer on the Re_d, the experiment data were plotted in Fig. 4.17 as a function of Re_d. This figure shows all the data measured for inner diameters of 1, 1.8 and 2.8 mm, heated lengths of 30 to 50 mm, inlet temperatures of 303, 323, 343 K and exponential periods of 6.38 s to 15.48 s at various flow velocities. The exponent, n, for d = 2.8 mm is finally determined as 0.8, which is the same with conventional correlations [4, 5]. However, the value of the exponent for d = 1 and 1.8 mm is 1.2, larger than 0.8 for conventional sized channels. Similar result has also been reported by Yu et al [8] and Adams et al. [9] for small sized channels. As mentioned earlier, Kandlikar [10] classified channels with hydraulic diameters of 0.01-0.2 mm as micro-channels, hydraulic diameters of 0.2-3 mm as mini-channels, and hydraulic diameters greater than 3 mm as conventional sized channels. The inner diameters of test tube used in this study are located in the range of min-channels. For d = 1 and 1.8 mm, the data show anomalous trend ($Re_d^{1.2}$) compared with correlations for conventional sized channels ($Re_d^{0.8}$). Inner diameter of 2.8 mm is near the threshold between min-channel and conventional sized channel. It might be the reason why dependence on Re_d for d = 2.8 mm is the same with conventional correlations ($Re_d^{0.8}$).

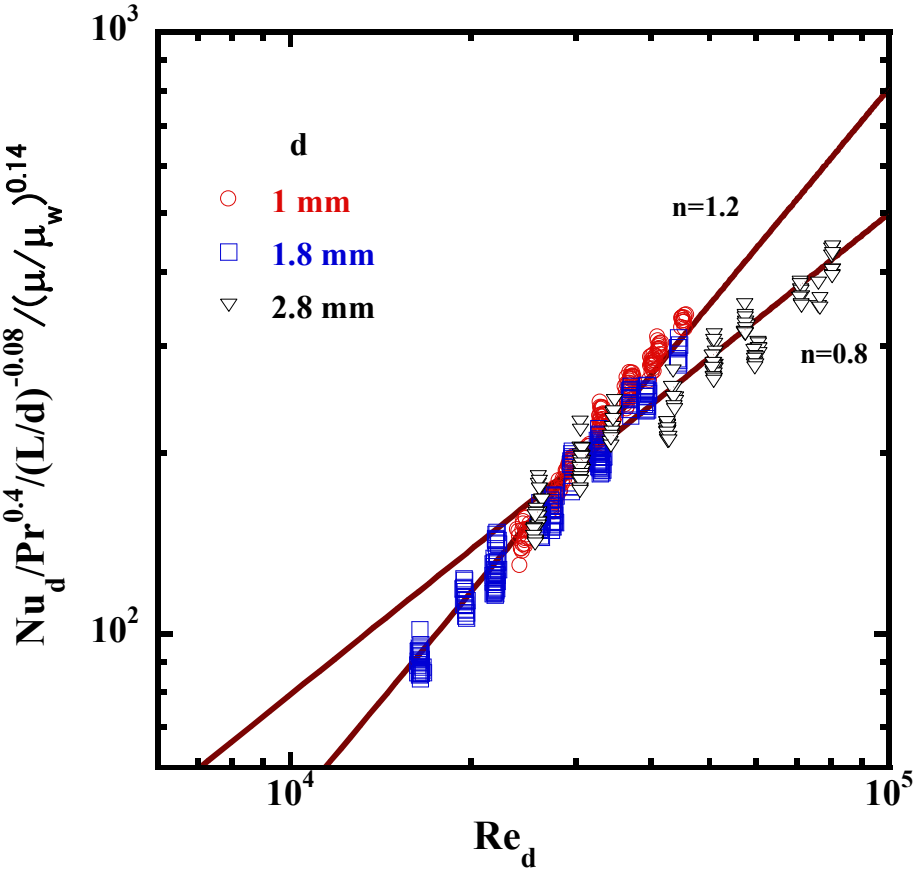

Fig. 4.17 Relation between $Nu_d/Pr^{0.4}/(L/d)^{-0.08}/(\mu/\mu_w)^{0.14}$ and Re for d=1, 1.8, 2.8 mm

4.1.4 Comparison with well-accepted correlations

The experimental Nu_d data were compared with the conventional correlations and the correlation developed for prediction of Nu_d in small sized channels.

4.1.4.1 Comparison with conventional correlations

A traditional expression for single-phase forced convection in macro channels was suggested by Dittus and Boelter [4] for Re_d>10000 as follows:

$$Nu_d = 0.023\,\mathrm{Re}_d^{0.8}\,\mathrm{Pr}^{0.4} \tag{4.1}$$

A more accurate correlation used for comparison was developed by Gnielinski [11] for turbulent flow over range of $3000 < Re_d < 5 \times 10^6$, as follows:

$$Nu_d = \frac{(f/8)\,\mathrm{Re}_d\,\mathrm{Pr}}{1.07 + 12.7(f/8)^{1/2}(\mathrm{Pr}^{2/3} - 1)}(1 + d/L)^{2/3} \tag{4.2}$$

Here, f is the Fanning friction factor for a smooth tube. It is calculated by using the Filonenko correlation [4.3] after setting the relative roughness equal zero.

$$f = (3.64 \log_{10} \mathrm{Re}_d - 3.28)^{-2} \tag{4.3}$$

Comparisons were also conducted with the following correlation presented by Hata et al. [6] for fully developed turbulent regime and inner tube diameter of 3, 6 and 9 mm:

$$Nu_d = 0.02\,\mathrm{Re}_d^{0.85}\,\mathrm{Pr}^{0.4}(\mathrm{L}/d)^{-0.08}(\mu/\mu_w)^{0.14} \tag{4.4}$$

Figure 4.18 shows the comparison of the experimental Nu_d with classical correlations developed for conventional sized channels. This figure clearly indicates that the experimental Nu_d values are generally higher than those predicted by the classical correlations for conventional sized channels. The deviation between the experimental and predicted Nu_d is more significant for higher Re_d for d = 1 and 1.8 mm. Namely, the Nu_d in turbulent flow depends more heavily on Re_d compared to macroscale correlations for d = 1 and 1.8 mm.

It is assumed that the deviation is due to effect of large relative roughness. The

roughness effect is generally negligible for conventional macroscale channels. But the roughness effect in small sized channels may increase the wall shear stress, thereby decreasing the thickness of conductive sublayer. In this way, the heat transfer rate in small sized channel is enhanced.

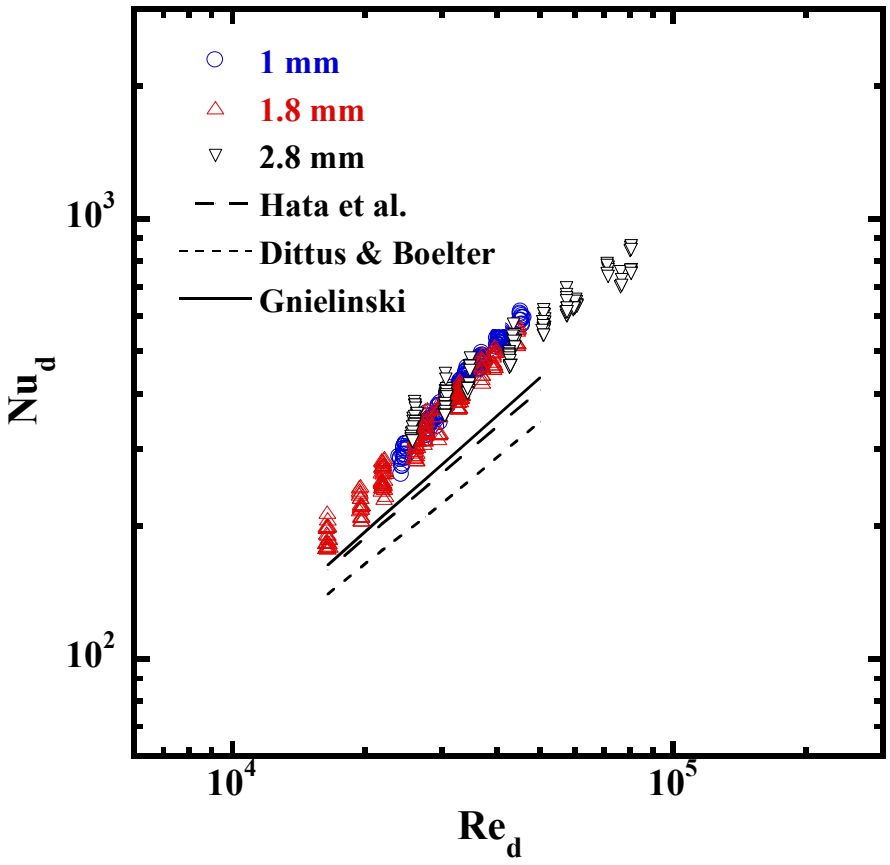

Fig. 4.18 Comparison between experimental Nu_d and classical correlations for conventional sized channels as a function of Re_d

4.1.4.2 Comparison with correlation for small sized channels

Adams et al. [9] investigated single-phase heat transfer in tubes with small diameters of 0.76 and 1.09 mm using water as working fluid. They modified Gnielinski'

correlation as follows:

$$Nu_d = Nu_{Gnielinski}(1+F) \tag{4.5}$$

where F is given by:

$$F = (7.6\times10^{-5})\,\mathrm{Re}\left(1-(d/d_0)^2\right) \tag{4.6}$$

where d_0 = 1.164 mm.

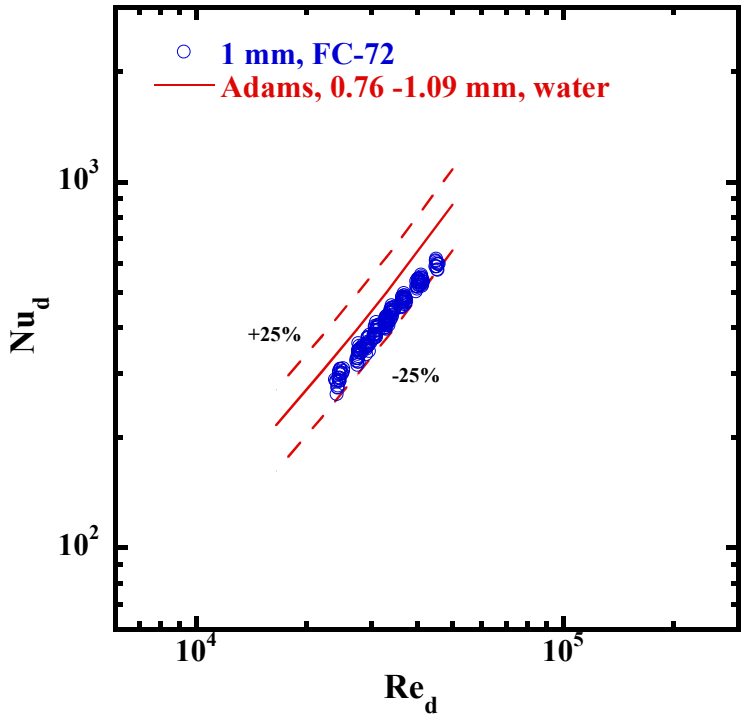

Fig. 4.19 Comparison between experimental Nu_d for d=1 mm and Adams' correlation

As shown in Fig. 4.19, the experimental data for FC-72 with tube diameter of 1 mm was compared with Adams' correlation, which was developed for water flowing through 0.76 and 1.09 mm diameter tubes. The experimental data show the same trend as Adams' correlation, and they fall along this correlation within -25%. The experimental data for

FC-72 are slightly lower than Adams' data obtained with water in almost the same diameters. This might be due to the lower thermal conductivity of FC-72.

4.1.5 Steady state turbulent heat transfer correlations

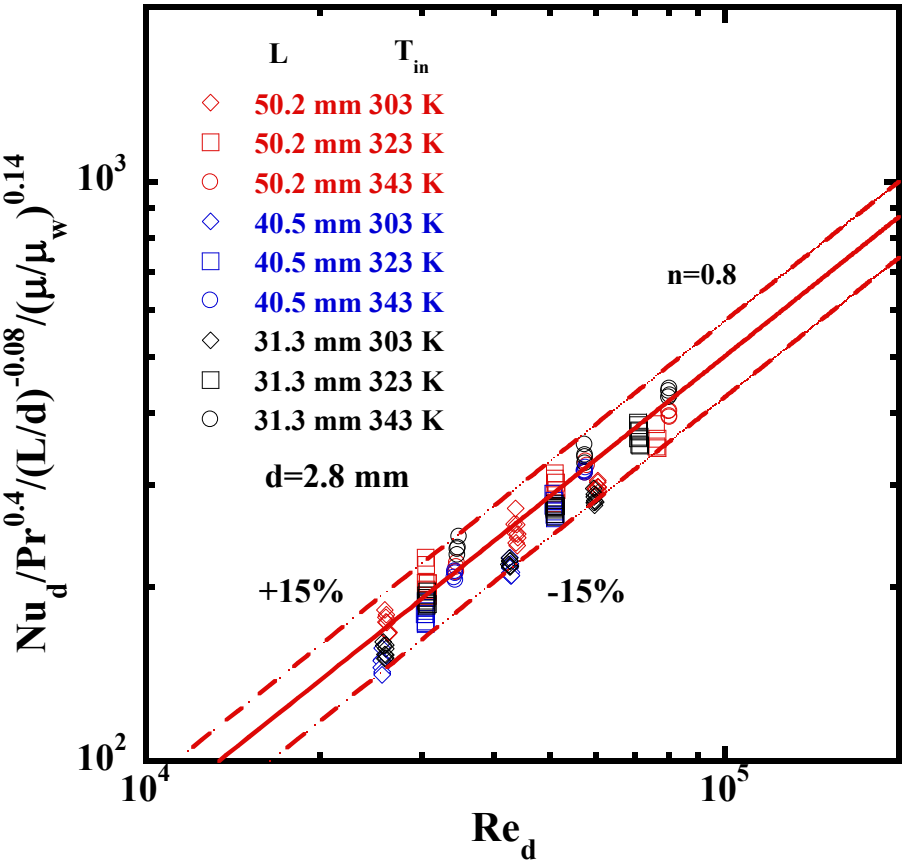

Fig. 4.20 Relation between $Nu_d/Pr^{0.4}/(L/d)^{-0.08}/(\mu/\mu_w)^{0.14}$ and Re_d for d=2.8 mm

Figure 4.20 shows all the data measured for inner tube diameters of 2.8 mm, heated lengths of 31.3, 40.5 and 50.2 mm, inlet temperatures of 303, 323, 343 K, inlet velocities of 3, 5, 7 m/s and exponential periods of 6.4-14.2 s. The empirical correlation is also depicted by solid line in this figure. A value for the constant coefficient was

determined as 0.052 by the least-squares method and the turbulent heat transfer correlation for d = 2.8 mm was developed as Eq. (4.7). The final correlation equation represents the experimental data (154 points) within ±15%.

$$Nu_d = 0.052\,\mathrm{Re}_d^{0.8}\,\mathrm{Pr}^{0.4}(\mathrm{L}/d)^{-0.08}(\mu/\mu_w)^{0.14} \tag{4.7}$$

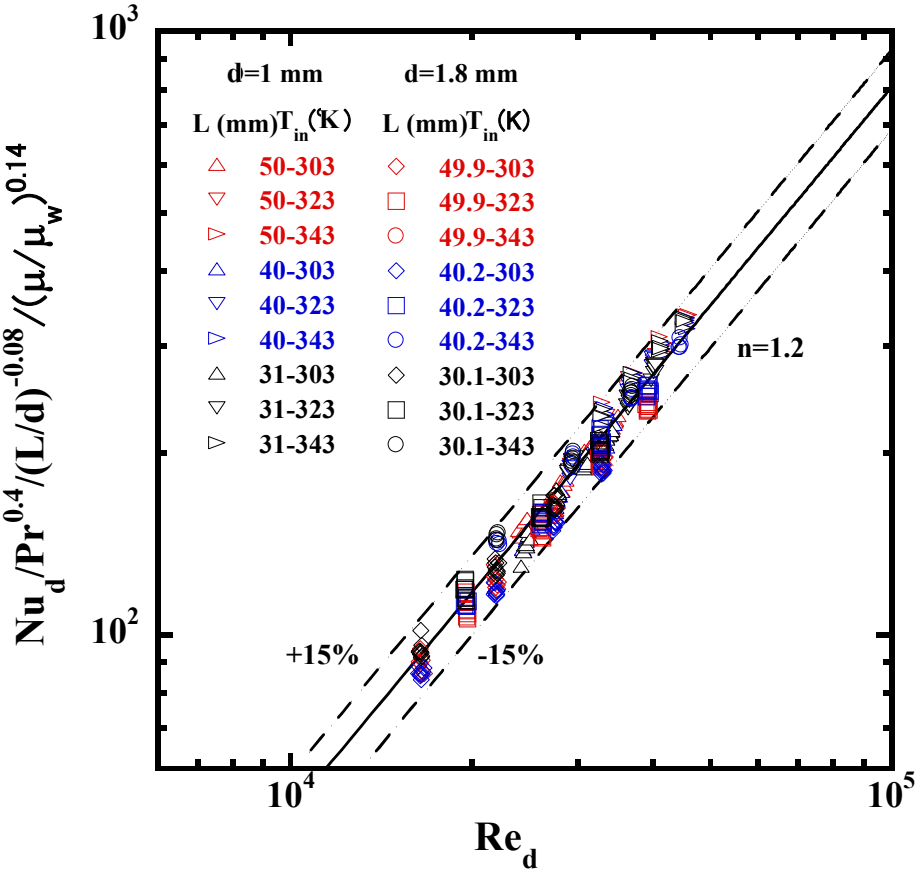

Fig. 4.21 Relation between $Nu_d/Pr^{0.4}/(L/d)^{-0.08}/(\mu/\mu_w)^{0.14}$ and Re_d for d=1 and 1.8 mm

Figure 4.21 shows the data measured for inner tube diameters of 1 and 1.8 mm, heated lengths of 30 to 50 mm, inlet temperatures of 303, 323, 343 K, and exponential periods of 6.4-14.2 s at various flow velocities. The constant coefficient was determined

as 0.000809 by the least-squares method. The turbulent heat transfer correlation for d = 1 and 1.8 mm was derived as Eq. (4.8). As shown in Fig. 4.21, the experimental data (440 points) fall along the proposed empirical correlation shown in solid line within ±15%.

$$Nu_d = (8.09 \times 10^{-4})\,\mathrm{Re}_d^{1.2}\,\mathrm{Pr}^{0.4}(\mathrm{L}/d)^{-0.08}(\mu/\mu_w)^{0.14} \tag{4.8}$$

4.2 Transient Turbulent Heat Transfer

Transient turbulent heat transfer involves dynamically varying heat flux or temperature. In this study, the transient turbulent heat transfer caused by exponentially increasing heat inputs has been systematically investigated for the vertical small diameter tubes.

Section 4.2 firstly introduces the experimental conditions, especially the definition of transient state. Then the effects of flow velocity, exponential period and tube inner diameter on transient turbulent heat transfer process are explored in detail. Finally, transient turbulent heat transfer correlation is proposed by combing the steady state values with effects of the Fourier number and tube inner diameter.

4.2.1 Experimental conditions

Transient turbulent heat transfer caused by various exponentially increasing heat inputs was experimentally investigated for several flow velocities and inlet liquid temperatures for small diameter tubes with different inner diameters and heated lengths at a certain pressure. The experimental conditions for transient study are almost identical with steady state experiments as tabulated in Table 4.1, except the exponential periods of heat generation rate. The exponential periods were varied from 27.3 ms to 15.48 s for d = 1 mm, from 15.7 ms to 14 s for d = 1.8 mm and from 25.6 ms to 14.2 s for d = 2.8 mm.

4.2.2 Characteristics of heat generation rate, heat flux and surface temperature difference

Fgure 4.22 shows typical time dependence of heat generation rate, Q, heat flux, q and surface temperature difference, ΔT_L (=T_s-T_L) at the inlet liquid temperature of 323 K, flow velocity of 11 m/s and exponential periods of 80.8 ms, 382.4 ms and 1.5 s, respectively. As shown in Fig. 4.22, heat flux and surface temperature difference increase exponentially with the increase of heat generation rate. A shorter period means a higher heat generation rate. Thus heat flux and surface temperature difference also

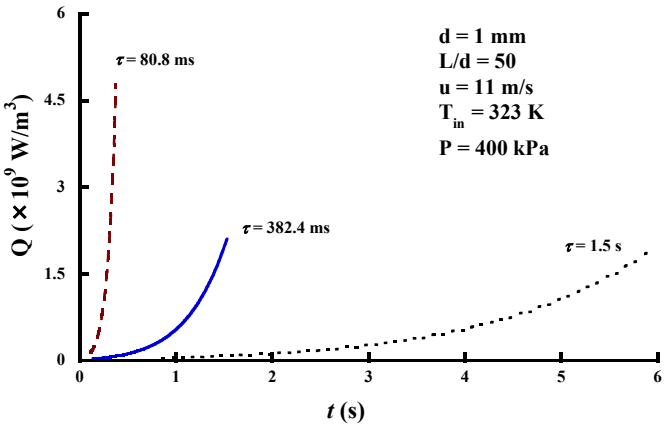

(a) Heat generation rate, Q

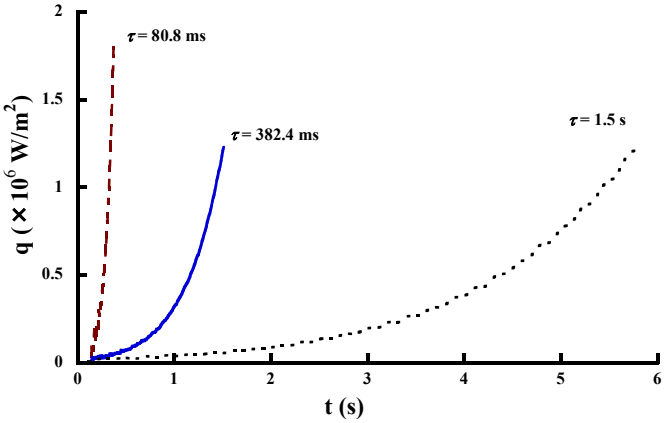

(b) Heat flux, q

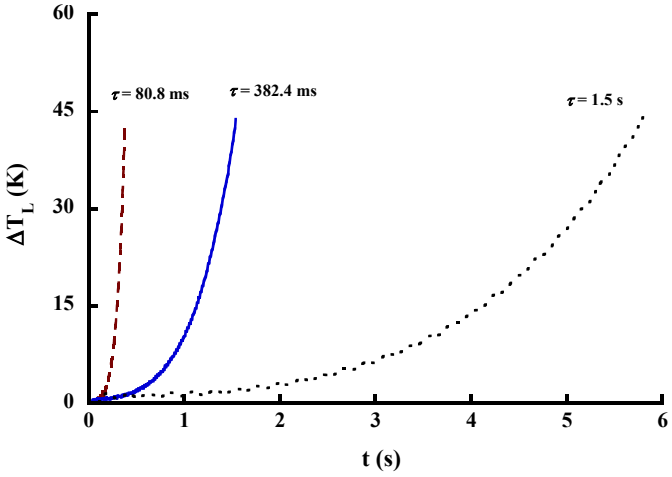

(c) Surface temperature difference, ΔT_L

Fig. 4.22 Time dependency of Q, q and ΔT_L at various τ

increase more rapidly while the period is shorter. Those values increase slower when the period is longer. It is clarified that the surface temperature difference and heat flux increase exponentially as the heat generation rate increases with exponential function of $Q = Q_0 \exp(t/\tau)$.

4.2.3 Transient heat transfer coefficient

Transient heat transfer coefficient, h, can be obtained from the measured heat flux and surface temperature difference ($h=q/\Delta T_L$). The instantaneous heat transfer coefficients were measured using a tube with inner diameter of 1.8 mm and heated length of 49.9 mm for flow velocity of 6 m/s, inlet liquid temperature of 323 K and exponential periods of 0.15, 1.4 and 13.9 s. The data was plotted against elapsed time and surface temperature difference in Fig. 4.23 and Fig. 4.24, respectively. As shown in those figures, the heat transfer coefficients dip and approach an asymptotic value at every period. Some researchers [12, 13] considered that the temperature is uniform in the liquid at the initial stage. The heat transfer coefficients were mainly determined by the transient conduction in the fluid. With the increase of thermal boundary layer and development of temperature distribution, the heat transfer coefficients approach the asymptotic value or steady state value. This process was influenced by the exponential

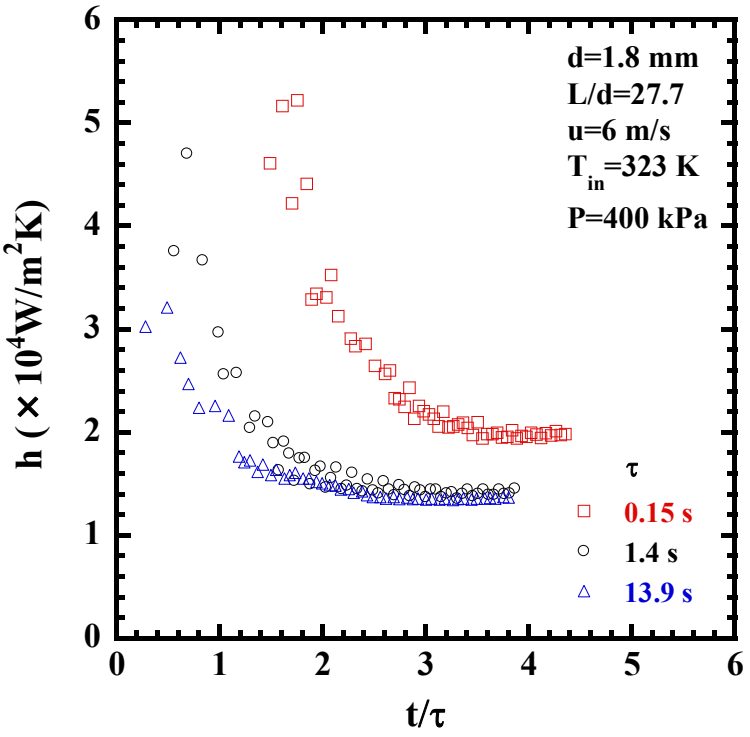

Fig. 4.23 Instantaneous h versus t/τ at different τ

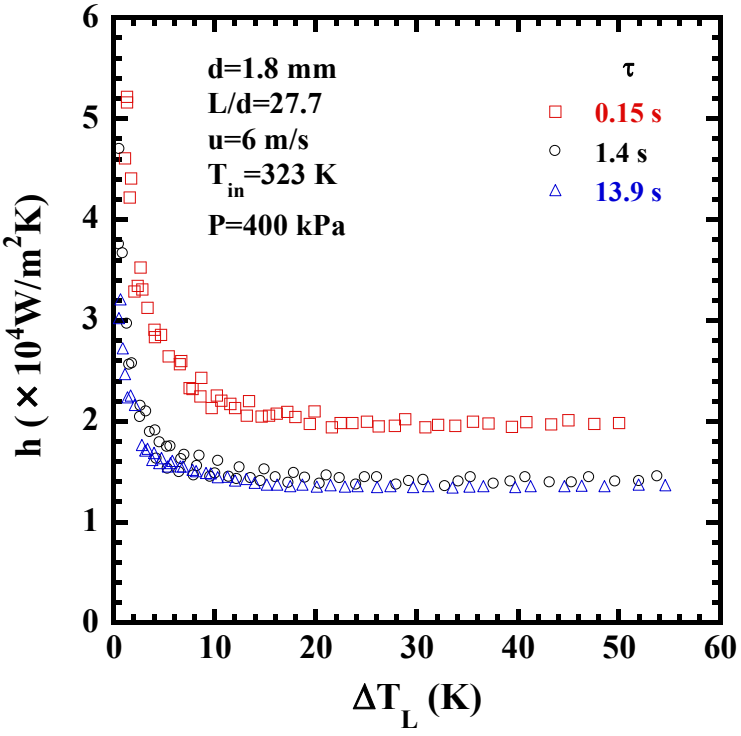

Fig. 4.24 Instantaneous h versus ΔT_L at different τ

periods of heat generation rate. It was also found that the transient heat transfer coefficients decrease and approach asymptotic values for all periods, velocities and other experimental conditions. Particular attention should be paid to the asymptotic value for each exponential period. Thus the data at surface temperature differences, ΔT_L, of 20, 30, 40 and 50 K should be taken as representative data hereinafter.

Figure 4.25 shows the relation of heat transfer coefficients, h and the exponential periods, τ, with flow velocity, u, as a parameter. The heat transfer coefficients measured using 1 mm diameter tube for flow velocities of 8, 9, 10 and 11 m/s, and inlet temperature of 303 K were plotted with the surface temperature differences of 20, 30, 40 and 50 K. With the increase of exponential periods, the heat transfer coefficients gradually decrease and approach an asymptotic value at each velocity. This trend is similar to observations by other researchers [1-3]. As shown in Fig. 4.25, both flow velocity and exponential period affect the transient heat transfer process.

As stated earlier, the experiments with exponential periods larger than 5 s can be practically regarded as steady state experiments because the increase of heat generation rate is so slow that the thermal boundary layer next to the tube inner surface is fully developed. The heat transfer coefficients did not depend upon the exponential period.

With a decrease of period from about 5 s, the heat transfer coefficients slightly

increase. The region from period of 5 s to a period at which heat transfer coefficient is 5% larger than the steady state value is considered as quasi steady-state. The quasi-steady state region is from period of 5 s to period of about 1 s in Fig. 4.25. In this region, the heat transfer coefficients become obviously higher for higher flow velocities. Meanwhile, the heat transfer coefficients approach the steady state for each velocity and they are weakly affected by the periods. It seems that the usual forced convection heat transfer predominates the heat transfer process. The heat transfer process in this region transports heat through the thermal boundary layer influenced by the liquid flow conditions.

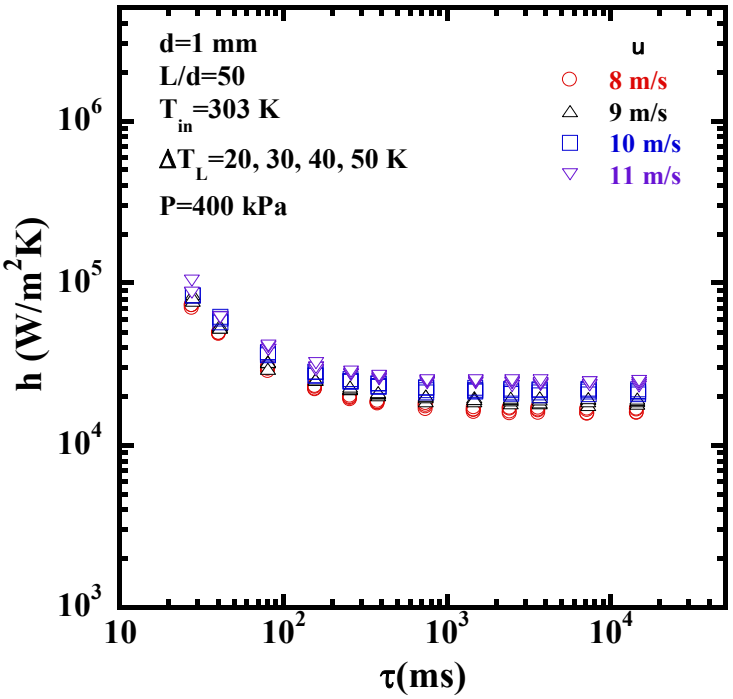

Fig. 4.25 h versus τ at various flow velocities for d = 1 mm

With further decrease of periods, the heat transfer coefficients gradually increase and they are much higher than that for steady state. This shows that the heat transfer process is in a transient state. The effect of heat conduction contribution increases gradually with a decrease of periods. And conductive heat transfer rather than the convective heat transfer component governs the heat transfer process for very short periods. This can be proven by the fact that the flow velocity has relatively small impact on heat transfer coefficients in the transient region. Liu [2] stated that the development of thermal boundary layer is slower than the increment of wall temperature due to very high heat generation rate. The heat conduction is high due to thin thermal boundary layer and severe temperature gradients. The heat conduction contribution on heat transfer process for transient state is higher than that for quasi-steady state.

The same results were also found for the tubes with inner diameters of 1.8 and 2.8 mm as shown in Fig. 4.26 and Fig. 4.27.

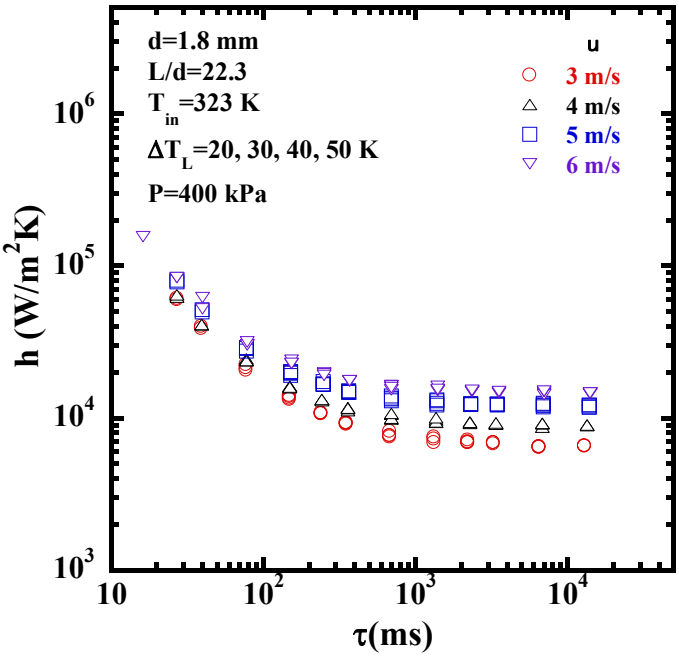

Fig. 4.26 h versus τ at various flow velocities for d = 1.8 mm

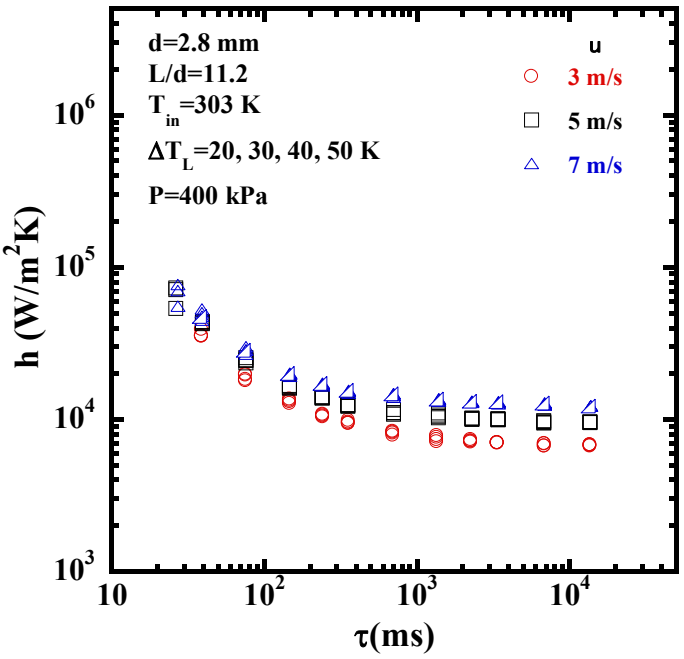

Fig. 4.27 h versus τ at various flow velocities for d = 2.8 mm

4.2.4 Transient Nusselt number

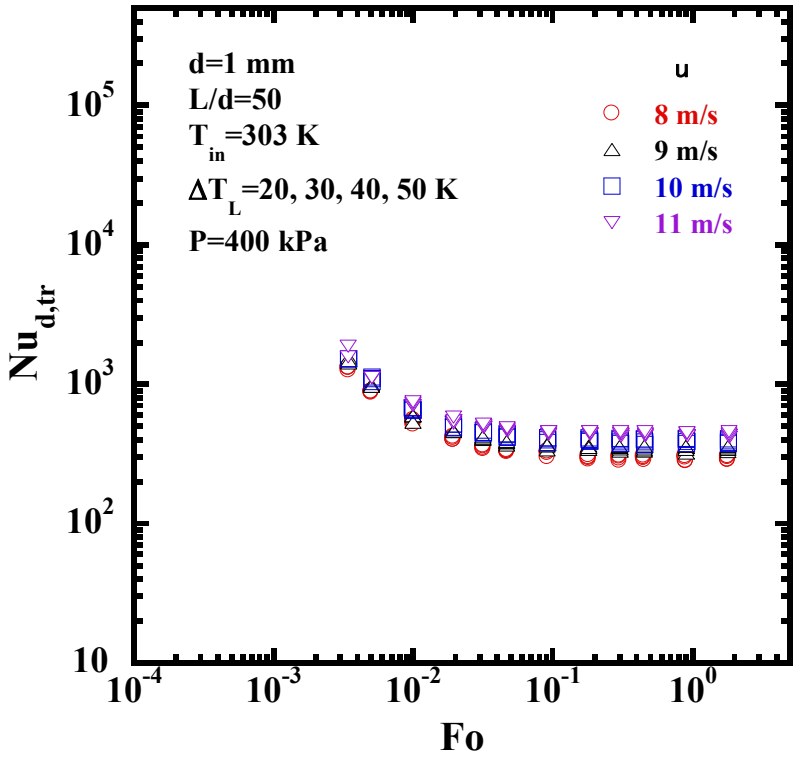

Fig. 4.28 $Nu_{d,tr}$ versus Fo at various flow velocities for d = 1 mm

The relations between heat transfer coefficients, h, and exponential periods, τ, for d = 1, 1.8 and 2.8 mm shown in Fig. 4.25 to Fig. 4.27 were rewitten in the form of variations of Nusselt number, $Nu_{d,tr}$, against Fourier number, Fo, in Fig. 4.28 to Fig. 4.30 with flow velocity as a parameter. The Fourier Number (Fo) is a dimensionless number which arises naturally from the nondimensionalization of the conduction equation. It is very widely used in the description and prediction of the temperature response of materials undergoing transient conductive heating or cooling.

Fourier number is defined as the following equation:

$$Fo = \frac{\alpha \tau}{r_i^2} \tag{4.9}$$

where α, τ, and r_i are the thermal diffusivity of liquid (m^2/s), exponential period (s), and the inner radius of test tube (m), respectively.

As shown in Fig. 4.28 to Fig. 4.30, $Nu_{d,tr}$ also decrease and approach an asymptotic value for each flow velocity. The flow velocity has clear influence on $Nu_{d,tr}$ for longer Fo, but exerts a relatively small effect on $Nu_{d,tr}$ for shorter Fo. The relation between $Nu_{d,tr}$ and Fo with flow velocity as a parameter shows the same trend as h versus τ for each velocity. Taking the aforementioned heat conduction contribution in the transient turbulent heat transfer process into consideration, it is reasonable to assume that the transient turbulent heat transfer characteristics could be described by introducing the non-denmensional time, Fo. As stated earlier, Fakoor-Pakdman [14,15] employed Fo to analyse the transient laminar forced convection heat transfer inside a circular tube under time-dependent heat flux. Kakaç [16] also numerically analyzed transient heat transfer for turbulent flow using Fo. Therefore, the empirical correlation for transient turbulent heat transfer caused by exponentially increasing heat inputs will be derived later by taking the effect of the non-dimensional time, Fo, into account.

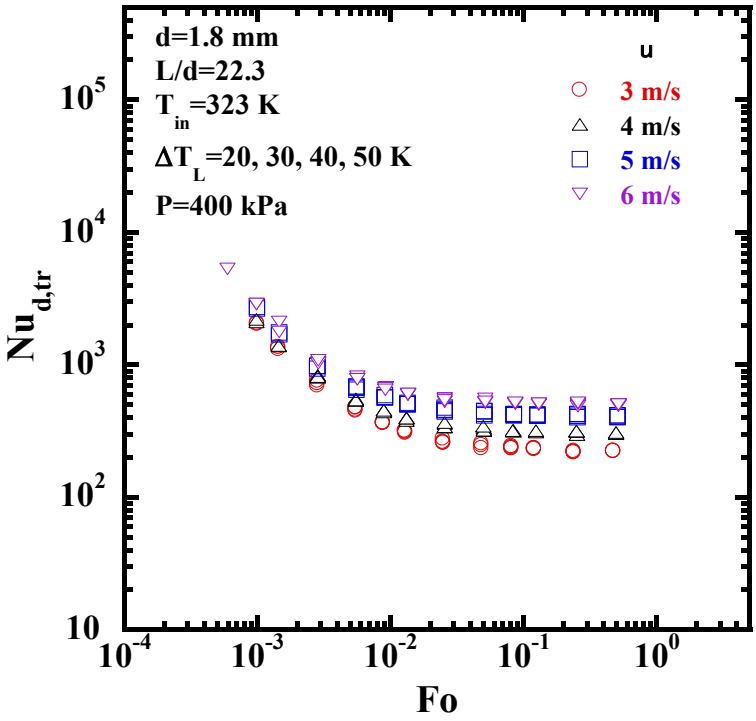

Fig. 4.29 $Nu_{d,tr}$ versus Fo at various flow velocities for d = 1.8 mm

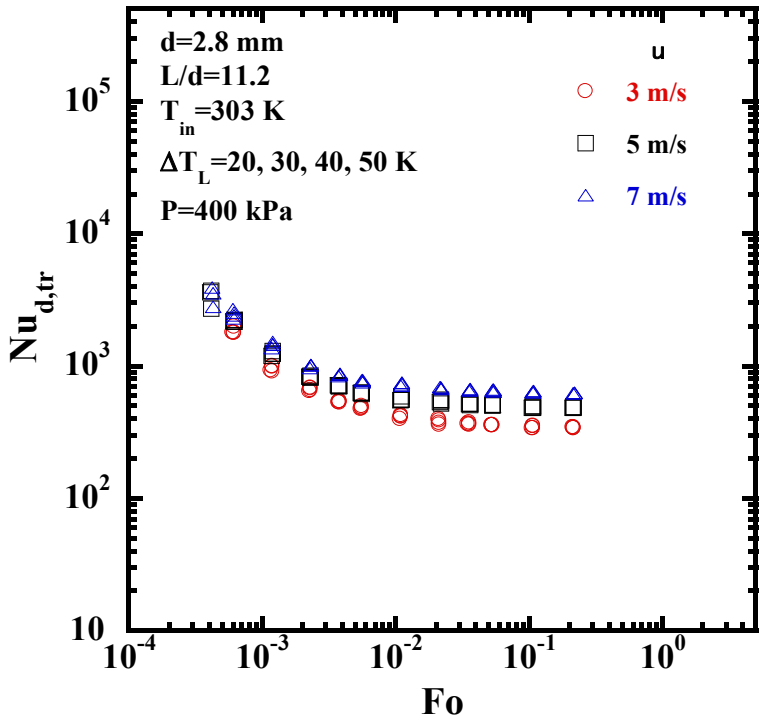

Fig. 4.30 $Nu_{d,tr}$ versus Fo at various flow velocities for d = 2.8 mm

4.2.5 Effect of *Fo* on transient turbulent heat transfer

Figures 4.31 to 4.33 show the ratios of transient turbulent Nusselt numbers, $Nu_{d,tr}$, to steady state ones, $Nu_{d,st,}$ against Fo for all the data measured using tubes with inner diameters of 1, 1.8 and 2.8 mm, respectively. The $Nu_{d,tr}$ /$Nu_{d,st}$ ratios approach unity for larger Fo, which implies the heat transfer shifts to steady state heat transfer. And the $Nu_{d,tr}$ /$Nu_{d,st}$ ratios increase with the decrease in Fo for smaller Fo. This means the heat transfer shifts to transient heat transfer. The transient turbulent heat transfer is affected by the Fo. It seems that the transient heat transfer correlation could be obtained by combing the steady state value with the effect of Fo since the increment of transient Nusselt numbers relative to steady state value depends on Fo. The largest transient turbulent heat transfer data become almost 6, 11 and 10 times the steady state for tube inner diameters of 1, 1.8 and 2.8 mm, respectively. For this reason, the study of transient turbulent heat transfer is fundamentally important for improving the reliability and efficiency of dynamic heat exchangers.

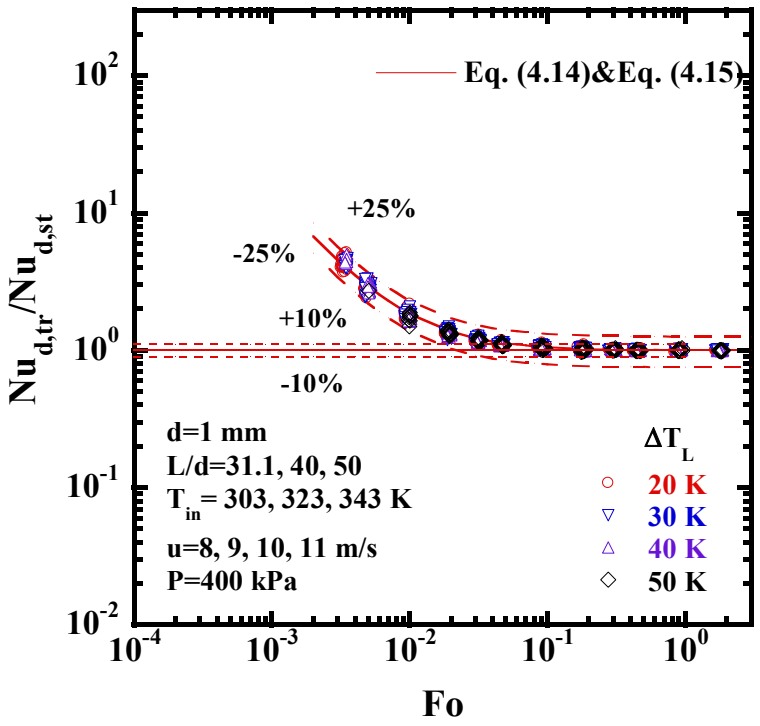

Fig. 4.31 $Nu_{d,tr}/Nu_{d,st}$ versus Fo for d =1 mm

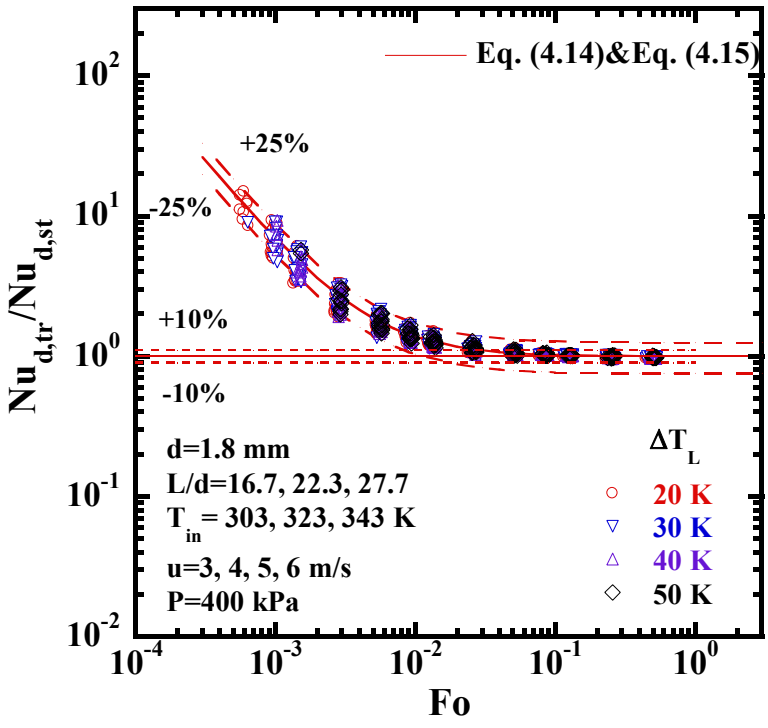

Fig. 4.32 $Nu_{d,tr}/Nu_{d,st}$ versus Fo for d =1.8 mm

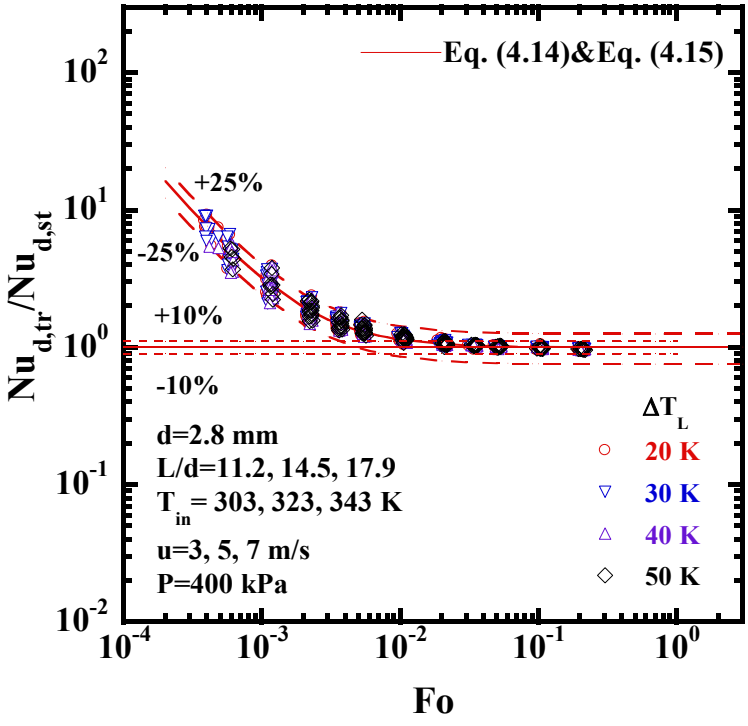

Fig. 4.33 $Nu_{d,tr}$ /$Nu_{d,st}$ versus Fo for d =2.8 mm

4.2.6 Effect of tube inner diameter on transient turbulent heat transfer

The experimental data measured for tube inner diameters of 1, 1.8 and 2.8 mm under various experimental conditions were plotted in Fig. 4.34 with the corresponding curves derived from Eq. (4.14) and Eq. (4.15). The ratios of transient turbulent $Nu_{d,tr}$ to steady state one for three tube inner diameters all increase with a decrease of Fo. However, the increment of transient state data relative to the steady state is higher for smaller diameter. It is assumed that the effect of heat conduction contribution for transient state increases with a decrease of tube inner diameter. The effect of tube inner diameter will also be

taken into account for developing transient turbulent heat transfer correlation.

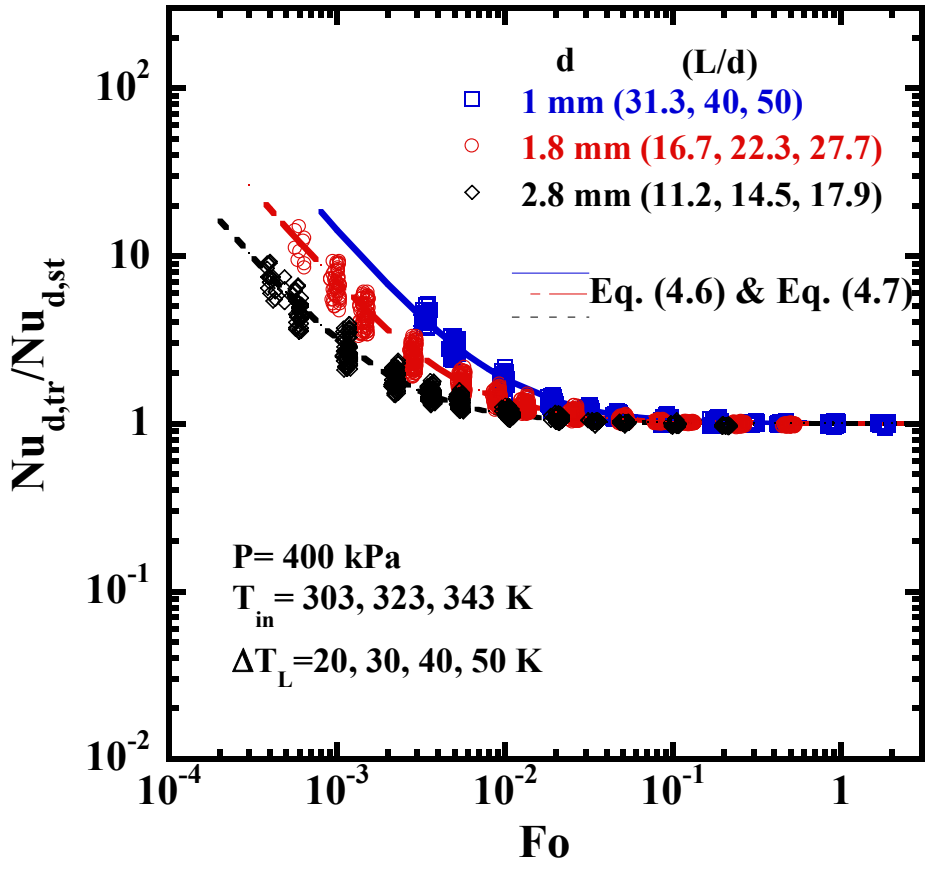

Fig. 4.34 $Nu_{d,tr}$ /$Nu_{d,st}$ versus Fo for d =1, 1.8 and 2.8 mm

4.2.7 Transient turbulent heat transfer correlation

To specify the increment of transient state data relative to the steady state, the following equation was defined.

$$Nu_{in} = \frac{Nu_{d,tr} - Nu_{d,st}}{Nu_{d,st}} \tag{4.10}$$

where, Nu_{in} is relative increment of Nusselt number between transient state and steady state, $Nu_{d,tr}$ is Nusselt number for transient state, and $Nu_{d,st}$ is Nusselt number for steady

state.

Figure 4.35 shows the experimental results for d = 2.8 mm in the form of Nu_{in} versus Fo. The Nu_{in} values linearly decrease with increase of Fo. The slop on this log-log graph is determined as -1.2. Those experimental data for d = 2.8 mm are correlated with the follwing equation:

$$Nu_{in} = \frac{Nu_{d,tr} - Nu_{d,st}}{Nu_{d,st}} = 5.53\times10^{-5}\, Fo^{-1.2} \tag{4.11}$$

Although some deviation exists in the larger Fo region, the Eq. (4.11) could roughly represent the experimental data for d = 2.8 mm within ±50%.

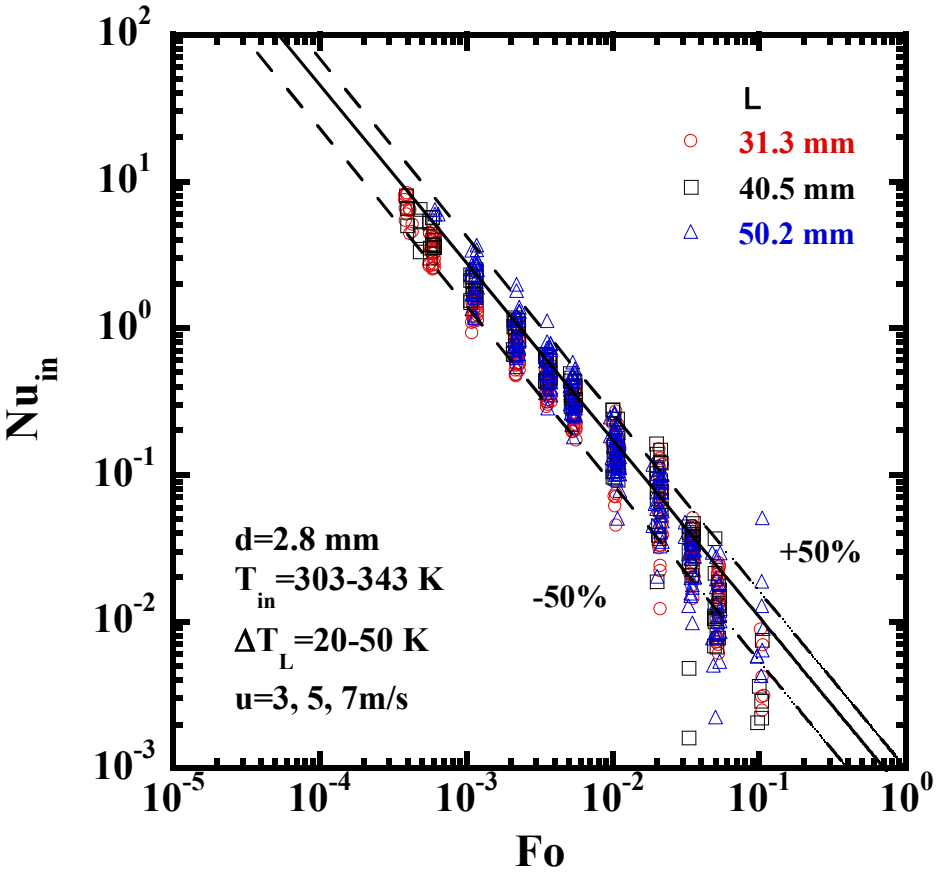

Fig. 4.35 Nu_{in} versus Fo for d = 2.8 mm

In the same method, the experimental data for d = 1 and 1.8 mm are correlated with

Eq. (4.12) and Eq. (4.13) respectively.

$$Nu_{in} = \frac{Nu_{d,tr} - Nu_{d,st}}{Nu_{d,st}} = 3.35\times10^{-4}\, Fo^{-1.2} \tag{4.12}$$

$$Nu_{in} = \frac{Nu_{d,tr} - Nu_{d,st}}{Nu_{d,st}} = 1.5\times10^{-4}\, Fo^{-1.2} \tag{4.13}$$

The transient turbulent heat transfer correlation for a wide range of exponentially increasing heat inputs on small diameter tubes has been obtained by combining the steady state values with effects of the *Fo* and tube inner diameter clarified in this work. It is expressed as follows:

$$Nu_{d,tr} = Nu_{d,st}(1 + C \cdot Fo^{-1.2}) \tag{4.14}$$

where, C is a constant to accommodate the effect of tube inner diameter and is expressed in the following equation.

$$C = 9.1\times10^{-3}\ \exp(-\frac{d}{d_{re}}) \tag{4.15}$$

where, d is the tube inner diameter and d_{re} (= 0.001 m) is the reference diameter. C = 3.35×10^{-4} for 1 mm diameter tube; C = 1.5×10^{-4} for 1.8 mm diameter tube and C = 5.53×10^{-5} for 2.8 mm diameter tube.

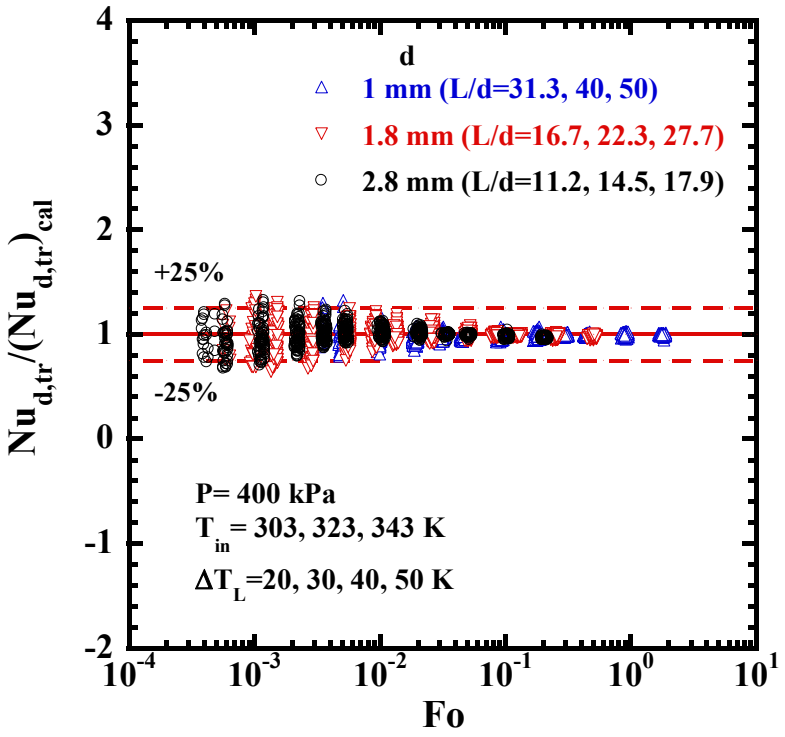

Fig. 4.36 $Nu_{d,tr}/(Nu_{d,tr})_{cal}$ versus Fo for d =1, 1.8 and 2.8 mm

Figure 4.36 shows the ratios of the experimental transient turbulent heat transfer data, $Nu_{d,tr}$, to the values calculated from transient turbulent heat transfer correlations of Eq. (4.14) and Eq. (4.15), $(Nu_{d,tr})_{cal}$, versus Fo for tube inner diameters of 1, 1.8 and 2.8 mm, inlet liquid temperatures of 303, 323 and 343 K, surface temperature differences of 20, 30, 40 and 50 K at various flow velocities. The obtained empirical correlations correlate all those experimental data (3253 points) within ±25%. For larger Fo, the data show a smaller deviation from the correlation because they approach the steady state. For steady state, the heat transfer process is governed by the usual heat convection and the heat conduction component is almost none. With a decrease of Fo, the heat transfer process becomes a complicated

phenomenon combining both heat convection and heat conduction. The heat transfer process may be affected by other factors besides *Fo*, flow velocity and inner diameter. Thus the data for smaller *Fo* show a relatively larger deviation from the proposed empirical correlation considering only the effects of *Fo* and inner diameter. Eq. (4.14) and Eq. (4.15) are also plotted in Figures 4.10 to 4.12 by solid lines. The empirical correlations represent the experimental data well.

4.3 Summary

4.3.1 Steady state turbulent heat transfer

Steady state turbulent heat transfer was systematically investigated for wide ranges of parameters such as velocity, inlet temperature and exponential period of heat generation rate. Circular tubes with different inner diameters (1, 1.8 and 2.8 mm) and heated lengths (about 30-50 mm) were used in this study. The conclusions are summarized as follows:

1) The Nusselt numbers for FC-72 flowing through tubes with diameters of 1, 1.8 and 2.8 mm are found to be higher than those predicted by classical correlations for conventional sized channels. It is assumed that the roughness effect enhances the heat transfer rate in small sized channels.

2) To accommodate the enhancement caused by the small sized channels, steady state

turbulent heat transfer correlations were developed in Eq. (4.7) and Eq. (4.8) for d = 1, 1.8 and 2.8 mm by taking into account the effects of L/d, μ/μ_w, Pr and Re_d. The deviation between the experimental data and the developed correlations is less than ±15%.

4.3.2 Transient turbulent heat transfer

The transient heat transfer process due to exponentially increasing heat inputs for turbulent flow of FC-72 was schematically investigated for different combinations of parameters such as flow velocity, inlet liquid temperature and period of exponentially increasing heat inputs using small diameter tubes with different inner diameters and heated lengths. The experimental results lead to the following conclusions:

1) The usual convective heat transfer dominates the heat transfer process for quasi steady state region. The heat conduction gradually governs the heat transfer process for transient state with a decrease of period.

2) It was clarified that the transient heat transfer process could be analyzed in terms of the dimensionless time, Fo.

3) The ratios of $Nu_{d,tr}/Nu_{d,st}$ approach unity for larger Fo, and they increase with the decrease in Fo for smaller Fo.

4) The increment of transient state data relative to the steady state is higher for smaller diameter as the effect of heat conduction contribution increases with a decrease of tube inner diameter.

5) Based on the effects of *Fo* and tube inner diameter, the empirical correlation of transient turbulent heat transfer was developed for a wide range of exponentially increasing heat inputs using small diameter tubes. Deviations between the experimental data and the empirical correlations were less than ±25%.

References

[1] Q. Liu, Z. Zhao, K. Fukuda, Transient heat transfer for forced flow of helium gas along a horizontal plate with different widths, Int. J. Heat Mass Transf. 75, (2014) 433–441.

[2] Q. Liu, Z. Zhao, K. Fukuda, Experimental study on transient heat transfer enhancement from a twisted plate in convection flow of helium gas, Int. J. Heat Mass Transf. 90, (2015) 1160–1169.

[3] K. Hata, N. Kai, Y. Shirai, S. Masuzaki, Transient turbulent heat transfer for heating of water in a short vertical tube, J. Power Energy Syst. 5, (2011) 414–428.

[4] Dittus, F., W., and Boelter, L., M., K., Univ. Calif. (Berkeley) Pub. Eng., Vol. 2, (1930) 443.

[5] Nusselt, W., Der Warmeaustausch zweischen Wand und Wasser im Rohr, Forsch. Geb. Ingenieurwes., Vol. 2, (1931) 309.

[6] K. Hata, N. Kai, Y. Shirai, and S. Masuzaki, Turbulent Heat Transfer for Heating of Water in a Short Vertical Tube, Journal of Power Energy System., vol. 5, no. 3, (2008) 414–428.

[7] Sieder E.N., Tate C.N. Heat transfer and pressure drop of liquids in tubes. Ind Eng

Chem 28, (1936)1429‑1435.

[8] D. Yu, R.O. Warrington, R. Barron, T. Ameel, An Experimental and Theoretical Investigation of Fluid Flow and Heat Transfer in Microtubes, Proceedings of ASME/JSME Thermal Engineering Joint Conf., Maui, HI, (1995), 523–530.

[9] Adams, T., Abdel-Khalik, S. I., Jeter, S. M., and Qureshi, Z. H., An Experimental Investigation of Single-phase Forced Convection in Microchannels, International Journal of Heat and Mass Transfer, vol. 41, no. 6–7, (1998) 851–857.

[10] Kandlikar, S.G., Fundamental Issues Related to Flow Boiling in Minichannels and Microchannels, Experimental Thermal and Fluid Science 26, (2002) 389–407.

[11] Gnielinski, V., New Equations for Heat Transfer in Turbulent Pipe and Channel Flow, International Chemical Engineering, Vol. 16, (1976) 359-368.

[12] R.C.C.Wang, B.T.F. Chung and L.C. Thomas, Transient convective heat transfer for laminar boundary layer flow with effects of wall capacitance and resistance, J. Heat Transfer 99(4), (1977) 513-519.

[13] H. Kawamura, Experimental and analytical study of transient heat transfer for turbulent flow in a circular tube, Int. J. Heat Transfer, vol. 20, (1977) 443-450.

[14] M. Fakoor-Pakdaman, M. Ahmadi, M. Bahrami, Unsteady laminar forced-convective tube flow under dynamic time-dependent heat flux, J. Heat

Transfer, 136, (2014) 041706-1-9.

[15] M. Fakoor-Pakdaman, M. Ahmadi, M. Bahrami, Temperature-aware time-varying convection over a duty cycle for a given system thermal-topology, Int. J. Heat Mass Transf. 87, (2015) 418–428.

[16] S. Kakaç, Transient forced convection heat transfer in a chnannel, Wärme- und Stoffübertragung, Vol. 1, (1968) 169-176.

CHAPTER 5

Subcooled Flow Boiling Heat Transfer in Vertical Small Diameter Tubes

Subcooled flow boiling refers to the situation that the bulk liquid temperature remains lower than the saturation temperature but the surface superheat is enough to generate bubbles. This chapter presents the experimental study on steady state and transient subcooled flow boiling heat transfer with FC-72 in vertical small diameter tubes. The steady state and transient flow boiling heat transfer processes are described in detail. The effects of flow velocity, inlet and outlet liquid subcooling and exponential period of heat generation on subcooled flow boiling and its CHF are explored. Empirical equations are proposed to fit the experimental data. The physical mechanism of steady state and transient subcooled flow boiling CHF in vertical small diameter tubes has also been discussed.

5.1 Experimental Conditions

Subcooled flow boiling heat transfer experiments have been conducted with FC-72 in vertical tube with inner diameter of 1.8 mm and effective length of 26.2 mm. FC-72 was

Table 5.1 Experimental conditions of flow boiling

Working liquid	FC-72
Test tube material	SUS304
Tube inner diameter (d)	1.8 mm
Effective length (L)	26.2 mm
L/d	14.56
Inlet flow velocity (u)	3, 4, 5 m/s
Inlet pressure (P_{in})	301.26-329.64 kPa
Outlet pressure (P_{out})	300 kPa
Inlet liquid subcooling ($\Delta T_{sub,in}$)	33.85-76.71 K
Outlet liquid subcooling ($\Delta T_{sub,out}$)	27.16-73.18 K
Inlet liquid temperature (T_{in})	293, 303, 313, 323, 333 K
Exponential period (τ)	81.31 ms-16.04 s

selected as the test liquid since it has low surface tension. The low surface tension characteristic is expected to affect the transition from non-boiling region to film boiling. The flow velocity varied from 3 to 5 m/s. Heat inputs to the test heater were exponentially increased with exponential periods, τ, ranging from 81.31 ms to16.04 s. The inlet liquid temperatures, T_{in}, were maintained at 293, 303, 313, 323 and 333 K.

Correspondingly, the inlet and outlet liquid subcooling were 33.85-76.71 K and 27.16-73.18 K respectively. The outlet pressure, P_{out}, was kept at 300 kPa for all experiment runs. The ranges of all experimental parameters covered in this study are summarized in Table 5.1.

5.2 Heat Transfer Coefficient in Non-boiling Region

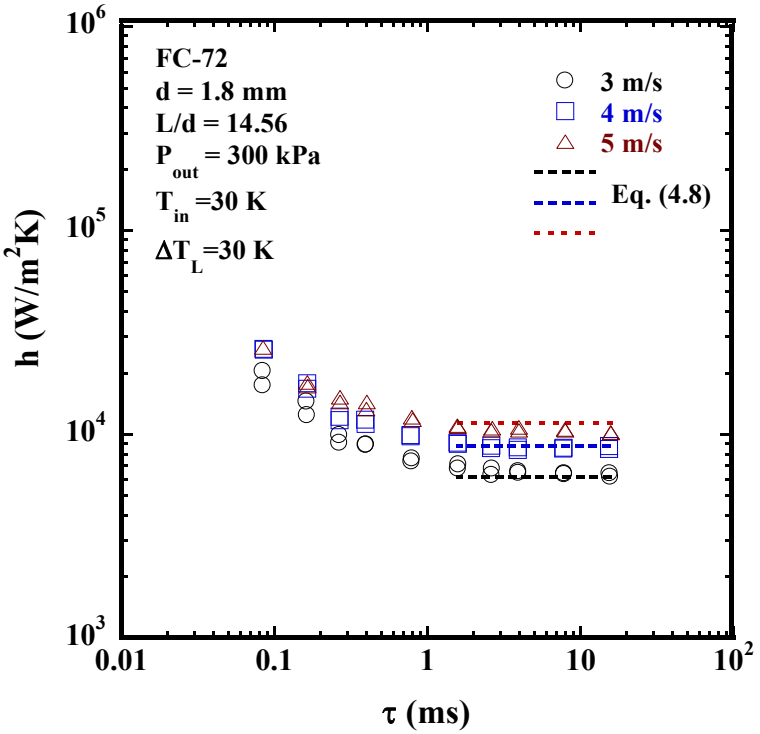

Fig. 5.1 Non-boiling heat transfer coefficient versus exponential period at ΔT_L=30 K

The heat transfer coefficients in the non-boiling region were measured at inlet velocities of 3, 4, 5 m/s for $\Delta T_L(T_S\text{-}T_L)$=30 K at outlet pressure of 300 kPa. The results are shown versus exponential periods in Fig. 5.1. For longer periods, the experimental

data of heat transfer coefficients versus exponential periods match basically with authors' steady state single-phase heat transfer correlations as expressed in Eq. (4.8). Therefore, the experiments conducted for longer periods are regarded as steady state. On the other hand, the heat transfer coefficients increase with decrease of period in shorter period region. The experiments performed under shorter periods are taken as transient state.

5.3 Time Dependence of Flow Boiling Characteristics

Figure 5.2 shows representative changes in tube inner surface temperature, T_s, heat flux, q, and heat input, Q, with elapsed time. The heat input to the test tube was increased quasi-steadily as a function of $Q_0 exp(t/\tau)$ with period of 15.68 s. This figure shows a typical heat transfer process of transition to film boiling through fully developed nucleate boiling (FDNB) as plotted with solid line in Fig. 5.4. Firstly the surface temperature increases with the increase of heat input. Boiling begins when the surface superheat is enough to initiate the evaporation as shown with square mark. In the nucleate boiling regime, surface temperature increases with a very low rate until reach the CHF point as shown with circle mark. In the boiling process, the heat flux increase rapidly with increase of heat input. During nucleate boiling process, a rapid

increase in heat flux up to CHF under small temperature difference is observed. Therefore, the nucleate boiling region has been widely employed in the industries.

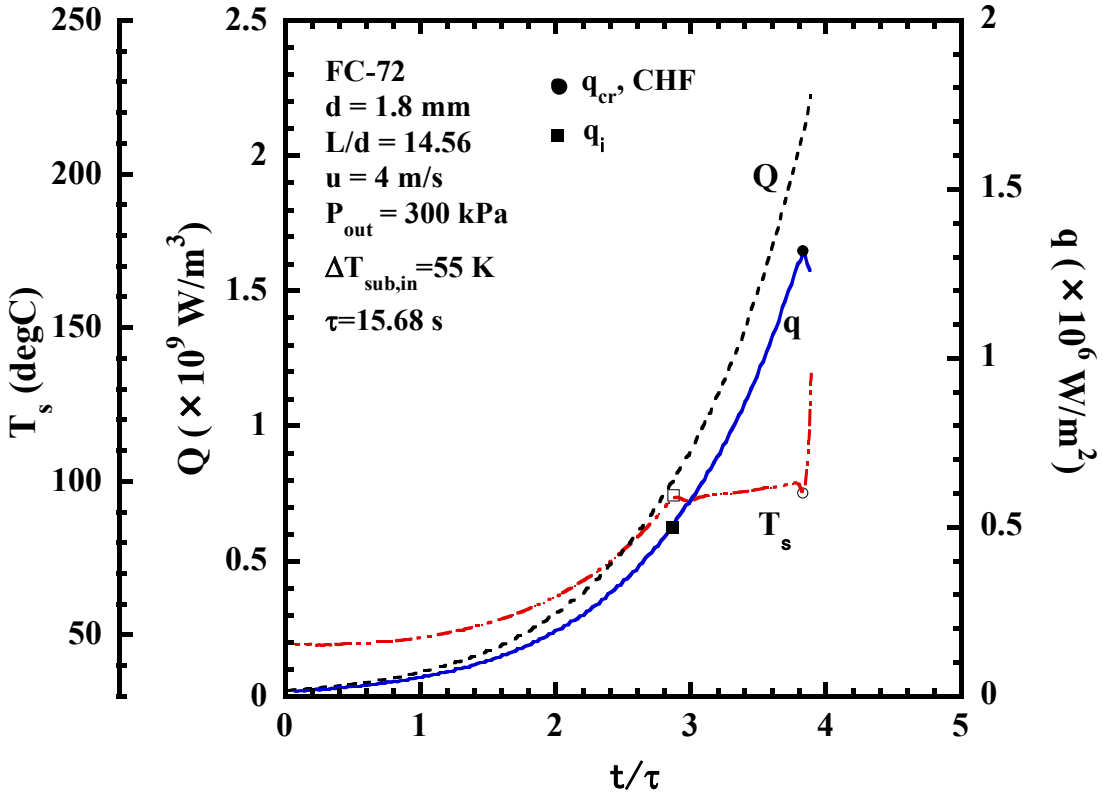

Fig. 5.2 Typical changes of heat generation rate, heat flux and surface temperature relating to elapsed time for transition to film boiling through FDNB (τ＝15.68 s)

Figure 5.3 shows the case of time dependence of q, Q and T_s for the exponential period of 163.98 ms, corresponding to the boiling graph shown with dashed line in Fig. 5.4. It shows a transition from non-boiling region to film boiling with increasing heat flux or so-called semi-direct transition. This kind of transition refers to imperfect nucleate boiling (the nucleate boiling region is in a very short time) prior to CHF

accompanying with rapid increase in the surface temperature. The surface temperature increases steeply to induce boiling incipience and the CHF, which is similar to the direct transition process occurred in the transient pool boiling process as shown in section 3.2. It is assumed that the semi-direct transition process is also due to explosive-like HSN in originally flooded cavities.

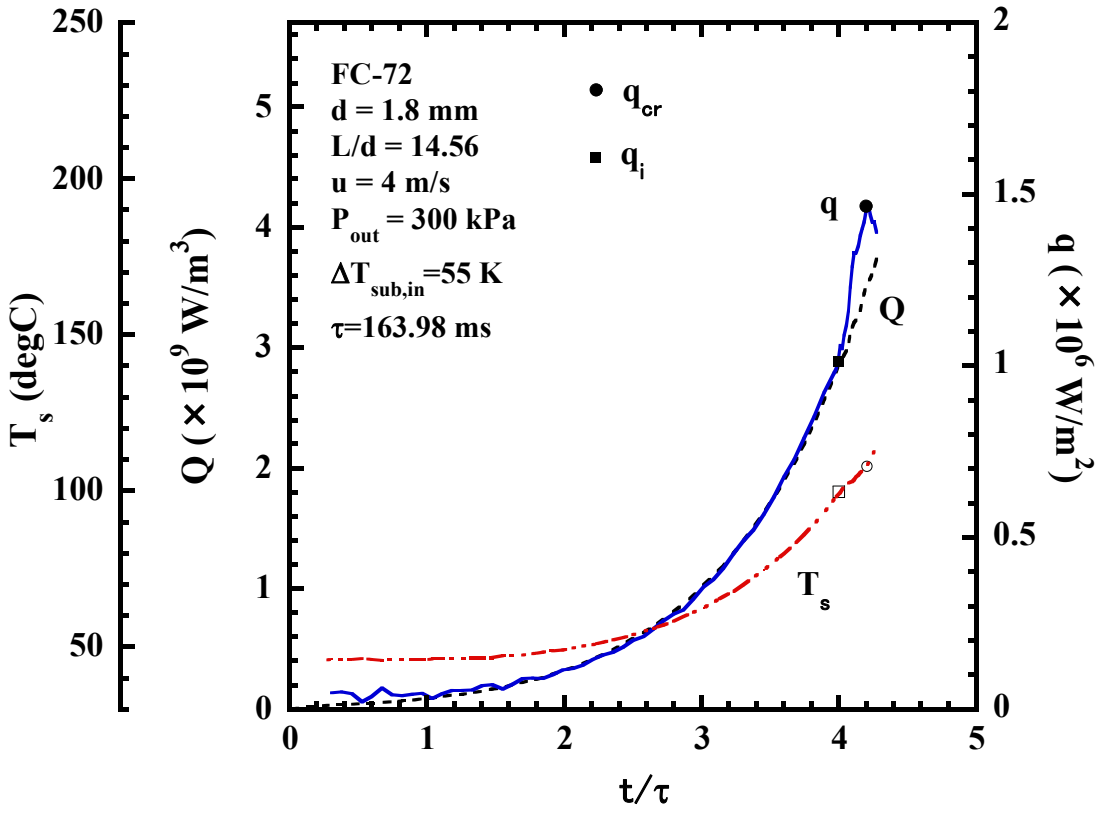

Fig. 5.3 Typical changes of heat generation rate, heat flux and surface temperature relating to elapsed time for semi-direct transition (τ＝163.98 ms)

5.4 Flow Boiling Heat Transfer Process

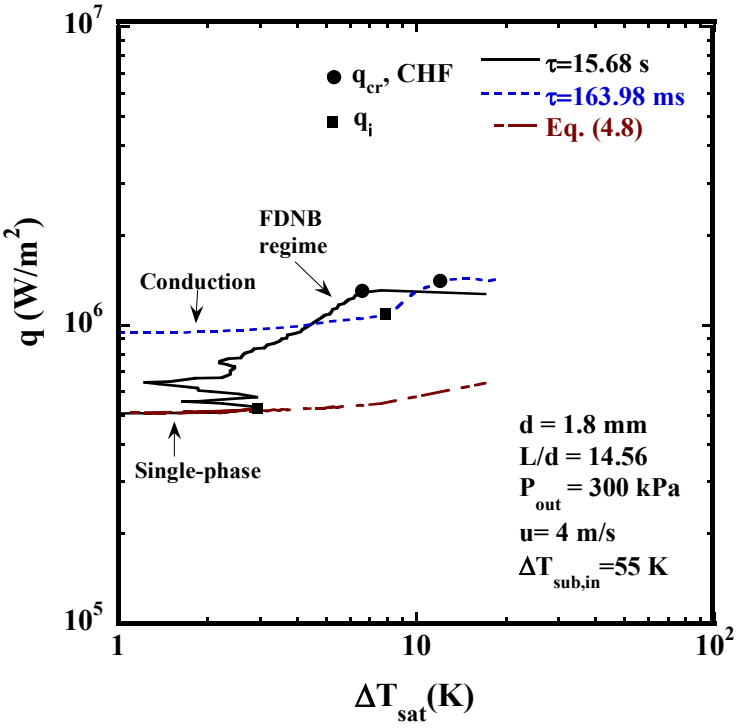

Fig. 5.4 Typical flow boiling curves at τ＝15.68 s and 163.98 ms

According to the transition from non-boiling regime to film boiling due to quasi-steady state and transient exponential heat generation, the flow boiling heat transfer processes are divided into the following two types, i.e.: transition from the non-boiling region to film boiling through FDNB and transition from non-boiling regime to film boiling through a short nucleate boiling or semi-direct transition. The two typical flow boiling heat transfer processes are plotted in Fig. 5.4 in the form of heat flux, q, versus surface superheat, ΔT_{sat}. The two blow boiling heat transfer processes correspond to periods of 15.68 s and 163.98 ms. Their time dependence of flow boiling

characteristics are described in section 5.3.

5.4.1 Transition from the non-boiling region to film boiling through FDNB (type 1)

The flow boiling heat transfer processes for periods of heat generation ranging from 1.58 s to 15.68 s at inlet velocity of 4 m/s and inlet subcooling of 55 K are all shown in Fig. 5.5. The typical transition from non-boiling region to film boiling through fully developed nucleate boiling (FDNB) are caused by quasi-steadily increasing heat inputs with exponential periods longer than a certain value as shown in Fig. 5.5. At first, the heat flux increase along the single-phase heat transfer curve obtained by the authors [1]. At the incipient boiling point as shown in black square mark, the wall superheat decrease due to the activation of originally flooded cavities. The heat flux then increase gradually with an increase in surface superheat along the FDNB curve to the CHF point marked with black circle mark. After the CHF point, heat transfer process shifts to transition boiling and film boiling. The transition from FDNB to film boiling occurs due to the hydrodynamic instability (HI) mechanism [2, 3] in the two-phase region near the tube inner surface. The process from non-boiling regime to film boiling through FDNB is defined as type 1 heat transfer process. The CHF for various periods can be separated

into two groups as shown in Fig. 5.11. The first group data for longer periods correspond to type 1 heat transfer process.

As shown in Fig. 5.5, the CHF data slightly increase with the decrease of period of heat generation. The surface superheat corresponding to the boiling incipience is defined as ΔT_i. The ΔT_i also increase with a decrease in period. The increasing trend of CHF and ΔT_i could be explained by the time lag of the HI [4].

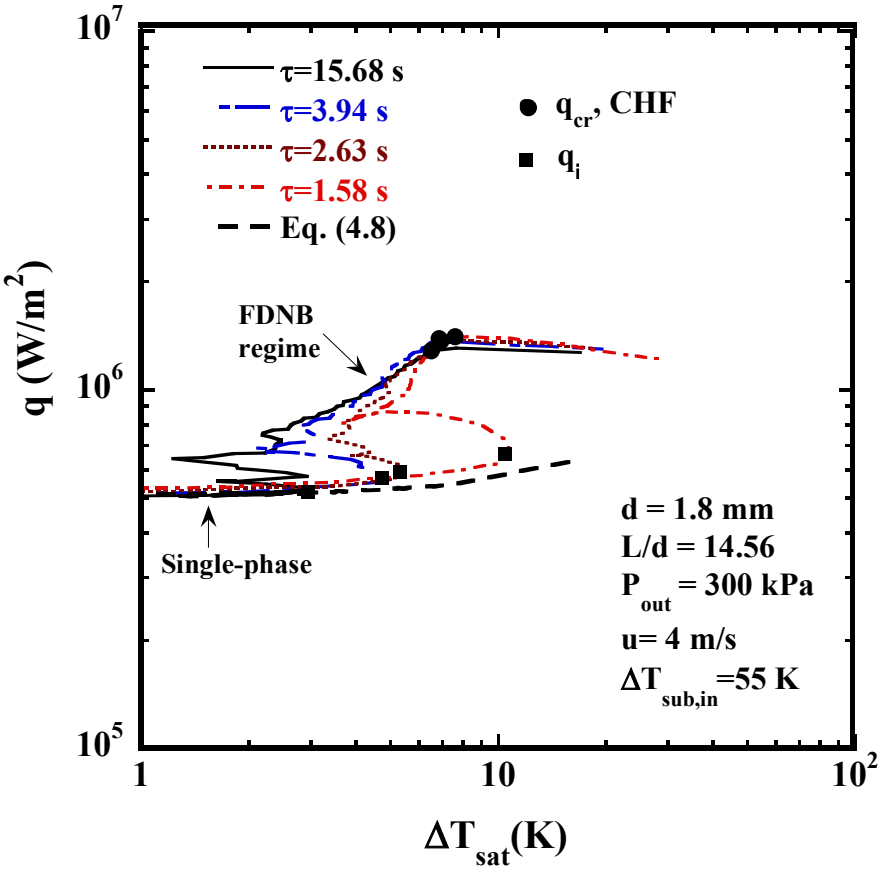

Fig. 5.5 Transition to film boiling through FDNB with quasi-steady heat input

5.4.2 Transition from non-boiling regime to film boiling through a short nucleate boiling or semi-direct transition (type 2).

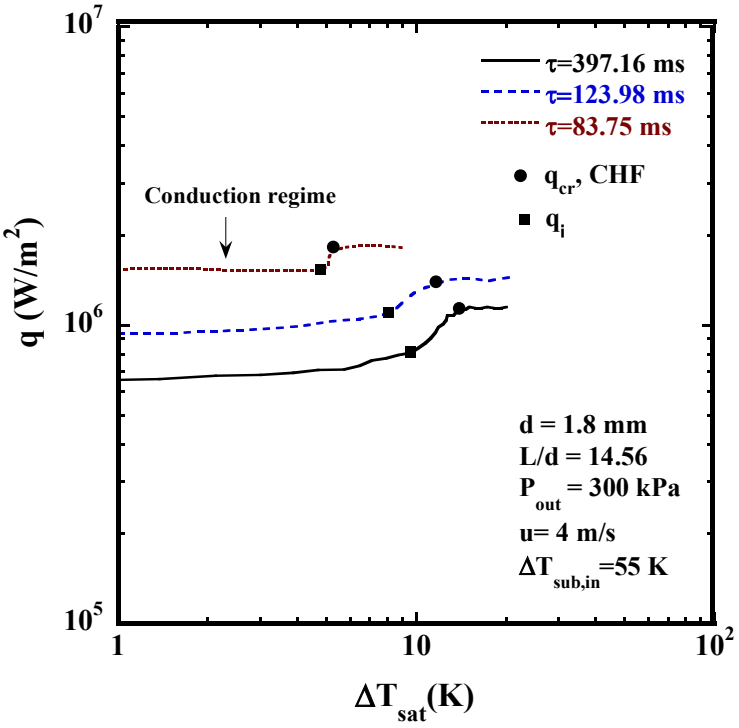

Fig. 5.6 Semi-direct transition to film boiling process with transient heat input

The heat transfer processes for periods of 83.75 to 397.16 ms at velocity of 4 m/s and inlet subcooling of 55 K are shown in Fig. 5.6. The heat flux increase along the conduction regime and suddenly increase from incipient boiling point (q_i) to CHF point (q_{cr}) with a small increase in the wall superheat. The transition from conduction to explosive boiling regime due to HSN in flooded cavities with increasing of heat flux in a short time and the transition from the boiling regime to film boiling is called a semi-direct transition [4]. The semi-direction transition has been observed for the period

shorter than a certain value. As shown in Fig. 5.11, the second group data for shorter periods correspond to semi-direct transition process.

5.5 Steady State Flow Boiling CHF

As mentioned in section 5.2, the heat transfer process for periods longer than 5 s is defined as steady state one because its heat transfer coefficient agrees with the steady state single phase heat transfer correlation. The effects of flow velocity, inlet and outlet subcooling on steady state flow boiling CHF have been discussed as follows.

5.5.1 Effect of flow velocity

Figure 5.7 shows the heat transfer process from single-phase region to boiling region for different flow velocities. The heat flux increases with the increase of T_s-T_{in} along the forced convection curve in the single-phase region. For the same temperature difference, higher flow velocity curve shows higher heat flux due to higher heat transfer coefficient. From the boiling incipience point, the heat flux increases along the nucleate boiling regime to CHF point. The CHF values increase with the increase of flow velocity.

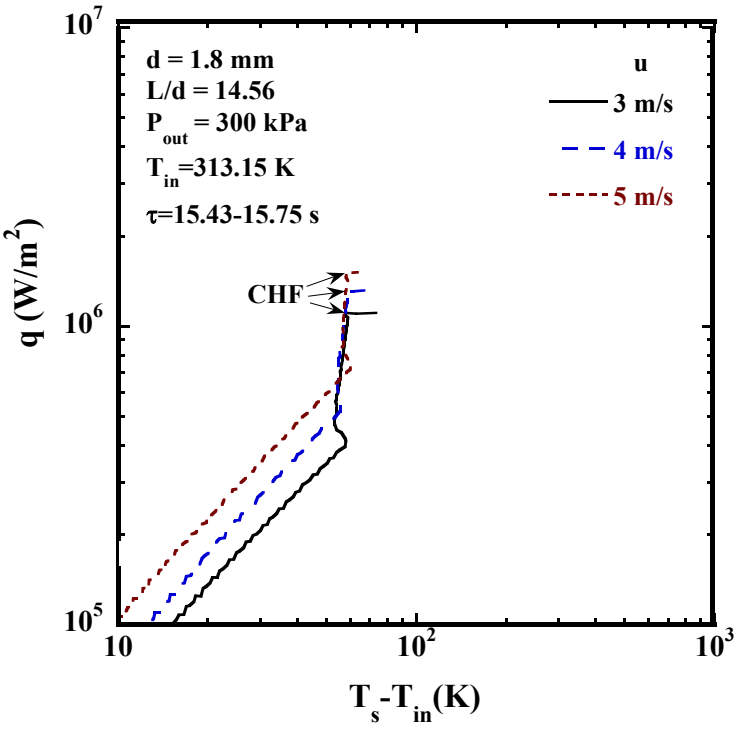

Fig. 5.7 Relation between q and T_s-T_{in}

5.5.2 Effect of inlet subcooling

Figure 5.8 shows the steady state flow boiling curves for inlet subcooling of 34, 44, 54 and 64 K at outlet pressure of 300 kPa and flow velocity of 3 m/s. The heat flux and surface superheat corresponding to the incipient boiling point are defined as q_i and ΔTi. The q_i and ΔTi increase with an increase in inlet subcooling. The CHFs also increase with increase of inlet subcooling. It indicates that higher subcooling requires a higher heat flux and surface superheat to initiate and sustain bubble activity.

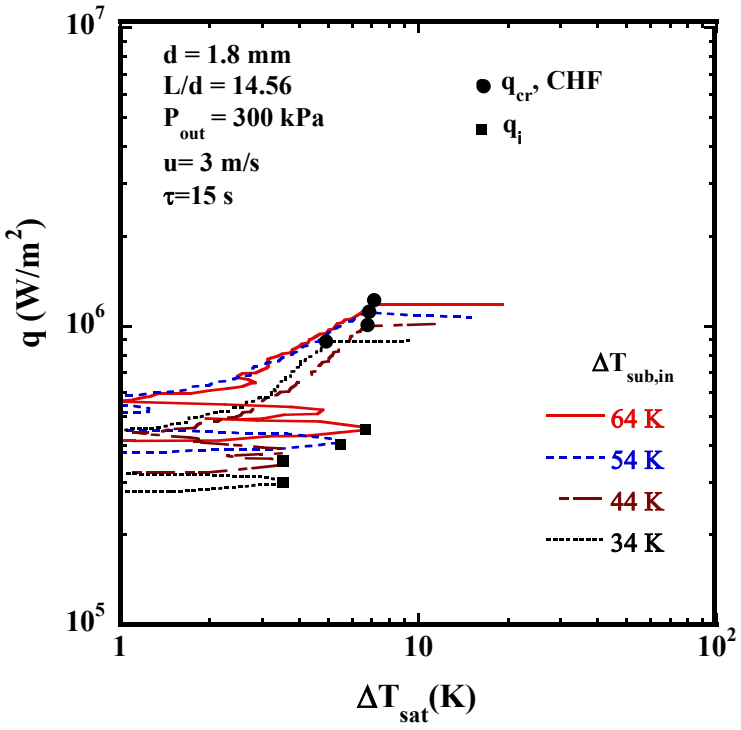

Fig. 5.8 Effect of inlet subcooling on boiling heat transfer curve

The CHF data measured using the tube with diameter of 1.8 mm and *L/d* of 14.56 are shown versus inlet subcooling with flow velocity as a parameter in Fig. 5.9. The CHF values increase with an increase in flow velocity at a certain $\Delta T_{sub,in.}$ The CHF values increase with the increase of $\Delta T_{sub,in}$ at each flow velocity. In the subcooled flow boiling, the bubbles generated on the heat surface condense as they leave the surface and contact with the subcooled bulk liquid. The condense rate increases with increase of subcooling. Therefore, higher heat flux is required to initiate and sustain bubble activity for the higher subcooling.

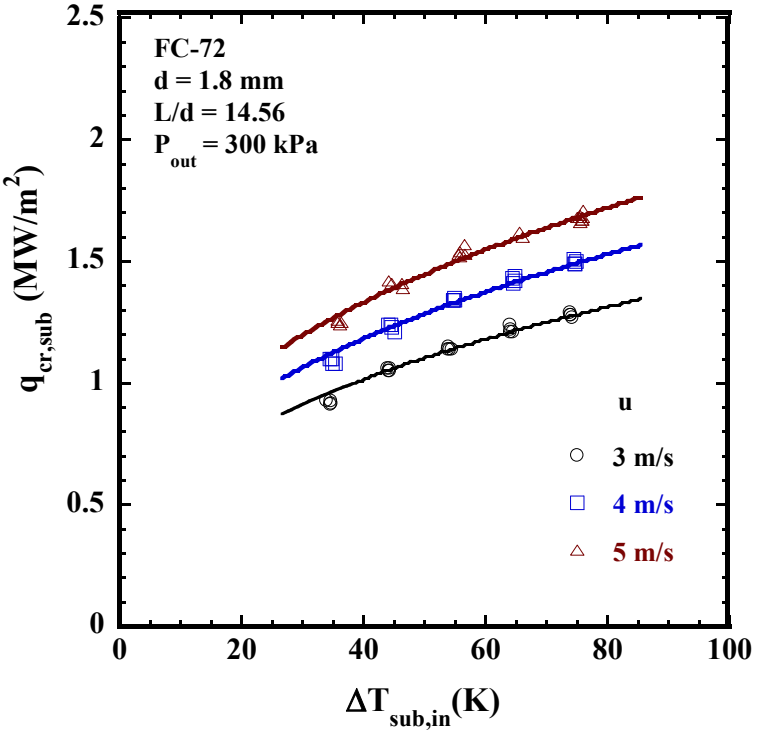

Fig. 5.9 $q_{cr,sub}$ versus $\Delta T_{sub,in}$ at various velocities

Gunther [5] proposed a flow boiling empirical correlation based on the study on the effect of velocity and subcooling for a flat 12.5 mm wide and 150 mm long heater strip placed in a rectangular section with flow of water as follows:

$$q_{cr,sub} = 71987 u^{0.5} \Delta T_{sub} \tag{5.1}$$

A similar empirical correlation combing the effects of flow velocity and inlet subcooling was developed to fit the experimental data. The empirical correlation is expressed as follows:

$$q_{cr,sub} = 1.45 \times 10^{5} u^{0.53} \Delta T_{sub,in}^{\ 0.37} \tag{5.2}$$

5.5.3 Effect of outlet subcooling

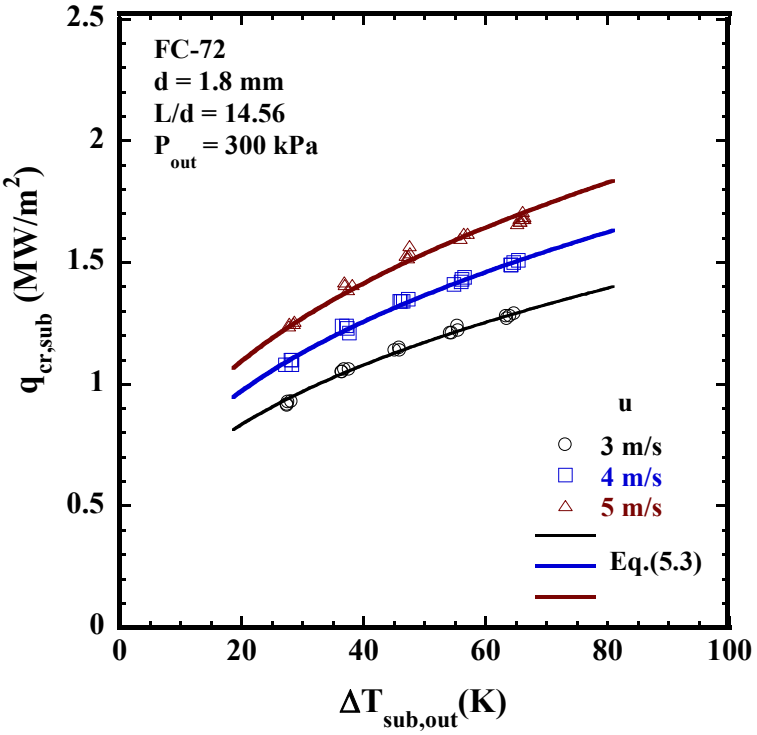

Fig. 5.10 $q_{cr,sub}$ versus $\Delta T_{sub,out}$ at various velocities

The CHF data versus outlet subcooling is shown in Fig. 5.10. The CHF values also increase with the increase of $\Delta T_{sub,out}$ at each flow velocity. Since the CHF point always appears near the outlet of flow channel, the relation between CHF and outlet succooling is very important. The following empirical equation has been developed to describe the relation between CHF and $\Delta T_{sub,out}$. As shown in Fig. 5.10, Eq. (5.3) matches the experimental data very well.

$$q_{cr,sub} = 1.54\times10^{5} u^{0.53} \Delta T_{sub,out}{}^{0.37} \tag{5.3}$$

5.6 Transient Flow Boiling CHF

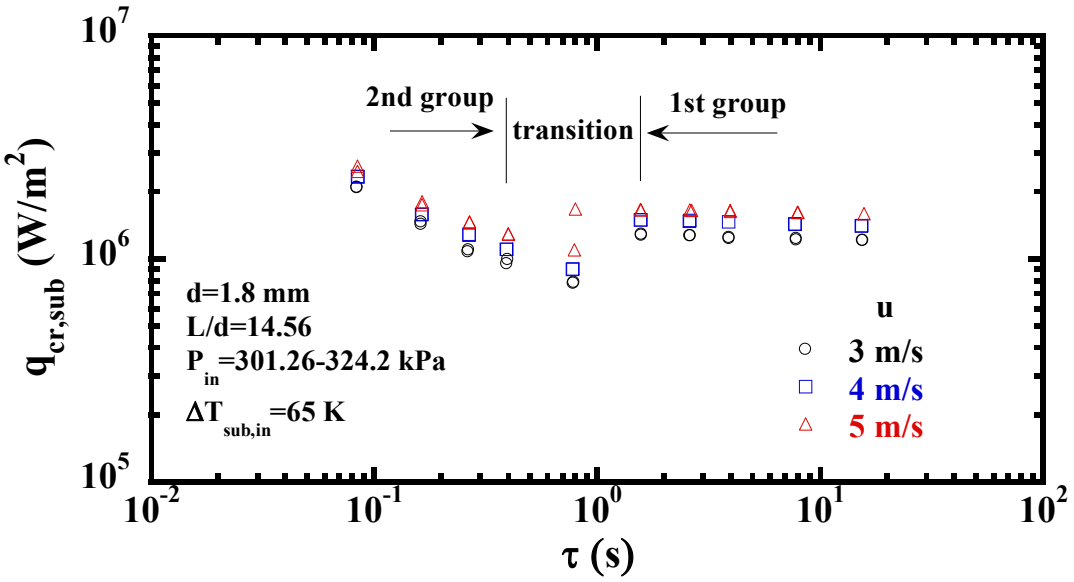

Fig. 5.11 Typical transient CHF for various periods at $\Delta T_{sub,in}$=65 K

The transient flow boiling CHF correspond to the maximum heat flux measured for exponential periods of rapid and quasi-steady state heat inputs. In this experimental study, the exponential periods varied from 81.31 ms to16.04 s.

Figure 5.11 shows the CHF data measured at flow velocity of 3, 4 and 5 m/s and inlet subcooling of 65 K versus exponential period ranging from 83.72 ms to 15.58 s. As shown in Fig. 5.11, the CHF values increase slightly from steady state with a decrease of period. It is explained by the time lag of HI. Then CHF values significantly decrease to a minimum one and finally increase again with the decrease of period. The transient CHF data could be separated into two groups, which represents CHF data for long and short period respectively. The first group CHF corresponds to type 1 flow boiling heat

transfer process, which could be explained by conventional HI mechanism. The second group CHF corresponds to type 2 flow boiling heat transfer process, which could be explained by HSN mechanism. In the case of 5 m/s, there are CHF values belonging to two different groups at period of 789.29 ms. It seems that there exists a transition region between the two CHF groups.

The surface superheat corresponding to the CHF (ΔT_c) versus exponential periods is shown in Fig. 5.12. The ΔT_c could also be divided into two groups based on the exponential periods. The ΔT_c for the first group is significantly lower than that for the second group. This phenomenon also confirms that there exist two different CHF mechanisms for long period and short period.

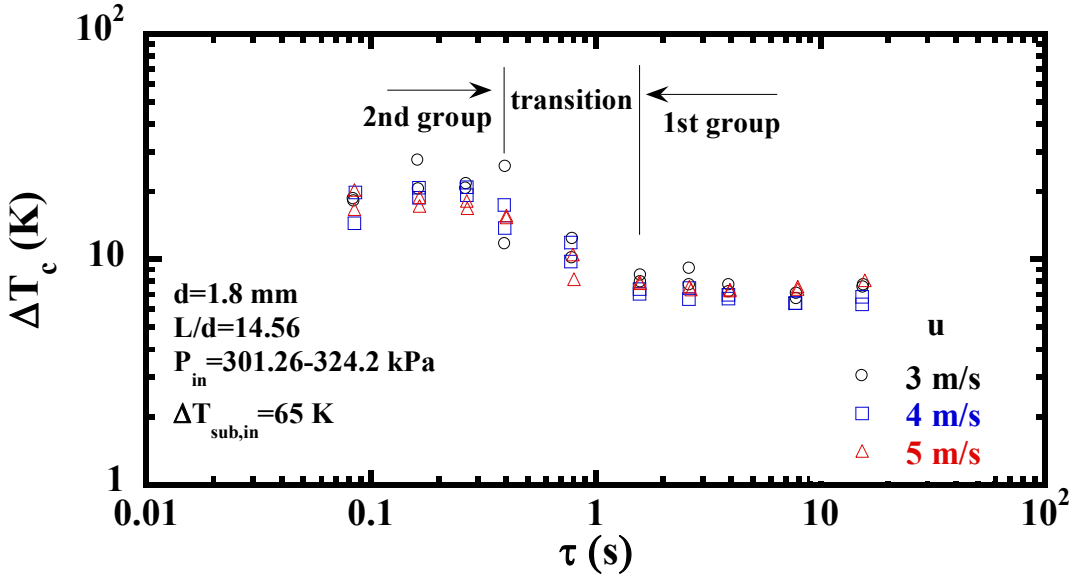

Fig. 5.12 Typical ΔT_c for various periods at $\Delta T_{sub,in}$=65 K

The CHF data and its surface superheat measured at inlet subcooling of 55 K and 45

K are shown in Fig. 5.13 to 5.16. They show similar results as the case of $\Delta T_{sub,in}$=65 K. The CHF values and ΔT_c could be divided into two groups based on the exponential periods of heat generation.

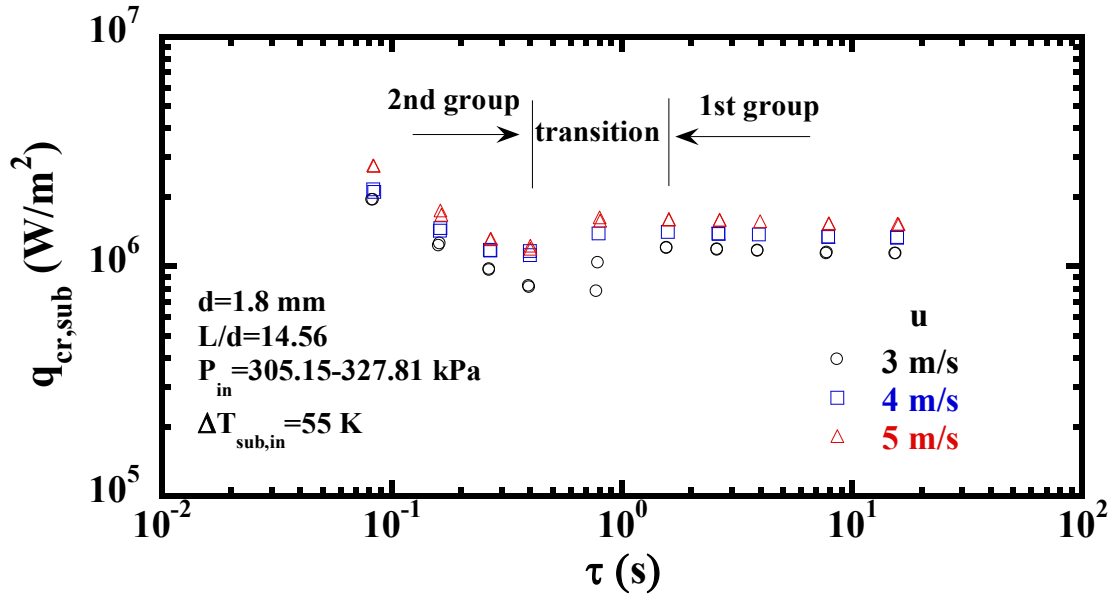

Fig. 5.13 Typical transient CHF for various periods at $\Delta T_{sub,in}$=55 K

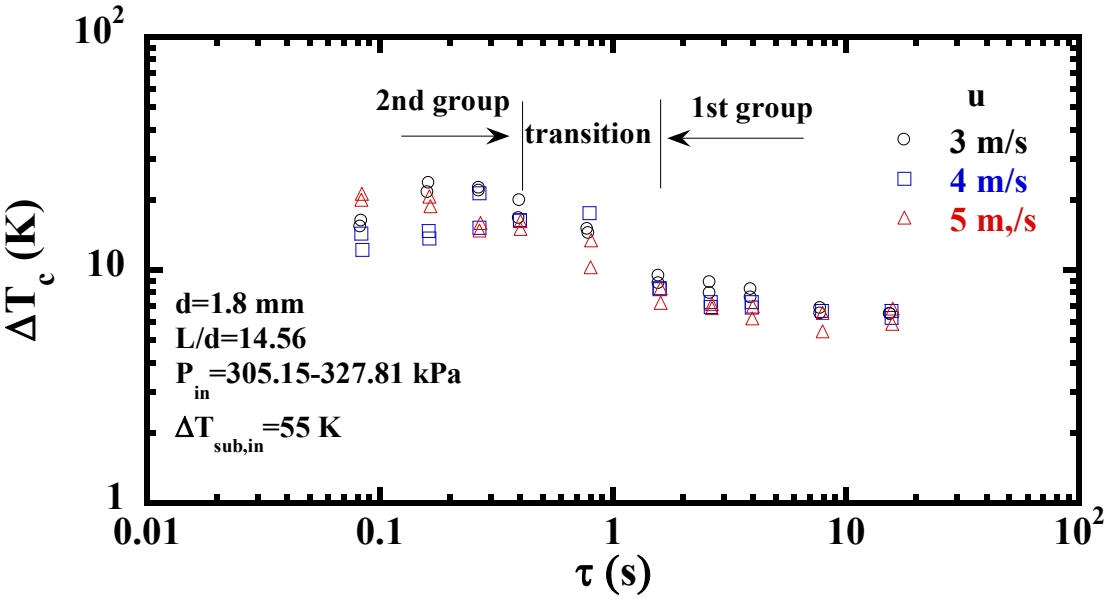

Fig. 5.14 Typical ΔT_c for various periods at $\Delta T_{sub,in}$=55 K

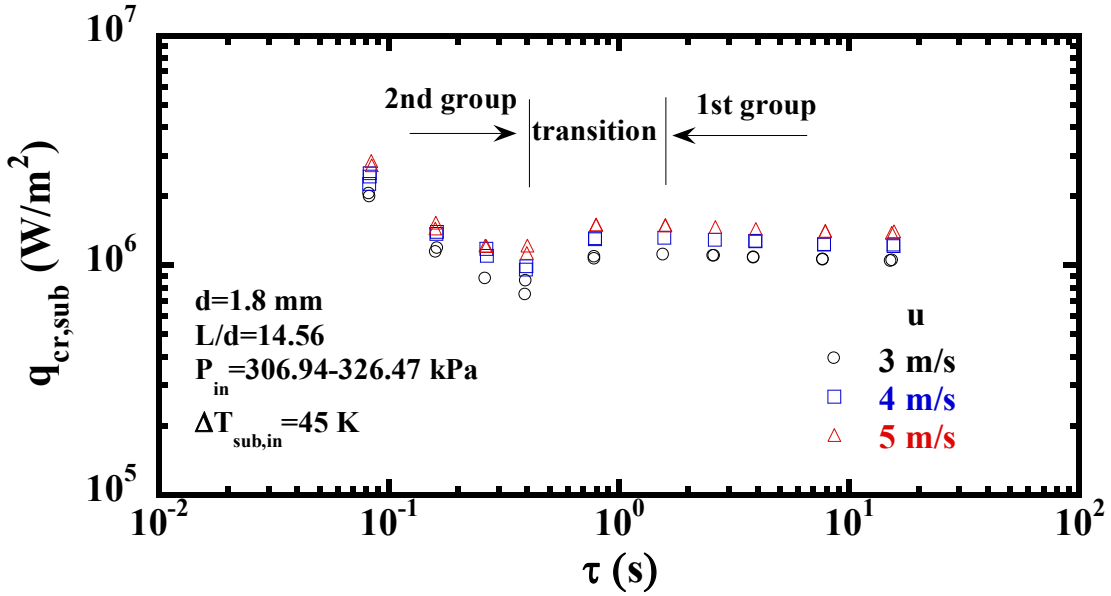

Fig. 5.15 Typical transient CHF for various periods at $\Delta T_{sub,in}$=45 K

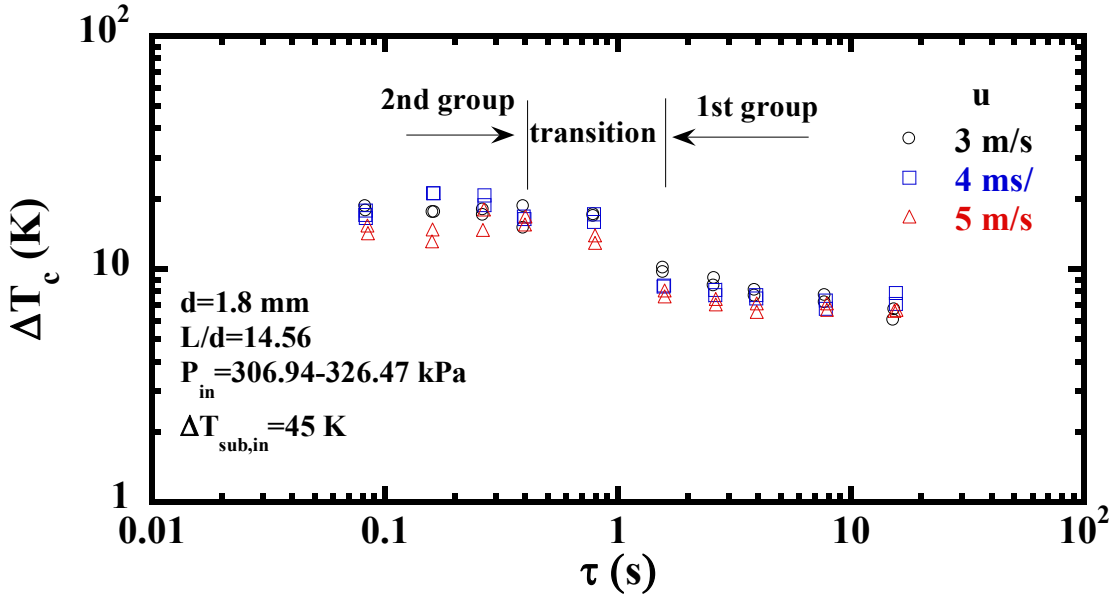

Fig. 5.16 Typical ΔT_c for various periods at $\Delta T_{sub,in}$=45 K

5.7 Summary

Subcooled flow boiling heat transfer experiments were conducted with FC-72 in vertical tube with inner diameter of 1.8 mm and effective length of 26.2 mm for exponentially increasing heat input with periods of 81.31 ms to 16.04 s. The flow velocity varied from 3 to 5 m/s and the inlet liquid temperature changed from 293 K to 333 K at a fixed outlet pressure of 300 kPa. The experimental results are summarized as follows:

1) The transition to film boiling process can be categorized into two types, representing two different CHF mechanisms. The transition from non-boiling to film boiling through FDNB and the transition from non-boiling region to film boiling through a short nucleate boiling are named as type 1 and type 2 process. Type 1 occurs at steadily increasing heat inputs and could be explained by conventional HI mechanism. Type 2 appears for rapid increasing heat inputs and it is induced by the explosive-like HSN from originally flooded cavities.

2) The steady state CHF values increase with the increase of flow velocity, inlet subcooling and outlet subcooling because in such a situation a higher heat flux is required to initiate and sustain bubble cavity. Empirical correlations combing effects of

flow velocity and subcooling have been proposed.

3) The transient CHFs due to exponentially increasing heat input could be divided into first and second group for long and short periods respectively. The first group data correspond to type 1 process. The second group data correspond to type 2 process.

References

[1] Yantao Li, Katsuya Fukuda, Qiusheng. Liu, Makoto Shibahara: Turbulent heat transfer with FC-72 in small diameter tubes, Int. J. Heat Mass Transf. 103, (2016) 428–434.

[2] Kutateladze S. S., Heat Transfer in Condensation and Boiling, AEC-tr-3770, USAEC (1959).

[3] Zuber N., , Hydrodynamic Aspects of Boiling Heat Transfer, AECU-4439, USAEC(1959).

[4] Sakurai, A. “Mechanism of Transitions to Film Boiling at CHFs in Subcooled and Pressurized Liquids Due To Steady and Increasing Heat Inputs”, Nuclear Engineering and Design, Vol. 197, (2000) 301-356.

[5] Gunther, F.C., “Photographic Study of Surface-Boiling Heat Transfer to Water with Forced Convection,” Transactions of the ASME, Vol. 73, No. 2, (1951) 115-123.

CHAPTER 6

Conclusions

The experimental study on pool boiling heat transfer, single-phase and two-phase flow boiling have been conducted with quasi-steady and transient heat input. The study of pool boiling heat transfer and single-phase heat transfer contributes to the understanding of mechanism of two- phase flow boiling heat transfer. The conclusions are summarized as follows.

6.1 Pool boiling Heat Transfer

The steady and transient pool boiling experiments were performed on a horizontal cylinder in a pool of ion-exchange-distilled water at pressures of 20 kPa to 101.6 kPa. The steady state and transient Critical Heat Flux (CHF) data under one atmosphere and sub-atmospheric pressures for the subcoolings ranging from zero up to 40 K with the exponential periods (τ) of heat input ranging from 20 s down to 10 ms were obtained and analyzed. The following conclusions are obtained:

1) For short periods of heat generation, the non-boiling heat transfer coefficients increase with a decrease of periods caused by transient heat conduction

contribution. However, in the long period region, the heat transfer coefficients approach an asymptotic value which is predicted by natural convection correlation.

2) It was found that the steady state CHF increase with the increase of subcoolings. And although the steady CHF data for one atmosphere are in agreement with conventional correlations, the CHF data for sub-atmospheric pressures show higher values.

3) The steady state CHF data for sub-atmospheric pressures are not in agreement with conventional correlations. Those CHF values within sub-atmospheric pressures increase with a decrease in pressure.

4) The transient CHF values under sub-atmospheric pressures could be divided into two groups based on the exponential periods, corresponding to short period region and long period region.

6.2 Single-phase Heat Transfer in Vertical Small Diameter Tubes

The steady state and transient heat transfer process for turbulent flow of FC-72 in vertical small diameter tubes was schematically investigated. The experiments were conducted at the flow velocities, u, changing from 8 to 11 m/s with corresponding Re_d in

the range of 23,400 to 45,900 for d = 1 mm, u changing from 3 to 6 m/s with corresponding Re_d in the range of 16,200 to 44,800 for d = 1.8 mm and u changing from 3 to 7 m/s with corresponding Re_d in the range of 25,200 to 81,800 for d = 2.8 mm. The range of Prandtl number, Pr, was from 8.4 to 10.8. Heat inputs to the test heater were exponentially increased with exponential periods ranging from 15.7 ms to 15.5 s. The inlet liquid temperatures were maintained at 303, 323 and 343 K and the system pressure was kept around 400 kPa. The test heaters used in this study were circular SUS304 tubes with small inner diameters of 1, 1.8 and 2.8 mm, wall thickness of 0.5 mm, and heated lengths around 30, 40 and 50 mm. The important conclusions that can be drawn based on the observations and analysis in the present study are summarized as in the following subsections.

6.2.1 Steady state turbulent heat transfer

1) The heat transfer coefficient linearly increases with the increase of flow velocity. Flow velocity has a strong effect on the temperature profile, thereby influencing the convective heat transfer process. The dependency of heat transfer coefficients on flow velocity for d = 2.8 mm coincides with conventional correlations. However, the cases of d = 1 and 1.8 mm show stronger dependency.

2) The heat transfer coefficient decreases with an increase in the L/d due to the thermal entrance effect for relatively short tubes.

3) The heat transfer coefficient becomes higher with the increase of μ/μ_w with a slope of 0.14 as viscosity of FC-72 varies greatly with change of temperature. Lower viscosity of the liquid at the walls increases the velocity gradient near the wall, thereby increasing the heat transfer coefficient.

4) The values of $Nu_d/Re_d^{0.8}/(\mu/\mu_w)^{0.14}$ increase with the increase of Pr with slope of 0.4. The trend of $Pr^{0.4}$ dependence accords with other well-known correlations.

5) For d = 1 and 1.8 mm, the data show anomalous trend ($Re_d^{1.2}$) compared with d = 2.8 mm in accordance with correlations for conventional sized channels ($Re_d^{0.8}$).

6) The Nusselt numbers for FC-72 flowing through tubes with diameters of 1, 1.8 and 2.8 mm are found to be higher than those predicted by classical correlations for conventional sized channels. It is assumed that the roughness effect enhances the heat transfer rate in small sized channels.

7) The experimental data are also compared with correlation for small channels. The experimental data for FC-72 are slightly lower than Adams' data obtained with water in almost the same diameters. It may be due to the lower thermal conductivity of FC-72.

8) To accommodate the enhancement caused by the small sized channels, steady state turbulent heat transfer correlations have been developed for d = 1, 1.8 and 2.8 mm by taking into account the effects of u, L/d, μ/μ_w, Pr and Re_d. The deviation between the experimental data and the developed correlations is less than ±15%.

6.2.2 Transient turbulent heat transfer

1) The usual convective heat transfer dominates the heat transfer process for quasi steady state region. The heat conduction gradually governs the heat transfer process for transient state with a decrease of period.
2) The relation between transient Nusselt number and Fourier number, Fo with flow velocity as a parameter shows the same trend as heat transfer coefficient versus exponential period for each velocity. It was clarified that the transient heat transfer process could be analyzed in terms of the dimensionless time, Fo.
3) The ratios of $Nu_{d,tr}/Nu_{d,st}$ approach unity for larger Fo, and they increase with the decrease in Fo for smaller Fo.
4) The increment of transient state data relative to the steady state is higher for smaller diameter. It is assumed that the effect of heat conduction contribution

increases with a decrease of tube inner diameter.

5) Based on the effects of *Fo* and tube inner diameter, the empirical correlations of transient turbulent heat transfer have been developed for a wide range of exponentially increasing heat inputs using small diameter tubes. Deviations between the experimental data and the empirical correlations were less than ±25%.

6) Based on the effects of Fo and tube inner diameter, the empirical correlations of transient turbulent heat transfer have been developed for a wide range of exponentially increasing heat inputs using small diameter tubes. Deviations between the experimental data and the empirical correlations were less than ±25%.

6.3 Subcooled Flow Boiling Heat Transfer in Vertical Small Diameter Tubes

Subcooled flow boiling heat transfer experiments were conducted with FC-72 in vertical tube with inner diameter of 1.8 mm and effective length of 26.2 mm for exponentially increasing heat input with periods of 81.31 ms to 16.04 s. The flow velocity varied from 3 to 5 m/s and the inlet liquid temperature changed from 293 K to

333 K at a fixed outlet pressure of 300 kPa. The experimental results are summarized as follows:

1) The transition to film boiling process can be categorized into two types, representing two different CHF mechanisms. The transition from non-boiling to film boiling through FDNB and the transition from non-boiling region to film boiling through a short nucleate boiling are named as type 1 and type 2 process. Type 1 occurs at steadily increasing heat inputs and could be explained by conventional HI mechanism. Type 2 appears for rapid increasing heat inputs and it is induced by the explosive-like HSN from originally flooded cavities.
2) The steady state CHF values increase with the increase of flow velocity, inlet subcooling and outlet subcooling because in such a situation a higher heat flux is required to initiate and sustain bubble cavity. Empirical correlations combing effects of flow velocity and subcooling have been proposed.
3) The transient CHFs due to exponentially increasing heat input could be divided into first and second group for long and short periods respectively. The first group data correspond to type 1 process. The second group data correspond to type 2 process.

APPENDIX

A.1 Wheatstone Bridge Method

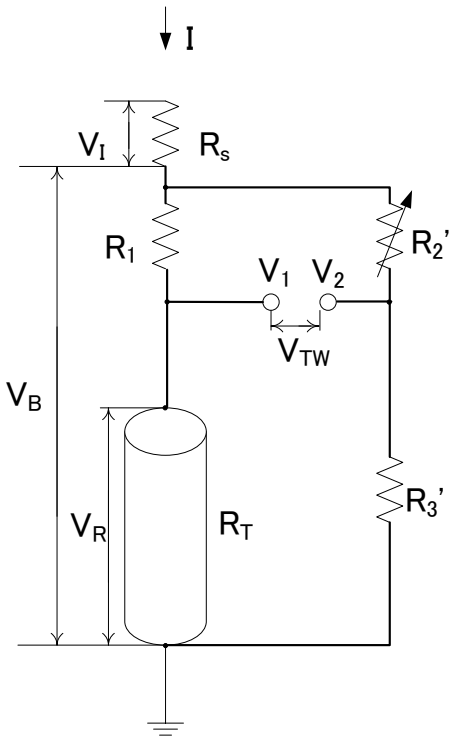

Fig. A.1 Circuit diagram of Wheatstone bridge

The standard bridge circuit, often called a Wheatstone bridge, is shown like in Fig. A.1. When the voltage between point V_1 and the negative side is equal to the voltage between point V_2 and the negative side, the null detector will indicate zero and the bridge is said to be “balanced.” To measure resistance with a Wheatstone bridge, an unknown resistance, V_T is connected in the branch, while the other three resistors are

precision devices of known value. One of the other three resistors (like R_2') can be adjusted until the bridge is balanced. When balance has been reached, the unknown resistor value can be determined from the ratios of the known resistances.

The derivation of a typical Wheatstone bridge is as follows:

$$V_1 = \frac{R_T}{R_1 + R_T} V_B \tag{1}$$

$$V_2 = \frac{R_3'}{R_2' + R_3'} V_B \tag{2}$$

Due to $R_1 + R_T << R_2' + R_3'$ (R_1=8.5115 mΩ, R_T≈12 mΩ, R_2=R_3=2000 Ω)

$$V_B = I(R_1 + R_T) \tag{3}$$

Substitute Eq. (3) into Eq. (1) and Eq. (2)

$$V_1 = \frac{R_T}{R_1 + R_T} I(R_1 + R_T) = R_T I \tag{4}$$

$$V_2' = \frac{R_3'}{R_2' + R_3'} I(R_1 + R_T) = \frac{R_3'(R_1 + R_T)}{R_2' + R_3'} I \tag{5}$$

The output voltage of the Wheatstone bridge, V_{TW}, is expressed as follows:

$$\begin{aligned} V_{TW} = V_1 - V_2 &= \left[R_T - \frac{R_3'(R_1 + R_T)}{R_2' + R_3'} \right] I \\ &= \frac{R_T R_2' + R_T R_3' - R_3' R_1 - R_3' R_T}{R_2' + R_3'} I \\ &= \frac{R_T R_2' - R_1 R_3'}{R_2' + R_3'} I \end{aligned} \tag{6}$$

Then

$$R_T = \frac{R_1 R_3' + \frac{V_{TW}}{I}(R_2' + R_3')}{R_2'} \tag{7}$$

When the bridge is in balance, V_{TW}=0. So Eq. (7) can be rewritten as:

$$R_T = \frac{R_1 R_3'}{R_2'} \tag{8}$$

The resistances of connections and connecting wires between R_1 and R_T are not considered for Wheatstone bridge method. Therefore, the measured resistance, R_T, is higher than the actual value. The corresponding measured average temperature of test heater is also higher than the actual one. Once the measured average temperature by Wheatstone bridge method exceeds the preset value, the heat input to the test heater would be cut-off. In this way, it provides an allowance for interlock protection. As to the precise measurement of a low resistance, R_T, the Kelvin double bridge circuit should be employed.

A.2. Kelvin Double Bridge Method

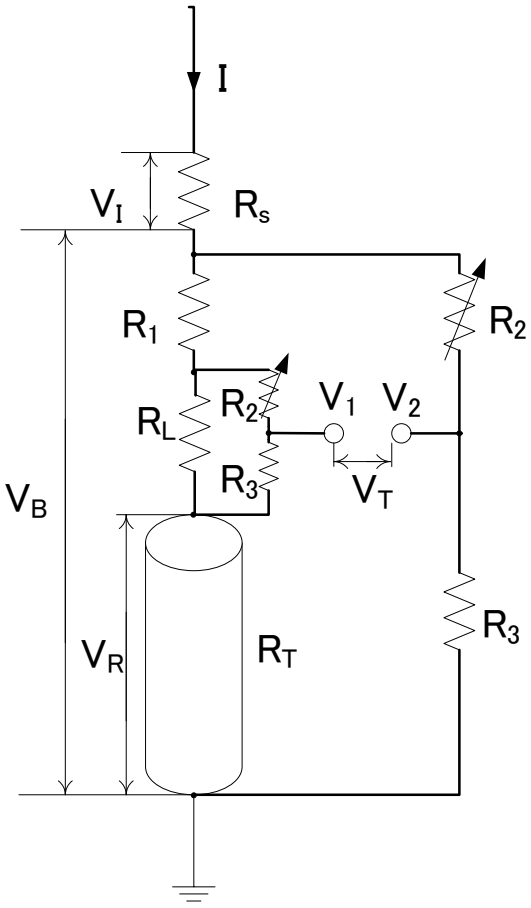

Fig. A.2 Circuit diagram of Kelvin double bridge

Kelvin double bridge is a variation of the Wheatstone bridge, used for measuring very low resistances. Its schematic diagram is shown in Fig. A.2.

If we were to use a standard Wheatstone bridge to measure low resistance, we have a problem in that the connections and connecting wires between R_1 and R_T possess

resistance, R_L, as well, and this stray resistance may be substantial compared to the low resistances of R_1 and R_T. Since we don't want to measure these stray wire and connection resistances, but only measure R_T, The Kelvin double bridge circuit is employed so that it won't be influenced by voltage dropped across the connections and connecting wires.

The voltafe drop across the connections and connecting wires, R_L, and test heater, R_T, is expressed in Eq. (9) and Eq. (10) as follows:

$$V_{R_L} = \frac{\frac{R_L(R_2+R_3)}{R_L+R_2+R_3}}{R_T+R_1+\frac{R_L(R_2+R_3)}{R_L+R_2+R_3}} V_B \tag{9}$$

$$V_{R_T} = \frac{R_T}{R_T+R_1+\frac{R_L(R_2+R_3)}{R_L+R_2+R_3}} V_B \tag{10}$$

$$V_1 = V_{R_T} + V_{R_3} \tag{11}$$

$$V_{R_3} = \frac{R_3}{R_2+R_3} V_{R_L} = \frac{\frac{R_L R_3}{R_L+R_2+R_3}}{R_T+R_1+\frac{R_L(R_2+R_3)}{R_L+R_2+R_3}} V_B \tag{12}$$

Submit Eq. (10) and Eq. (12) into Eq. (11),

$$V_1 = \frac{R_T V_B}{R_T + R_1 + \frac{R_L(R_2+R_3)}{R_L+R_2+R_3}} + \frac{\frac{R_L R_3}{R_L+R_2+R_3}}{R_T + R_1 + \frac{R_L(R_2+R_3)}{R_L+R_2+R_3}} V_B$$
$$= \frac{V_B}{R_T + R_1 + \frac{R_L(R_2+R_3)}{R_L+R_2+R_3}} (R_T + \frac{R_L R_3}{R_L+R_2+R_3}) \quad (13)$$

Due to $R_L << R_2 + R_3$,

$$V_1 = \frac{V_B}{R_T + R_1 + R_L} (R_T + \frac{R_L R_3}{R_2+R_3}) \quad (14)$$

$$V_2 = \frac{R_3}{R_3+R_2} V_B \quad (15)$$

$$V_T = V_1 - V_2 = \frac{V_B}{R_T + R_1 + R_L} (R_T + \frac{R_L R_3}{R_2+R_3}) - \frac{R_3}{R_3+R_2} V_B \quad (16)$$

The electrical resistance of the heater branch was much smaller than the remainder of the electrical paths. Thus,

$$V_B = I(R_T + R_1 + R_L) \quad (17)$$

Submit Eq. (17) into Eq. (16),

$$V_T = I(R_T + \frac{R_L R_3}{R_2+R_3}) - \frac{IR_3(R_T+R_1+R_L)}{R_3+R_2} \quad (18)$$
$$= IR_T - \frac{IR_3(R_T+R_1)}{R_3+R_2}$$
$$= \frac{IR_T R_2}{R_3+R_2} - \frac{IR_1 R_3}{R_3+R_2}$$

Then the output voltage of the Kelvin double bridge circuit is obtained as:

$$R_X = \frac{R_1 R_3 + \frac{V_T}{I}(R_3 + R_2)}{R_2} \tag{19}$$

When the bridge is in balance, V_T=0.

$$R_X = \frac{R_1 R_3}{R_2} \tag{20}$$

Eq. (20) is the usual equation for the Kelvin double bridge. It indicates that the connections and connecting wires resistance has no effect on the measurement.